

Personalized Chemotherapy Treatments for Microsatellite Instable Gastroesophageal Adenocarcinomas

Adam Daniel Hoffman

Faculty of Medicine

Division of Experimental Surgery

McGill University, Montreal, Canada

Supervisor: Dr. Lorenzo E. Ferri MD, PhD

November 2022

A thesis submitted to McGill University in partial fulfillment of the requirements of the degree
of Master of Science in Experimental Surgery



McGill

© Adam Daniel Hoffman, 2022

TABLE OF CONTENTS

ABSTRACT	4
RÉSUMÉ	6
ACKNOWLEDGEMENTS	8
PREFACE & AUTHOR CONTRIBUTIONS	10
LIST OF ABBREVIATIONS	11
LIST OF FIGURES & TABLES	14
CHAPTER ONE: REVIEW OF THE LITERATURE	15
1.1 GASTRIC & ESOPHAGEAL CANCER OVERVIEW	15
1.1.1 GASTROESOPHAGEAL CANCER ORIGINS & STATISTICS	15
1.1.2 GASTROESOPHAGEAL MOLECULAR SUBTYPES & CLINICAL BIOMARKERS	17
1.1.3 GASTROESOPHAGEAL ADENOCARCINOMA TREATMENTS	19
1.2 PATIENT-DERIVED ORGANIDS IN PRECISION MEDICINE	22
1.2.1 ORGANIDS COMPARED TO MOUSE MODELS	22
1.2.2 RECAPITULATE PATIENT TUMOUR	26
1.2.3 DRUG SCREENING CAPABILITY & PERSONALIZED CARE	27
1.3 MICROSATELLITE INSTABILITY-HIGH MECHANISM & CLINICAL RELEVANCE	31
1.3.1 ROLE OF MISMATCH REPAIR DEFICIENCY IN CANCER PROGRESSION & STATISTICS	31
1.3.2 IDENTIFYING MICROSATELLITE INSTABILITY STATUS	33
1.3.3 ASSOCIATED MUTATIONS	34
1.3.4 CHEMOTHERAPY: VIABLE TREATMENT OR INTRINSIC CHEMORESISTANCE	38
1.3.5 WRN HELICASE SYNTHETIC LETHALITY	39
1.3.6 IMMUNOTHERAPY POTENTIAL	42
1.4 PROJECT RATIONALE, OBJECTIVES & HYPOTHESIS	44
CHAPTER 2: EXPERIMENTAL DESIGN & METHODOLOGY	46
2.1 CLINICAL DATA & COHORT	46
2.2 PATIENT SAMPLE COLLECTION	46
2.3 TUMOUR VOLUME CHANGE	46
2.4 PATIENT-DERIVED ORGANOID CULTURE	47
2.5 MICE SURGERY & PATIENT-DERIVED XENOGRAFT ORGANIDS	50
2.5.1 MOUSE SURGERY FOR PDX:	50
2.5.2 TUMOUR XENOGRAFT SUBCUTANEOUS IMPLANTATION	51
2.5.3 PDXO DERIVATION	51
2.6 HISTOLOGY & ANTIBODIES	52

2.7 BRIGHTFIELD IMAGING	54
2.8 <i>IN VITRO</i> DRUG SCREENING	55
2.9 DRUG STOCKS	56
2.10 DNA COLLECTION, EXTRACTION & SEQUENCING	56
2.11 STATISTICAL ANALYSIS	58
CHAPTER 3: RESULTS	59
<hr/>	
3.1 MSI-HIGH PATIENTS ARE CLINICOPATHOLOGICALLY WELL-MATCHED TO MSS	59
3.1.1 CHARACTERISTICS OF PATIENT COHORT DISPLAY EFFECTIVE MATCHING	59
3.1.2 NO SIGNIFICANT DIFFERENCES IN SURVIVAL WERE OBSERVED BETWEEN MSI-HIGH & MSS PATIENTS GIVEN NEOADJUVANT CHEMOTHERAPY	64
3.2 TUMOUR HISTOLOGY & MSI STATUS IS RECAPITULATED BETWEEN PRIMARY TUMOUR & PDOs/PDXOs	68
3.3 CLINICAL CHEMOSENSITIVITY CORRELATES WITH PATIENT-DERIVED ORGANOID/XENOGRAFT ORGANOID CHEMOSENSITIVITY	72
3.3.1 MOST PDOs/PDXOs RECAPITULATED THE CLINICAL RESPONSE OF RESPECTIVE PATIENTS'	72
3.3.2 NO SIGNIFICANT NEOADJUVANT CHEMOTHERAPY RESPONSE DIFFERENCE BETWEEN MSI-HIGH & MSS PATIENTS CLINICALLY, & MSI-HIGH & MSS PDOs/PDXOs <i>IN VITRO</i> .	78
3.4 GENOMIC SEQUENCING & ALTERNATIVE TARGETED THERAPIES EXHIBIT PROMISING OUTCOMES	83
CHAPTER 4: DISCUSSION	91
<hr/>	
REFERENCES	99

ABSTRACT

INTRODUCTION: The gastroesophageal adenocarcinoma (GEA) molecular subtype of microsatellite instability (MSI) high is characterized by mismatch repair (MMR) deficiency, leading to an increased mutation burden and augmented chance of intrinsic chemoresistance. Due to the lack of clinical evidence, it is not possible to determine the epidemiology of patients within the MSI-high GEA group responding to chemotherapy, and which chemotherapies work best. *We hypothesize that the poor response of MSI-high GEAs to chemotherapies is due to the increased mutational burden, which can be overcome by concurrently identifying and targeting multiple genetic alterations.*

METHODS: An ideally matched MSI-high and microsatellite stable (MSS) patient cohort was selected from a >350 GEA patient biobank. Selected patient-derived organoids (PDOs)/patient-derived xenograft organoids (PDXOs) were developed, regularly thawed, maintained, and passaged in a Matrigel-based environment. Tumour content and MSI status of PDOs/PDXOs were confirmed with paraffin block embedding, subsequent slide sectioning, H&E staining, and mismatch repair protein staining. To identify differentially and frequently altered genes per PDO line, >1 million cells were frozen for whole exome sequencing (WES) to compare with primary tumour WES. To determine whether organoid models replicate clinical responses, cells were treated with the same chemotherapy received by the patient. In addition, high throughput screening with potential inhibitors against a few target genes was conducted.

RESULTS: A cohort consisting of 23 MSI-high and 23 MSS patients was well-matched based on tumour location, grade, neoadjuvant chemotherapy, sex, and age. H&E staining revealed that PDOs recapitulated the histology of the respective primary tissues. IHC staining of 4 mismatch repair proteins demonstrated PDOs (11 MSI-high, 13 MSS) can maintain MSI-high

status *in vitro*. A spectrum of genetic mutations of a small cohort (5 MSI-high, 3 MSS) was determined using primary tumour. Extracted DNAs from 22 PDOs (10 MSI-high, 12 MSS) are available for WES and target validation. The chemosensitivity of 18 PDOs (10 MSI-high and 8 MSS) was examined. Using previous data, the WES of 13 patient-derived xenografts (3 MSI-high, 10 MSS) revealed potential targets for MSI-high patients. Afterwards, preliminary robotic testing was performed *in vitro* (2 MSI-high, 2 MSS PDOs) with 16 FDA-approved drug compounds to validate the effectiveness of molecularly targeted therapy.

CONCLUSIONS: No significant overall survival, disease-free survival, and clinical chemosensitivity difference were observed between MSI-high and MSS patient groups. Through standard-of-care chemotherapy screening on PDOs, no significant chemosensitivity difference was observed between MSI-high and MSS. WES yielded promising alternative targets for MSI-high cases, such as *ARID1A*.

RÉSUMÉ

INTRODUCTION: Adénocarcinomes gastro-oesophagiens (GEAs) avec un sous-type moléculaire caractérisé par une instabilité élevée des microsatellites (MSI) et par un déficit de réparation des mésappariements (MMR), présente plus de mutations au niveau de la tumeur et un risque accru de chimiorésistance intrinsèque. En raison du manque de preuves cliniques, il n'est pas possible de déterminer l'épidémiologie des patients du groupe MSI-GEA élevé (MSI-H) qui répondent à la chimiothérapie, ni quelles chimiothérapies fonctionnent le mieux pour eux. Nous émettons l'hypothèse que la faible réponse à la chimiothérapie des patients faisant partie du groupe MSI-H s'explique par l'augmentation de la charge mutationnelle et que cette réponse pourrait être améliorée en identifiant et en ciblant simultanément plusieurs altérations génétiques.

MÉTHODES: Une cohorte de patients parfaitement compatibles MSI-H et microsatellite stable (MSS) a été sélectionnée à partir d'une biobanque de plus de 350 patients. Des organoïdes dérivés des tumeurs des patients (PDO) ou dérivés de xénogreffe tumorale (PDXO) ont été développés et maintenus en vie dans une matrice extracellulaire appelée Matrigel. Le contenu tumoral et le statut MSI-H/MSS des PDO/PDXO ont été confirmés en fixant les cellules dans des blocs de paraffine et en faisant soit une coloration hématoxyline/éosine (H&E) ou de l'immunohistochimie avec les anticorps spécifiques aux protéines de réparation des défauts d'appariement sur des sections. Afin de comparer le contenu génétique des PDO avec celui de la tumeur originale, plus d'un million de cellules ont été congelées et soumises au séquençage du génome complet (WES). Afin de déterminer si le modèle *in vitro* d'organoïdes reproduit bien la réponse clinique de la tumeur à la chimiothérapie, les cellules ont été traitées avec le même traitement que celui reçu par le patient. Finalement, un criblage à haut débit avec des inhibiteurs potentiels contre quelques gènes cibles a été réalisé.

RÉSULTATS: Une cohorte composée de 23 patients MSI-H et de 23 patients MSS a été créée en utilisant comme critères l'emplacement et le grade histologique de la tumeur, la chimiothérapie néo adjuvante reçue par le patient, ainsi que son sexe et son âge. La coloration H&E a révélé que les PDO récapitulent l'histologie de leurs tissus primaires. L'immunohistochimie de 4 protéines de réparation des défauts d'appariement a démontré que les PDO (11 MSI-H, 13 MSS) maintiennent leur statut de MSI-H ou MSS *in vitro*. La quantité de mutations génétiques d'une fraction de la cohorte (5 MSI-H, 3 MSS) a été évaluée dans les tumeurs primaires. De plus, l'ADN extrait de 22 PDO (10 MSI-H, 12 MSS) est disponible pour le séquençage du génome et pour la validation de cibles thérapeutiques. La sensibilité à la chimiothérapie de 18 PDO (10 MSI-H et 8 MSS) a aussi été examinée. En utilisant des données de séquençage obtenues pour 13 xénogreffes dérivées de patients (3 MSI-H, 10 MSS), plusieurs cibles thérapeutiques potentielles pour les patients MSI-H ont été identifiées. Certaines de ces cibles ont été testées *in vitro* (2 MSI-H, 2 MSS) avec 16 composés médicamenteux approuvés par la FDA afin de valider l'efficacité de la thérapie moléculaire ciblée.

CONCLUSION: Du point de vue clinique, aucune différence significative de survie globale, de survie sans maladie et de sensibilité à la chimiothérapie n'a été observée entre les groupes de patients MSI-H et MSS. Les tests *in vitro* sur les PDO ont permis de confirmer qu'aucune différence significative de sensibilité à la chimiothérapie n'existe entre les deux mêmes groupes. Par contre, le séquençage a révélé des cibles thérapeutiques alternatives prometteuses pour les patients MSI-H, comme par exemple *ARID1A*.

ACKNOWLEDGEMENTS

I would like to show my appreciation to Dr. Lorenzo Ferri for supervising me as a Master's student. He welcomed me into his lab and was a great mentor, facilitating my development professionally and interpersonally. His work ethic, leadership, and passion helped motivate me to try my best and strive for excellence. The vast experience in the field that he demonstrated during our meetings was vital in guiding the project toward meaningful objectives. He always provided unique perspectives and clinical insight into our conversations. I hope to apply the presentation, communication, and scientific skills that I developed throughout my future endeavours. I genuinely enjoyed the laboratory experience and am deeply thankful for the opportunity. Dr. Veena Sangwan provided research expertise in organoid development that acted as a foundation for this project. Dr. Nick Bertos gave project suggestions and used his valuable experiences with MUHC logistics to help move research requisitions forward. I am very grateful to Julie for creating a friendly environment in the lab, in which I could ask questions and learn new techniques. You assisted me throughout my entire thesis, and I could always rely on your expertise. France was approachable and a great communicator when allocating mouse responsibilities, which was essential for the xenograft work done. Sanjima gave instrumental advice and feedback throughout my journey. She importantly taught me how to think like a researcher, showing me how to plan and prepare for experiments. I am thankful for the conversations we shared, as I developed professionalism in how to conduct myself within the workplace that were vital to the completion of my research. Sanjima, Iris and Kulsum were a pleasure to work alongside, sharing thought-provoking and meaningful experiences. You all helped make me feel welcome in the lab, and importantly, we tried some of the best food Montreal has to offer during our dinners. You were always available for discussion and

emotional support, and I value our friendship. In particular, constant video updates from Kulsum's bunny Cloudy gave me something to look forward to every day while writing this thesis. Additionally, I am incredibly fortunate for my supportive parents Lawrence and Risa, and my brother Ryan. Our calls after a late night in the lab conducting experiments provided a voice of reason that grounded me during hectic weeks. A special thank you to my grandparents Wilf, Bonnie, Joe and Robbie; your endless support kept me motivated throughout my studies. This thesis is dedicated to my loving grandmother Robbie, who passed away shortly before this thesis was completed. I will carry on your legacy of compassion, thoughtfulness and family-oriented drive throughout my life in your memory.

PREFACE & AUTHOR CONTRIBUTIONS

This thesis was produced in compliance with the McGill University Graduate and Postdoctoral Studies Faculty's requirements. The thesis was written entirely by the author. The experimental design, laboratory activity, and data analysis that contributed to the final findings presented in this thesis were carried out primarily by the author under the supervision of Dr. Lorenzo Ferri. Moreover, Dr. Veena Sangwan (Assistant Professor), Betty Giannias (lab manager), France Bourdeau (animal technician), Julie Berube (research assistant), Dr. Sanjima Pal (postdoctoral fellow), Iris Kong (Ph.D. candidate) and Kulsum Tai (MSc candidate) all contributed in the planning and completion of experiments. Dr. Nick Bertos (biobanking manager) coordinated all biobanking efforts. Dr. Greta Evaristo and Dr. Pierre-Olivier Fiset helped with immunohistochemistry. Dr. Swneke Bailey and Nathan Osman assisted with genomic analysis.

LIST OF ABBREVIATIONS

AGC: Advanced gastric cancer

ALI: Air-liquid interface

AUC: Area under the curve

BE: Barrett's esophagus

CAF: Cancer-associated fibroblasts

CAR: Chimeric antigen receptor

CDH1: E-Cadherin

CDKN2A: cyclin-dependent kinase inhibitor 2A

CIN: chromosomal instability

CNV: Copy number variation

CR: Complete response

CRC: Colorectal cancer

CT: Computerized tomography

DCF: Docetaxel + cisplatin+ Fluorouracil

DDR: DNA damage response

DFS: Disease-free survival

dMMR: deficient mismatch repair

EA: Esophageal adenocarcinoma

EBV: Epstein-Barr Virus

EC: Esophageal cancer

ECF: Epirubicin + cisplatin + fluorouracil

ECM: Extracellular matrix

EGF: Epidermal growth factor

EGFR: Epidermal growth factor receptor

ESCC: Esophageal squamous cell carcinoma

FDA: Food and Drug Administration

FLOT: Fluorouracil + oxaliplatin + docetaxel

GA: Gastric adenocarcinomas

GC: Gastric cancer

GEA: Gastroesophageal adenocarcinoma

GEJ: Gastroesophageal junction

GI: Gastrointestinal

GS: genomic stable

HER2: Human epidermal growth factor receptor 2

HNSCC: Head and neck squamous cell carcinomas

H. pylori: Helicobacter pylori

ICI: Immune checkpoint inhibitor

IHC: Immunohistochemistry

IM: Intestinal metaplasia

LCO: Lung cancer organoid

MMR: Mismatch repair

MGH: Montreal General Hospital

MRN: Medical record number

MSI: Microsatellite instability

MSI-high: Microsatellite instability-high

MSS: Microsatellite stable

MUHC: McGill University Health Center

OS: Overall survival

PD: Progressive disease

PD-1: Programmed cell death 1

PD-L1: Programmed death ligand 1

PDO: Patient-derived organoid

PDX: Patient-derived xenograft

PDXO: Patient-derived xenograft organoid

PFS: Progression-free survival

PR: Partial response

pMMR: Proficient MMR

PTC: Patient tumour cluster

RECIST: Response evaluation criteria in solid tumours

SCNA: Somatic copy number alteration

SNV: Single nucleotide variant

SOX: S-1 + oxaliplatin

SD: Stable disease

TBIO: Tumour biopsy

TILS: Tumour infiltrating lymphocytes

TMB: Tumour mutational burden

TME: Tumour microenvironment

TSUR: Tumour surgery

LIST OF FIGURES & TABLES

Figure 1. Organoids prepared from primary tumour samples are processes for storage, drug screening, and imaging

Figure 2. MMR protein staining process for PDO/PDXO slides.

Figure 3. Clinical treatment timeline overview comparing MSI-high to MSS

Figure 4. Kaplan-Meier curves of overall survival & disease-free survival according to MSI status (MSI-high vs. MSS) &/or treatment (surgery only vs. surgery & neoadjuvant chemotherapy)

Figure 5. Primary tumour & PDO/PDXO H&E & MMR protein staining images of MSI-high & MSS

Figure 6. RECIST % tumour change CT images & corresponding PDO/PDXO chemosensitivity curves

Figure 7. Clinical neoadjuvant chemosensitivity waterfall plot of RECIST % tumour change according to MSI status (MSI-high vs. MSS)

Figure 8. DCF-treated PDO/PDXO response curves according to MSI status (MSI-high vs. MSS)

Figure 9. TMB & genomic alterations of MSI-high & MSS primary tumour oncoplot

Figure 10. PDO drug compound response curves to chemotherapy regimens & alternative targets

Table 1. Clinicopathological overview comparing MSI-high with MSS

Table 2. PDOs/PDXOs recapitulate the clinical response of patients

Table 3. IC50 organoid responses for 16 drug compounds

CHAPTER ONE: REVIEW OF THE LITERATURE

1.1 Gastric & esophageal cancer overview

1.1.1 Gastroesophageal cancer origins & statistics

Cancer is a leading cause of death that decreases life expectancy in every country of the world ¹. Gastric cancer (GC) globally ranks fifth for incidence and fourth for mortality, being responsible for over one million new cases worldwide in 2020, with approximately 769,000 deaths. If combining all cancers, the worldwide incidence rate was 19% higher in men than in women. GC has 2-fold higher rates in men than in women, acting as the most commonly diagnosed cancer and the leading cause of cancer-related death in several South Central Asian countries. Separating by cancer location in the body, the stomach at 5.6% has the 5th highest incidence and 4th highest mortality at 7.7% for both sexes. In comparison, esophageal cancer (EC) is tied for 7th highest incidence at 3.1% and 6th highest mortality at 5.5% for both sexes.

In Canada, 233 900 new cancer cases and 85 100 cancer deaths are expected during 2022 ². Concerning colorectal, stomach, and EC in Canada; 24 300, 4100, and 2500 new cases respectively will likely occur. Estimates for 2022 Canadians project about one-quarter of cancer deaths to be from lung cancer, with colorectal at 9400, esophagus at 2400 and stomach at 2000. Due to the lack of systemic screening and the absence of early signs, the majority of patients present with locally advanced illness, culminating in a 5-year survival rate of less than 20% ³. Moreover, male gender, age >55, a history of cigarette use, a diet poor in fruits and vegetables, and obesity are risk factors for GC and EC. Esophagus and stomach cancers affect more males than females, with projected deaths of 1800 males to 540 females for the esophagus, and 1250 males to 30 females for the stomach. The age-standardized ratios of GC and EC heavily varied

between countries with 10 times more GC cases than EC in men in several South American countries, Algeria and the Republic of Korea, while EC was much more prevalent in sub-Saharan African countries ¹. Both cardia GC and esophageal squamous cell carcinoma (ESCC) had high rates in several Asian populations.

Gastric adenocarcinomas (GA) are located in the pylorus and antrum for 50-60% of cases, 25% in the cardia, and 15-25% in the body or fundus ⁴. The majority of GCs are adenocarcinomas, which can be subdivided according to the Lauren classification into the three main GA subtypes intestinal, diffuse, and mixed ⁵. Intestinal is characterized by a glandular or papillary structure that frequently originates from intestinal metaplasia; diffuse displays poorly cohesive tissue; mixed shows areas of both intestinal and diffuse histology ^{4,5}. Intestinal-type GC and EC both emerge through pathological progression sharing fundamental features in which chronic inflammation leads to intestinal metaplasia (IM) ^{6,7}. For intestinal-type GC, IM occurs when normal gastric mucosa becomes chronic atrophic gastritis, followed by multifocal atrophy and IM, followed by dysplasia and carcinoma appearance ⁷.

The majority of ECs are associated with infectious agents, such as the bacterium *Helicobacter pylori* (*H. pylori*) and Epstein–Barr virus (EBV) ⁸. Importantly, the intestinal-type GC arising from the antrum or corpus portions of the stomach is increasingly associated with chronic *H. pylori*-associated gastritis and IM ⁹. On the other hand, diffuse-type GC is associated with the presence of both pre-existing *H. pylori* infection and inflammation ^{10,11}. There is a strong positive relationship between cardia GC and *H. pylori* infection as it can induce both inflammation and metaplasia ^{12,13}. Tumours of the upper gastrointestinal (GI) tract such as Barrett's esophagus (BE), esophageal adenocarcinoma (EA), and GAs may show similar immunohistochemical findings ⁴. EA cases typically show glandular differentiation and involve

the lower one-third of the esophagus. In EAs, acid and bile reflux-induced chronic esophagitis leads to BE, which is when the native epithelial lining is adapted to a columnar one with excess goblet cells ^{7,14}. Additionally, BE was shown to originate from gastric cardia in functional studies using organoids ¹⁵. The metaplasia in BE includes gastric glands, making it more histopathologically complex than simply intestinal differentiation with goblet cells ⁷.

1.1.2 Gastroesophageal molecular subtypes & clinical biomarkers

The combination of whole exome sequencing, bulk RNA, and single-cell transcriptomics help to offer insight into the ambiguity of classifying GC and EC as distinct cancers ^{7,16}. GC has been molecularly categorized into four distinct genetic subgroups: EBV (9%), Microsatellite instability (MSI) - high (22%), GS (genomic stable) (20%), and CIN (chromosomal instability) (50%) ¹⁷. Each subtype is distinguished by distinct genetic abnormalities, many of which are amenable to therapeutic intervention. EBV is characterized by increased methylation, MSI-high by elevated mutation rates, GS by the absence of aneuploidy with hypermethylation, and CIN by aberrant copy number patterns ^{17,18}.

Historically, the anatomical location and histological appearance of GC and EC made it difficult to examine or conceptually comprehend their relationship. Currently, their anatomical and histological characteristics overlap ⁷. There is no clear distinction though between CIN GAs and EAs ¹⁹. Gastroesophageal adenocarcinomas (GEAs) exhibit a steady gradation of subtypes, with increasing incidence of the CIN phenotype proximally, with 71 of 72 EAs being categorized as CIN, no EAs being MSI or EBV positive ¹⁹. MSI- and EBV-positive tumours were found among gastroesophageal junction (GEJ) adenocarcinomas that were not obviously of esophageal origin ¹⁹. The significant molecular similarity between EAs and CIN gastric malignancies gives

indirect evidence for the stomach origin of BE and EA, suggesting that GEAs may be seen as a single entity^{17,19}. Previous animal models imply that BE and EA may develop from proximal gastric cells or embryonic remnant cell populations at the GEJ, even though the genesis of BE remains disputed^{14,20}. This CIN gradient is comparable to that of colorectal carcinomas, with CIN prevalence increasing distally toward the rectum²¹. These parallels between EA and CIN gastric tumours do not, however, imply that all CIN GEAs are identical.

Esophageal carcinomas can be molecularly clustered into adenocarcinomas or squamous cell carcinomas¹⁹. EAs and ESCCs were compared to head and neck squamous cell carcinomas (HNSCC) and GAs, revealing that ESCC resembled HNSCC more than EA based on mRNA expression, DNA methylation, and somatic copy number alteration (SCNA) data. After thorough examination, squamous tumours were justified to be molecularly distinguishable from adenocarcinomas. Therefore, results indicate against combining EA with ESCC in clinical trials of neoadjuvant, adjuvant, or systemic treatments since EAs were shown to be more similar to stomach cancer than ESCCs¹⁷.

Proximal and distal stomach tumours of intestinal-type GC and EA have been shown to share several characteristics⁷. The growing realization is that intestinal-type GC and EA may be modest variants of a single tumour type with a shared origin⁷. Similar to EA, the more prevalent intestinal type of GC occurs as a result of gastric epithelium adopting an intestine-like condition⁶. The discovery of *H. pylori* and its relation to chronic gastric inflammation helped with the understanding of IM²². The change in prevalence of intestinal-type GC from the more distal stomach has been followed by a decrease in *H. pylori* infection rates, along with improvements in diet and cleanliness^{23,24}. Although there are other lethal types of GCs, such as the diffuse type, these tumours differ from EAs more on a histopathological and molecular level⁷.

1.1.3 Gastroesophageal adenocarcinoma treatments

Chemotherapy is the treatment of choice for advanced stomach cancer; nevertheless, responses are varied and little is known about the mediators of chemotherapy response ¹⁶. Response evaluation criteria in solid tumours (RECIST) is extensively used in clinical practice to evaluate the efficacy of individual therapy, which is primarily dependent on image-based assessment ²⁵. The standard of treatment for patients with resectable gastric/GEJ adenocarcinomas is perioperative platinum-based chemotherapy with surgery ^{26,27}.

The MAGIC trial for resectable GEAs included three-week cycles of epirubicin + cisplatin + fluorouracil (ECF) followed by surgery, and then three further ECF cycles, which resulted in a substantial increase in five-year overall survival (OS) of the perioperative chemotherapy group at 36% compared to the surgery alone group at 22% ²⁷. Moreover, the French FNCLCC/FFCD trial observed patients with resectable GEAs that underwent perioperative chemotherapy of fluorouracil with cisplatin significantly raised their OS to 38% vs. 24% and disease-free survival (DFS) to 34% vs. 19% ²⁸. The CLASSIC trial showed that GC DFS significantly improved to 68% in the adjuvant capecitabine plus oxaliplatin group compared to 53% in the observation alone group ²⁹. Nevertheless, these studies are currently outdated and exclude docetaxel, which has shown great efficacy in both the first and second-line treatment of metastatic GC ²⁶. Currently, systemic cytotoxic chemotherapy (with or without radiation) administered before surgery gives the greatest chance of cure. The Ferri group was the first to establish the effectiveness of docetaxel as a viable neoadjuvant for GEAs ³⁰. In gastric and GEJ adenocarcinomas, perioperative fluorouracil + oxaliplatin + docetaxel (FLOT) increased median OS time to 50 months in comparison to 35 months with perioperative ECF ²⁶. Lastly of note, oxaliplatin has been seen to display small survival advantages with less toxicity compared to

cisplatin, making the FLOT regimen the optimal chemotherapy available ^{31,32}. However, FLOT when retrospectively compared to fluorouracil + cisplatin+ docetaxel (DCF) is relatively interchangeable since oxaliplatin and cisplatin are both platinum-based ^{33,34}. Even though these docetaxel-based therapies are the most effective approaches to date with an initial response rate of >60%, there are still 40% of patients with innate resistant tumours who receive toxic and futile treatment before curative-intent surgical resection ³⁵. Moreover, recurrence due to acquired resistance occurs in 50% of initial responders, leading to only a 30% sustained response rate.

Patients afflicted with advanced stomach cancer have a poor survival outlook; thus, identifying and validating new targets is of utmost therapeutic importance ²⁴. The neoadjuvant treatment of cancer patients has progressed over the last decade from therapy based on tumour type to treatment based on the molecular features of a tumour or its surroundings. After achieving only minor results, motivation is rising to conduct additional phase III comparative studies, with some using biomarker-based methodologies for patient selection. The T-cell-inflamed gene-expression profile, human epidermal growth factor receptor 2 (HER2) status, programmed death ligand 1 (PD-L1) expression, and tumour mutational burden (TMB) are biomarkers that may predict responsiveness to anti-programmed cell death 1 (PD-1) treatment across many tumour types ³⁶. Trastuzumab, a monoclonal antibody against HER2, also known as ERBB2, was studied in conjunction with chemotherapy for the treatment of advanced HER2-positive gastric and GEJ cancer ³⁷. Trastuzumab is most often used to treat breast cancer, but may also be used to treat GEAs ³⁸.

Multiple international phase III studies have recently confirmed the combination of anti-PD-1 medicines with conventional frontline fluorouracil and platinum chemotherapy for the treatment of GEAs ^{1,39-42}. Notably, the worldwide phase III CheckMate-649 study demonstrated

the effectiveness of PD-1 target nivolumab in conjunction with chemotherapy as the first-line treatment for advanced gastric cancer (AGC), resulting in the drug's expedited clearance by the US Food and Drug Administration (FDA) in April 2021⁴³. Differential outcomes have been observed between patients with PD-L1-high and PD-L1-low tumours, with the absence of benefit for nivolumab in PD-L1 low AGCs⁴³. This indicates the need for a greater understanding of the cellular and molecular processes underlying responsiveness in GEA malignancies.

Subsequently, interim analysis of the ongoing KEYNOTE-811 study revealed the effectiveness of PD-1 target pembrolizumab in combination with trastuzumab and chemotherapy in patients with locally advanced or metastatic HER2-positive AGC, resulting in FDA clearance on May 2021⁴¹. Cytotoxic chemotherapies may modify the tumour microenvironment (TME) and enhance immune-mediated tumour death, which may be amplified with PD-1 inhibition and reinvigorate anti-tumour T-cell responses^{16,44,45}. Oxaliplatin and other platinum drugs may upregulate PD-L1 expression on dendritic cells and increase immune cell infiltration in mouse colorectal models^{46,47}. Although preclinical research suggests that fluorouracil and oxaliplatin have the potential to create immunogenic conditions in the TME, there is no clear proof that this happens in patients. A full explanation of the pre-and post-treatment TME during conventional fluorouracil/platinum monotherapy alone in AGC remains a substantial knowledge gap and obstacle to a better comprehension of clinical results with PD-1 combos^{48,49}.

Currently, there is no standard treatment regimen for patients with advanced metastatic gastric cancer who have progressed after two or more courses of chemotherapy⁵⁰. The effectiveness and safety of vascular endothelial growth factor receptor 2 tyrosine kinase inhibitor apatinib were evaluated, and considerably increased median OS and progression-free survival (PFS) compared to the placebo group. Next, trifluridine/tipiracil substantially increased OS

relative to placebo in an extensively pretreated cohort of patients with AGC and was well tolerated ⁵¹. Trifluridine/tipiracil may be a novel therapeutic option for this group, which has a significant unmet medical need. Lastly, chimeric antigen receptor (CAR) T-cell therapy of CT041 displayed promising effectiveness in GC ⁵². This treatment was well tolerated and showed increased efficacy in patients with elevated Claudin18.2 expression.

1.2 Patient-derived organoids in precision medicine

1.2.1 Organoids compared to mouse models

A human cancer organoid biobank may be created directly from neoplastic tissue or by genetically modifying normal tissues ⁵³. The vast majority of biobanking investigations have shown that patient-derived organoids (PDOs) replicate the features of primary tumours at the level of bulk tumour DNA sequencing ⁵⁴. Patient tumour clusters (PTC) enhance translational research, may have a role in clinical decision-making, and can be adapted for difficult-to-establish cancer subtypes ^{55,56}. It is currently possible to generate long-term tumour organoid cultures from a variety of human epithelial tissues, including colon ⁵⁷⁻⁵⁹, breast ^{60,61}, liver ⁶², lung ^{63,64}, pancreas ⁶⁵⁻⁶⁸, prostate ⁶⁹⁻⁷¹, endometrial ^{72,73}, and gastroesophageal ⁷⁴⁻⁷⁷.

Spheroids or tumour spheres are aggregations of tumour cells that offer benefits over 2D monolayer cultures due to their resemblance to solid tumours ⁷⁸. Organoids are multicellular *in vitro* structures produced from adult or embryonic stem cells that have the potential to self-organize and self-renew ⁷⁹. The capacity of tumour organoids to preserve properties of the original tumour distinguishes them for individual patient-level cancer research. Due to the success of establishing tumour PDOs, they can potentially be used for precision medicine-guided clinical decision-making that maximizes patient outcomes. Organoids may be generated for

various cancers utilizing various mediums that can impact the therapy response ^{56,80}. Epidermal growth factor (EGF) and Noggin are sufficient for the majority of organoid culture growth, however, the media can be specialized depending on the area of interest ⁵⁶. 3D cultures and organoid cultures from tumour and healthy tissues of cancer patients use Matrigel as a replacement for the extracellular matrix (ECM) component ^{56,81,82}. The success rate of 3D cultures without spheres or Matrigel is poor ⁵⁵. Some synthetic ECM hydrogels are used as an alternative to Matrigel, acting as a suitable carrier for tumour implantation. The ECM aspects such as cellular ratios, medium composition and physical characteristics can be tailored at lower prices than Matrigel ^{65,66}.

The utilization of patient-derived xenograft (PDX) models in translational cancer research can offer valuable *in vivo* drug screening, biomarker investigation, and the preclinical assessment of personalized medicine initiatives ⁸³. These models are created by subcutaneous or orthotopic implantation of tiny parts of human tumours in immunodeficient mice, which are then propagated to obtain cohorts of animals with identical tumours on which to conduct preclinical trials ⁸³. In the great majority of instances, the main tumour and the PDX were an exact match. They resembled their respective original tumours substantially more than unmatched pairings, retaining histologic and transcriptional characteristics after many passes ⁸⁴. As a result, mice for *in vivo* investigations are a valuable method for studying tumour development, progression, metastasis, and medication response mechanisms.

However, PDXs may undergo tumour evolution unique to mice ⁸⁵. Colorectal cancer (CRC) PDXs were shown to undergo metastasis and clonal selection but can fail to effectively portray the clonal heterogeneity of the derived human tumour ⁸⁵. PDXs also present many disadvantages, including a low engraftment rate and weak metastatic potential, a

microenvironment distinct from that of the underlying tumour, the presence of intratumour heterogeneity, and engraftment in mice with highly damaged immune systems ⁸⁶.

In vitro analysis can also be conducted on derived organoids from PDX-implanted tumours. They can genotypically and phenotypically recapitulate the patient's tumour, providing an additional means to establish organoid models ⁸⁷. Drug reaction findings of patient-derived xenograft organoids (PDXOs) were even shown to correlate with the *in vivo* PDX findings ⁶⁴. Nonetheless, PDXOs still experience the drawbacks of being xenograft derived with a lower culture success rate than PDOs, approximately 2-3 month *in vivo* tumour growth wait period, and clonal changes from being implanted initially as a PDX.

The noteworthy advantages of PDOs are that they more accurately resemble the original tumour than cell lines and are more adaptable than PDX models ⁸⁸. Tumour organoids are simpler to create, less expensive to maintain, and do not need the use of experimental animals, which is consistent with animal welfare ethics. Additionally, they allow for patient-specific molecular and phenotypic characterizations, generation of biobanks for disease modelling/mechanistic investigations, and are high throughput drug screening-friendly. Fortunately, PDOs can reproduce the morphological and genetic characteristics of cancers ⁵⁶. Lung cancer organoids (LCOs) were able to display a minimum of three distinct morphologies, including solid spheres, luminal spheres, and loosely linked granular sheets ⁶⁴. Organoid shape examples were also shown in breast cancer PDOs to be mature luminal, luminal progenitor, and basal/stem cells ⁸⁹. In CRC PDOs, the histological characteristics are shown, including lumen structure and mucus production ⁵⁹.

While tumour organoids are revolutionary, they do possess drawbacks such as their inability to capture the TME, such as fibroblasts or immune cells ⁹⁰. This issue has been

somewhat alleviated by the development of co-cultures, as discussed further below, but remains a barrier, particularly in terms of immunotherapy testing. Once a culture has been established, the growth rate differs across intra- and inter-patient samples as well as tumour types, and slow-growing samples may delay prompt decision-making. Uncertainty remains as to whether this accurately reflects features of the original tumour and/or if it might introduce unintended biases into *in vitro* drug testing that relies on cellular growth. There can be variable success rates across tumour types, and clinical translation is limited to a subset of patients^{59,81}. Furthermore, cultivating organoids is time-consuming, and the requirement for a particular culture medium with a variety of growth factors is expensive, and depending on the experimental outcome, must be carefully evaluated. Access to patient samples may also be limited, particularly in situations of rarity⁹¹. Finally, normal epithelial cell contamination might be deleterious to the purity of organoid cultures⁷⁰.

A caveat in the use of cell lines is their prolonged adaptation to tissue culture conditions, which could lead to genetic and epigenetic alterations over time⁹². While examining the long-term passaging of LCOs the morphologies were maintained, and identical growth curves indicated maintenance of expansion ability⁶⁴. The proportion of cancer cells in the organoids continued to rise, corresponding with the discovery that our LCOs solely encouraged the development of tumour organoids⁶⁴. Analysis of long-term organoid cultures indicates that the phenotypic, genetic diversity, and mutational markers of the original tumour sample are conserved in PDOs^{54,93}. Cultures and circumstances for developing tumour organoids are often designed for normal tissue growth⁷⁹. Accordingly, the presence of normal cells in tumour resections may result in the overgrowth of normal organoids as opposed to tumour organoids⁶³. This may be prevented by using culture settings that preferentially promote tumour cell growth.

1.2.2 Recapitulate patient tumour

Tumour biopsies and resections utilized for clinical diagnosis are incapable of capturing the complete intratumoral heterogeneity responsible for the accumulation of tumour clones with innate or acquired resistance ⁵⁶. Tumour organoids replicated tumour genomes in the majority of instances; however, there were a few exceptions where the absence of recapitulation may have been caused by intratumoral heterogeneity or expansion of premalignant dysplastic epithelium. Organoids give an excellent genetic model of the original tumour and imitate the intricacy of cancer cells developing in the human body ^{53,74}. It has been shown that PDOs can preserve the tumour clonal hierarchy and intratumoral heterogeneity ⁹⁰. This clonal drift of organoids during extended culture durations seems to be a quite minor concern for CRC and ovarian cancer PDOs investigated ⁹⁴.

Histologic examination of the organoids indicated that they retained the features of the respective original tumours and PDXs ⁸⁴. Representative Hematoxylin and eosin (H&E) stainings of various histologic cancer types may be made and accurately represent the patient's original tumour as PDOs ⁵⁶. H&E staining revealed that the LCOs exhibit three-dimensional structures identical to those of *in vivo* malignancies, maintaining histologic resemblances to the primary tumour ^{64,95}.

PTCs that were subdivided into many wells on a microchip, had their genomic consistency determined by comparing genomic and transcriptome profiles between PTCs in various wells and their respective original tumours ⁵⁵. The somatic mutations, copy number variations (CNVs), and transcriptome profiles were very consistent, showing that the amounts and compositions of the PTCs were comparable across wells, maintaining genome primary tumour characteristics. For instance, DNA copy number gains and losses were retained in LCOs,

which frequently displayed clearer and more distinct signals than the original lung cancers due to the enrichment of cancer cells⁶⁴. PDOs of ovarian cancer develop fast, acting as genetically and functionally identical models to the tumours from which they are produced⁹⁶. If CRISPR alteration is conducted, gut organoids may be subcloned, allowing for a detailed analysis of cancer gene function⁵³. For example, when essential DNA repair genes are removed using CRISPR and the resultant mutant organoid clones are subcloned after some time, unique mutational signatures arising from poor DNA repair are seen. Mutation accumulation in organoids defective in the mismatch repair (MMR) gene *MLH1* accurately mimicked mutation profiles of deficient mismatch repair (dMMR) CRCs.

1.2.3 Drug screening capability & personalized care

A key goal of precision medicine is the identification of therapies that target the specific biology of each patient's ailment⁵⁶. Personalizing therapy requires the creation of unique biomarkers and prediction models to get more permanent results with fewer adverse effects⁹⁰. PDOs correctly predict medication response, making them extremely applicable in personalized medicine for individualized patient care^{53,74}. Emerging research shows that PDOs are excellent clinical response predictors and may accurately indicate patient medication response^{53,79,88,90}. Taking a tumour sample from a patient, creating and propagating organoids, exposing the patient-derived tumour organoids to a variety of medications, and then treating the patient with the optimal drug or combination of therapies is feasible^{82,97,98}. PDOs show early promise in drug research, and clinical studies utilizing organoids should be conducted to investigate whether organoids are reliable cancer mimics that may objectively predict a patient's response to medicines^{53,80,82,99}. In particular, Vlachogiannis *et al.* (2018) showed a favourable link between

PDO and patient response, reporting a 88% positive predictive value and a 100% negative predictive value.

It would serve as the definitive bench-to-bedside paradigm for cancer therapy that may reveal the direct effect of treatment on cancer cells. Multiple groups have reported that PDO cultures replicate patient responses to chemotherapies in ovarian cancer ⁹⁸, head/neck/oral/esophageal ⁷⁴, oral mucosal, ¹⁰⁰, pancreatic ductal adenocarcinoma ^{67,101}, CRC ^{90,97,102}, and gastroesophageal ⁹⁰. Demonstrating a specific example of utility, a patient was clinically diagnosed with stage III gastric adenocarcinoma and had neoadjuvant S-1 + oxaliplatin (SOX) therapy. PTC prognosis was then able to predict that the clinical result of SOX therapy would match the patient's response as observed on CT scans with a tumour volume reduction according to RECIST guidelines ^{25,55}.

Complete genetic profiling will be of immense assistance to cancer patients. Using this knowledge in conjunction with an ever-expanding arsenal of rationally tailored drugs will provide the unparalleled potential to match patients with the best therapy possible ^{67,103}. Molecular profiling of tumour organoids was linked with drug-screening findings, indicating that PDOs might complement current methods for characterizing cancer susceptibilities and enhancing therapy responses ^{67,81,82}. Culture medium also played a role in PDO phenotype, as shown by significant differences in responsiveness to standard-of-care chemotherapies, different morphologies, and transcriptomes across media used for the same PDO cultures ⁸⁰. PDOs also serve as models for the development of medications that circumvent inherent or acquired resistance, which is especially relevant in the evaluation of DNA repair pathways and replication fork stability in ovarian cancer PDOs ⁹⁶.

Currently, PDOs may be used to choose second-line or adjuvant medicines since it takes around 4-6 weeks to produce and evaluate PDOs⁶⁶. In a LCO model, the drug sensitivity testing process was reduced to one week by lowering the number of organoids needed for assays and increasing the number of organoids that may be produced from a patient's sample⁶⁴. Shortening PDO creation and drug testing to one week would allow PDO therapy recommendations in a more clinically relevant timeframe⁵³.

The TME influences tumour growth and treatment response; nevertheless, it is difficult to describe since it is hard to maintain viability in tissue culture and modify *ex vivo*. The microenvironment is crucial, and it is acknowledged that it influences therapeutic outcomes, yet PDOs often lack vascular tumour microenvironment and immune cells^{79,88,91,104}. Co-culturing tumour organoids with neutrophils, tumour infiltrating lymphocytes and cancer-associated fibroblasts (CAFs) would help establish viable TME models, allowing for practical PDO immuno-oncology applications^{53,65}. An example of PDO co-cultures includes evaluating how PDOs interact with CAFs to confer resistance to conventional and investigational medications, and whether they may be employed to maximize therapeutic response *ex vivo*¹⁰⁵. Another instance used an air-liquid interface (ALI) to culture PDOs with immunological and fibroblastic components from primary tumour pieces, in which the T cell clonal diversity of these ALI cultures parallels that of the patient's peripheral blood T cells¹⁰⁶. ALI cultures have been applied to the evaluation of immune checkpoint therapies in several human tumours with variable clinical responses, including melanoma, lung cancer, and renal cell carcinoma. Furthermore, PDOs derived from tumours with a high mutational load, such as MSI-high CRC and tobacco-related non-small cell lung cancer, may be cultivated with the patient's peripheral blood lymphocytes to create CD8+ T cell clones that grow in response to potential neoantigens¹⁰⁶. In

theory, such co-cultures might be utilized to maximize the response of effector T cells against a patient's neoplastic cells or to produce a high number of effector T cells that can target neoplastic cells for adoptive cell transplantation.

Existing organoid-on-a-chip approaches are constrained by either poor throughput or a lack of on-chip flexibility ¹⁰⁷. For translational applications of tumour organoids in drug discovery, development, and individualized therapy screening, high-throughput microfluidic organoid-on-a-chip devices are in great demand. The organ chip model gives insight into physical parameters (e.g., fluid flow, peristalsis) and biological components such as stromal cells (e.g., endothelium, immune cells), while giving a window into molecular-scale biochemical, genetic, and cellular responses in real-time ^{91,104,108,109}. The tumour-on-a-chip model can be employed for fundamental investigations concentrating on the TME and for drug preclinical testing in immunocompetent conditions ¹¹⁰.

To create a lung-on-a-chip that mimics the mechanically active alveolar-capillary interface of the living human lung, alveolar epithelial cells and microvascular endothelial cells are cultured in a microdevice with the physiological flow and cyclic suction applied to the side chambers to reproduce rhythmic breathing movements ¹¹¹. Lung organ-on-a-chip drug testing showed near-perfect consistency with clinical results ⁶⁴. Similarly, on-a-chip technology is capable of reconstituting the immunocompetent tumour microenvironment which could be used to test immunotherapy options in a low-throughput setting ³⁸. 3D co-cultures in microfluidic devices integrating four cell populations: cancer, immune, endothelial, and fibroblasts, were used to reconstruct the human tumour environment of HER2+ breast cancer ³⁸. Trastuzumab showed the ability to selectively enhance extended cancer-immune contacts, resembling the antibody-dependent cell-mediated cytotoxicity immune response ³⁸. Trastuzumab tended to enhance

interaction times with surrounding immune cells, whereas CAFs appeared to reduce mean and maximum contact times. The intestinal organ chip contains two parallel microfluidic channels; an upper luminal channel, in which biopsy-driven intestinal organoids are seeded, and a lower vascular channel, in which intestine-specific endothelial cells are seeded ¹¹². Cell culture microchannels are separated by a porous ECM-coated elastic membrane, that may be expanded and contracted by applying a cyclic vacuum to hollow side chambers, simulating the peristaltic-like mechanical motions of the intestine and physiological fluid flow. As a result, intestinal epithelial cell monolayer formation and growth of villi-like structures can be examined. Morphological study of the on-chip device resembles that of the small intestine, and a comparison of gene scores revealed that the intestinal chip is more similar to the duodenum than PDO models. Previous studies have shown that the organ chip technology's strength lies in its ability to mimic organ-level complexity by progressively integrating different cell types one-at-a-time ^{108,109}. Future directions include integrating the remaining important components of the living intestine into the chip, such as intestinal fibroblasts and immune cells (e.g., macrophages, intraepithelial lymphocytes, and dendritic cells).

1.3 Microsatellite instability-high mechanism & clinical relevance

1.3.1 Role of mismatch repair deficiency in cancer progression & statistics

Microsatellites are short tandem repeats of simple DNA sequences, commonly found in human coding and noncoding regions ¹¹³. Cellular MMR machinery is necessary for the identification and replacement of single-nucleotide mismatches, and the correction of minor insertions and deletions that might occur during DNA replication, especially at microsatellite

sequences. Alterations in the MMR system results in genomic instability, neoantigen production, and immune response in cancer ¹¹⁴. MMR with deficiency is clinically defined as the immunohistochemistry (IHC) evaluated absence of any of the 4 MMR proteins MLH1, PMS2, MSH2 and MSH6, with proficient MMR (pMMR) in contrast being identified if all four MMR proteins are present. MSI may develop from Lynch Syndrome due to mutations in the MMR genes, and dMMR status predicts MSI-high status with approximately 90% accuracy ¹¹⁵. Among the truncating, missense, and in-frame variants identified, MLH1 and MSH2 had the greatest incidence of potential loss-of-function modifications, while only certain hotspot areas were targeted by likely oncogenic mutations in PMS2 and MSH6 respectively ¹¹⁴. Another element to consider is that owing to their heterodimeric structure, the loss of expression of one protein may also be attributable to the loss of expression of its associated protein ¹¹⁶. Of note, the majority of MSI-high patients had nuclear MLH1/PMS2 deletion ¹¹⁷. Therefore, loss of PMS2 alone would suggest a problem in PMS2, but when both MLH1 and PMS2 expression is lost, this is likely due to loss of MLH1, since this leads to an unstable PMS2. The same holds for the rarer MSH6 and MSH2 accordingly¹¹⁶.

MSI-enriched DNA exhibits increased mutations such as frameshift and single-nucleotide variations, leading to elevated TMB scores, and hypermethylation at the MLH1 promoter ¹⁷. These tumours are often dense with immune cells whose gene expression can greatly impact the transcriptome as a whole ⁸⁴. Consequently, MSI-high cancers display increased tumour-infiltrating lymphocytes and higher expression of PD-L1 ¹¹⁸. Suitably, 80% of MSI gastric tumours have *MLH1* methylation ¹¹⁹. The *MLH1* gene is epigenetically silenced in the context of a CpG island methylator phenotype in sporadic dMMR stomach malignancies ¹²⁰. MSI

phenotype was mostly related to MLH1 protein expression reduction, MLH1 promotor hypermethylation, and the absence of BRAFV600E mutation^{115,121}.

From the literature, MSI-high cancer displays significant variability in currently reported incidence; in gastric between 5.6-33.3%, in GEJ at 0-8.3%, and in esophageal at 0-4%¹²²⁻¹²⁴.

One paper showed that age is related to MSI status in GC, as the proportion of MSI-high GC grows progressively with increasing age, amounting to 48% of patients over the age of 85 years, but 8% of all GC patients¹²⁵. Moreover, 56% of MSI-high patients were female and were identified at a median age of 72 years¹⁷. In a retrospective study by Vos *et al.* (2021), dMMR/MSI-high was elevated in 15% of tumours, and patients tended to be older, female and intestinal subtype. In another comparable study, 12% of tumours had the MSI-high phenotype and were more prevalent in individuals over 70 years of age^{84,125}. This corresponds to research indicating that the MSI-high phenotype occurs in about 10% of GEAs^{121,126}. Furthermore, Asian GC varies from non-Asian malignancies, and additional information is needed to assess the degree of the impact¹²⁷. MSI-high is seen in 9-22% of non-metastatic GC patients^{128,129}. In advanced instances of GC, MSI-high is detected in 3-14% of cases^{130,131}. Internally at the McGill University Health Center (MUHC), gastric/GEJ patients between 2011 and 2019 were examined by Dr. Greta Evaristo with 28/226 (12%) having MMR loss, while 25/28 (89%) exhibited MLH1/PMS2 loss.

1.3.2 Identifying microsatellite instability status

MSI status can be determined with genomic sequencing analyzing TMB, IHC dMMR expression against pMMR, and PCR evaluation^{84,132}. MSI-high tumours have a higher TMB score and more modifications compared to MSS¹³³. Using a mutational burden score method,

scientists can distinguish MSI-high and microsatellite stable (MSS) groups ¹³⁴. The clinically applicable proteins of MLH1, PMS2, MSH2 and MSH6 will show an absence of brown pigment compared to surrounding normal tissue on an IHC slide if protein loss, and pigment presence if the function is retained. Additionally, the MSI Analysis System Kit version 1.2 (Promega) is commonly used within studies reported in scientific journals to analyze MSI status ⁸⁴. Genomic DNA is extracted for fluorescence PCR-based study of a mononucleotide repeat marker panel of NR-21, BAT-26, BAT-25, NR-24, and MONO-27/NR-27 ^{84,118,135,136}. The presence of allelic size differences at two or more loci is categorized as MSI-high, whereas all other instances are classified as MSS ^{118,137}.

1.3.3 Associated mutations

The three most mutant genes in GC are *TP53*, *SMAD4*, and *PIK3CA* ¹⁷. Notably, the MSI-high subtype was related to hypermutation in genes including *KRAS* (23.3%), the *PI3K-PTEN-mTOR* pathway (42%), *ALK* (16.3%), *ARID1A* (44.2%), *ERBB2* (16.3%), and *ERBB3* (14%) ¹³⁸. Furthermore, the top mutated genes in 14 MSI-high patients were *ANKRD11* (78%), *ARID1A* (71%), *KMT2B* (71%), *BCORL1* (64%), *IGF1R* (50%), *KDM5* (50%), *POLD1* (50%), and *TSC1* (50%) ¹³³. Tumours can be further classified as MSS/*TP53*+ (intact P53 function) and MSS/*TP53*- (onco-suppressor function loss) ¹³⁸. The MSI/*TP53*+ subtype was linked with EBV infection more often than other subtypes, had an active *TP53* pathway, and had a greater frequency of *APC*, *ARID1A*, *KRAS*, *PI3KCA*, and *SMAD4* mutations compared to MSI/*TP53*- ¹³⁸.

Exome sequencing of 22 gastric cancer samples in a small cohort revealed common *ARID1A* mutations in the MSI and EBV subgroup ¹³⁹. The inactivation of chromatin-modifying enzyme genes, most often *ARID1A* ^{18,140}, encodes a member of the SWI-SNF chromatin

remodelling family, in 83% of GC with MSI-high, 73% of those with EBV infection, and 11% of those without EBV and displaying MSS status ¹³⁹. EBV tumours exhibited the greatest degree of genome-wide hypermethylation, minimum demethylation, and a high ratio of nonsynonymous to synonymous single nucleotide variant (SNV) mutations ¹⁸. Both MSI and EBV cancers lacked *TP53* mutations and were chromosomally stable ¹⁸. Additionally, *TP53* mutation was favourably linked with CIN and demethylation but negatively associated with promoter CpG island hypermethylation ¹⁸. The mutation spectrum for *ARIDIA* changes across molecular subtypes of GC and the incidence of mutations is adversely correlated with *TP53* mutations ¹³⁹. In a separate study, *ARIDIA* was demonstrated to have the greatest frequency percentage mutated among MSI-high PDXs ⁸⁴.

Clinically, *ARIDIA* mutations were linked with a better prognosis ¹³⁹, corresponding with a longer time to treatment failure in colon cancer, in contrast to *TP53* mutations which correlate with a shorter time to treatment failure ¹⁴¹. *ARIDIA* was discovered to be related to greater sensitivity to the kinase inhibitor dasatinib in pancreatic cancer PDOs, which was first identified in ovarian cancer ⁶⁵. Intriguingly, in terms of drug-gene interaction, only missense mutations in *ARIDIA*, but not nonsense or frameshift mutations, were associated with a greater drug sensitivity ⁶⁵. Moreover, it was revealed that molecular subtype-specific mutational processes target the same driving genes ¹⁸. In MSI cancers, *RNF43* and *CDHI* were commonly inactivated by indels affecting mononucleotide repeats, while MSS patients had missense, nonsense, or indels in non-repeat areas, similar to what was previously found for *ARIDIA*. *ROS1*, *ALK*, or *NTRK* rearrangements are abundant in dMMR cancers and cause hypersensitivity to matching kinase inhibitors ^{142–144}. Resistance to these matching targeted drugs may develop as a result of *NTRK1* mutations or genetic changes that activate the MAPK pathway ^{145–147}.

Uniquely, 2.5%–3.9% of patients with MSI-high CRCs do not have germline mutation or MLH1 methylation, and these cancers have been identified as having two somatic MMR mutations^{148–150}. These CRC patients showed a greater prevalence of *PIK3CA* somatic mutations¹⁵¹. In addition to these distinct mutational patterns, the genomic landscape of CRC implicates the PI3K pathway as a driving factor in carcinogenesis¹⁵². Initial emphasis was on *PIK3CA* because it plays a crucial regulatory function in this pathway and was shown to be mutated in 30% of CRCs¹⁵³.

Multiple abnormalities in genes involved in TGF transduction pathways have been identified in CRC, including mutations in SMAD family genes, *BMPRIA*, and TGF β receptors. Unresolved is the effect of these mutations on immune cell recruitment in human CRC, however, several preclinical models have shown that disruption of these genes leads to a chronic inflammation that promotes CRC growth¹⁵⁴.

ATM was found to be the most frequently altered DNA damage repair (DDR) gene in CRC patients⁶⁴. Patients with *ATM* mutations had considerably higher overall survival than those without. Moreover, *ATM* inhibitors enhanced anti-PD-1 treatment in a mouse model. It was also found that *ATM* inhibition and radiation might increase tumoral immunogenicity, hence enhancing the efficiency of immune checkpoint inhibitors (ICIs)¹⁵⁵. Therefore, *ATM* may be a promising immunotherapy biomarker, and *ATM* inhibitors in combination with ICI and radiation may be an effective treatment regimen.

The *PTEN* gene contains instructions for producing an enzyme present in almost all bodily tissues. The enzyme works as a tumour suppressor, meaning that it helps regulate cell division by preventing cells from expanding and dividing too quickly or uncontrollably. Similarly, Bilbao *et al.* (2006) and Catass *et al.* (1998) observed a greater prevalence of

mutations in the *PTEN* gene in endometrial carcinoma with MSI. It has been shown that *PTEN* gene inactivation, caused mostly by mutations, plays a crucial role in the growth of tumours. In 24% of instances, this inactivation was caused by frameshift mutations in polyA/T repeats. The frameshift and nonsense mutations result in the production of proteins that are inactive or less stable^{156,157}. In one case, a patient with unresectable dMMR leiomyosarcoma with biallelic loss of *PTEN* was able to achieve CR from pembrolizumab treatment. Similarly, in non-colorectal GI cancers that get comparatively less benefit from ICIs, select subsets, such as those with *PTEN* alterations, may derive a greater advantage from ICIs¹⁴¹.

The presence of MSI-high in GEAs was negatively correlated with the prevalence of *APC* gene mutations¹⁵⁸. Findings suggest that somatic mutation of the *APC* gene has a significant role in the etiology of gastric adenoma and dysplasia, but has a limited function in the development of neoplasia to adenocarcinoma¹⁵⁸. The antecedents of intestinal-type gastric adenocarcinomas are gastric adenomas or dysplasias without *APC* mutations, but with or without MSI-high status¹⁵⁸. Additionally, it has been shown that tumours with activated WNT/-catenin pathways resulting from *APC* or *CTNNB1* mutations are poorly penetrated by immune cells due to the absence of immune cell trafficking¹⁵⁹.

Previous high-throughput sequencing studies, for instance, revealed that tumour-suppressed genes such as *TP53* and cyclin-dependent kinase inhibitor 2A (*CDKN2A*) may be responsible for genomic instability in a variety of sporadic malignancies^{160,161}. MSI, *BRAF* mutation, and greater tumour grade were positively correlated with *CDKN2A* methylation.

In 25% of non-MSI-H patients, the *ERBB2* gene was amplified and identified as a targetable driver. Patients with the greatest amount of *ERBB2* amplification and an unchanged RTK/RAS/P13K pathway had the longest progression-free survival among the HER2+ patients

treated with anti-HER2 monoclonal antibody trastuzumab. Patients with RTK-RAS-PI3K pathway co-alterations and *ERBB2*- or *ERBB2*+ had a shorter progression-free survival¹³⁴.

In 27%-64% of GCs, *EGFR* is overexpressed, and its significance as an oncogene in this cancer is well-established^{162,163}. However, there is no unanimity about the predictive usefulness of *EGFR* status in patients with GC. Moreover, a 2013 meta-analysis analyzing the data collected in 5 separate studies on a total of 1,600 patients showed that *EGFR* expression is not an independent predictor of survival in GC¹⁶⁴. However, *EGFR* mutations correlated with the responses of LCOs to the tyrosine kinase inhibitor gefitinib⁶⁴.

A tiny proportion of GCs result from germline mutations in E-Cadherin (*CDH1*), which are linked to cancers with diffuse-type histology¹⁶⁵. Tumour growth, invasion, migration, and metastasis can result from *CDH1* dysregulation. Additionally, homologous recombination repair somatic mutations are the most common among DNA damage response (DDR) genes across 33 kinds of cancer¹⁶⁶. The most prevalent mutations linked to homologous recombination deficit are *BRCA1*, *BRCA2*, *RAD51*, *BLM*, and *RAD50*.

1.3.4 Chemotherapy: viable treatment or intrinsic chemoresistance

Kaplan-Meier and Cox regression analyses were used to evaluate clinicopathological features and survival between patients who received neoadjuvant/adjuvant treatment and those who did not, stratified by MSI status¹²⁶. Comparing MSI-high to MSS, the 5-year OS was 78% vs. 59% and DFS was 72% vs. 52%. When stratified into chemotherapy plus surgery vs. surgery alone groups, MSS patients improved from chemotherapy plus surgery against surgery alone with a 5-year OS of 62% vs. 53% and DFS of 57% vs. 41%. However, MSI-high patients did not benefit from chemotherapy + surgery over surgery alone with a 5-year DFS of 70% vs. 77% and

OS of 75% vs. 83%. Based on a meta-analysis of patient-level data from four clinical trials, dMMR/MSI-high GEA was a negative predictor of chemotherapy effectiveness in terms of OS and DFS. In contrast, a meta-analysis on adjuvant chemotherapy for dMMR/MSI-high GEA suggested a therapeutic advantage in terms of OS, but not DFS ¹⁶⁷. Moreover, the MSI score might have a prognostic value, as individuals with higher scores were identified to have a decreased recurrence rate ⁸⁴.

In CRC, patients with dMMR are treated with molecularly-targeted treatments and chemotherapeutic drugs. Patients with a subtype of MSI-high react poorly to chemotherapy, perhaps due to their elevated TMB, TME influence, and tumour progression ^{168,169}. Therefore, clarity is required on the usefulness of chemotherapy in both a neoadjuvant and adjuvant setting for dMMR/MSI-high GEAs. Clinical knowledge of how to match and choose medication combinations is a critical need for the pharmaceutical industry and physicians to combat treatment resistance in patients ^{170,171}. MSI-high patients are termed chemoresistant, but the specific chemotherapy regimen resistance is not clear, as large clinical studies examining MSI-high GEAs with potent drug component docetaxel in FLOT/DCF regimens are lacking. As a consequence, the apparent clinical chemoresistance led to the suggestion of chemotherapy omission and/or ICIs for better patient survival results ¹²⁶.

1.3.5 WRN helicase synthetic lethality

The *WRN* gene is a member of the RecQ family of DNA helicases and encodes for the Werner protein, which plays crucial functions in genomic integrity, DNA repair, replication, transcription, and telomere maintenance ^{172–175}. Patients with loss-of-function mutations in the *WRN* gene can lead to rapid aging and cancer susceptibility ¹⁷⁵. *WRN* operates as both a 3'–5'

exonuclease and 3'–5' helicase in activities such as DNA repair and replication¹⁷⁴. *In vitro* and *in vivo*, *WRN* is preferentially necessary for dMMR/MSI-high cell survival, and *WRN* deletion in dMMR/MSI-high cells promotes double-stranded DNA breaks and extensive genomic instability, encouraging death^{135,174–176}.

By examining dependency scores, projects Achilles CRISPR/Cas9 and DRIVE independently identified *WRN*, as the highest preferential dependence score, essential for cancer cell proliferation, in MSI-high cell lines compared to MSS^{174,177,178}. Greater than 90 percent of models, including models with various genetic origins, molecular settings, and oncogenic changes, were reliant on *WRN*, indicating that *WRN* dependence is a nearly universal characteristic of dMMR/MSI-high CRC cells. *WRN* was the leading candidate for preferred reliance in MSI-high because its depletion triggers double-stranded DNA breaks and promotes cell cycle arrest/apoptosis^{174,179}. Using functional screens, the dependent link for which *WRN* helicase mediated synthetic lethality (SL) in MSI-high GEAs has been found, but the particular genetic pathways that lead to cell death need more investigation^{174,179}. Functional expression of MSH2 and MLH1 was maintained in 7% of dMMR CRC mice that were *WRN*-independent, demonstrating that *WRN* reliance is impacted by the underlying MMR-pathway genes that are changed.

SL is an interaction in which the co-occurrence of two genetic events results in cell death while the occurrence of one event alone does not. Fortunately, there exists an exploitable SL connection in which the co-occurrence of dMMR and RecQ DNA helicase *WRN* inhibition results in cell death, yet neither event alone is deadly^{174,179,180}. Although *WRN* is the only human RecQ enzyme with a unique exonuclease domain, the MSI-high SL interaction is proven to be driven by the loss of helicase function^{135,174}. This connection between SL and MSI-high cancer

cells establishes *WRN* as a potential therapeutic target for MSI-high cancers, since silencing *WRN* seems to substantially lower cell viability ^{174,175}.

Before mitosis, activation of the G2/M checkpoint in response to DNA damage requires MMR activity ¹⁸¹. Therefore, *WRN* activity in MSI-high cells may be essential for the resolution of DNA damage events and the prevention of premature mitotic entrance. *WRN* silencing decreased the percentage of MSI-high cells in the S phase and increased the number of cells in the G1 or G2/M phase, indicating cell cycle arrest in G1 or G2/M ^{135,174}. Staining indicated that *WRN* silencing induced apoptosis and cell death in MSI-high cells. In contrast, MSS cell lines exhibited no enhanced cell cycle arrest or death after *WRN* silencing. Notably, cell lines produced by people with Werner syndrome exhibit faulty mitotic recombination and are sensitive to genomic instability ¹⁸². In MSS cancer cells and non-transformed cells, however, *WRN* depletion exhibited none or very modest impact on viability, indicating that pharmacological suppression of *WRN* might enable an MSI-high cancer-directed treatment that preserves normal cells and tissues.

WRN dependence should be investigated further in advanced or therapy-resistant cancers. *WRN* is a potential SL target in dMMR/MSI-high CRC tumours as a monotherapy or in conjunction with targeted medicines, chemotherapy, or immunotherapy ¹³⁶. MSI-high CRC cells resistant to clinically relevant targeted treatments or chemotherapy were shown to maintain a SL dependence with *WRN*, regardless of the mutational background of the tumour or the therapeutic regimen given ¹³⁶. The pharmacological suppression of *WRN* helicase provides an opportunity to create unique targeted treatments for MSI-high GEAs ^{135,174}. *WRN* inactivation specifically reduces the viability of MSI-high cells, but not of MSS cells in colorectal and endometrial cancer cell lines ^{135,174–176}. On the contrary, a lack of selectivity against dMMR cells has also been

observed, with off-target effects, and cytotoxicity to normal cells¹⁸³. Interestingly, inhibition of *WRN* may act synergistically with immunotherapy, since lack of DNA repair modifies the neoantigen landscape and increases the mutational load, resulting in an increased immune response^{136,184,185}. Low mutability in dMMR cancers was also shown to be inversely associated with ICI responsiveness^{186,187}.

1.3.6 Immunotherapy potential

Immunological characteristics, including MSI status, tumour infiltrating lymphocytes (TILs), PD-L1 expression, and the TME profile, are among the possible prognostic biomarkers for checkpoint inhibitors in advanced gastric/GEJ cancer¹⁸⁸. Multiple PD-1 inhibitors have been shown to increase OS in conjunction with chemotherapy in the first-line scenario¹⁸⁹. There is evidence that GEAs with dMMR status may respond to therapy with ICIs, particularly in patients with advanced illness¹¹⁴. MSI-high positive tumours have elevated PD-L1 expression, which may be related to the inflammatory TME and immune response¹⁸⁸. PD-1 is mostly expressed in T cells of the immune system, whereas PD-L1 is predominantly expressed in cancer cells and antigen-presenting cells. Immunotherapy with PD-1 and PD-L1 checkpoint inhibitors is effective against MSI-high CRC tumours due to their high TMB, and elevated neoantigen levels^{126,188,190,191}. It has been found that the responsiveness to ICIs correlates with TMB, dMMR status and PD-L1 expression^{134,188,192}. MSI-high/dMMR status also helps predicts the effectiveness of anti-programmed death-1 ICIs in combination with chemotherapy in patients with advanced GEAs^{43,193}. Furthermore, HER2-negative status is associated with greater PD-L1 expression rates, so accordingly HER2 is a possible biomarker for anti-PD-L1 treatment, along with dMMR status⁴⁰.

As of June 2020, the US Food and Drug Administration authorized pembrolizumab for the treatment of solid cancers with an increased tumour mutation load ¹¹⁸. Results revealed that both the amount and functional status of tumour-infiltrating T cells in the TME are necessary for an optimum pembrolizumab-induced antitumour response ¹¹⁸. The clinical effectiveness of PD-1 antibodies in metastatic GC has been adequately confirmed. The overall response rates to pembrolizumab monotherapy among the 67 MSI-high patients participating in the Keynote-059, -061, and -062 studies were 57%, 47%, and 57%, respectively ^{40,194,195}. These results were better than those of chemotherapy-treated patients in studies with a control arm ^{40,194,195}. Incorporating pembrolizumab with or without chemotherapy may be more effective than chemotherapy alone in treating advanced metastatic MSI-high GEA patients across all lines of therapy ¹⁹³.

Pembrolizumab monotherapy showed promising efficacy and tolerability in patients with advanced gastric/GEJ cancer who had received at least two prior lines of therapy. Both PD-L1-positive and PD-L1-negative patients had durable responses ⁴⁰. Pembrolizumab enhanced 24-month OS to 20% vs. 8% compared to chemotherapy paclitaxel in PD-L1-positive gastric/GEJ cancer, and was associated with 53% fewer adverse events than paclitaxel.

Next, nivolumab + ipilimumab-based neoadjuvant treatment was given for MSI-high patients with resectable GEAs, exhibiting no unexpected effects ¹⁹⁶. Nivolumab is an anti-PD-1 medication while ipilimumab is an anti-CTLA-4 medication, which is an antibody that strengthens the immune system by enhancing T-cell activity and proliferation. Nivolumab is the first PD-1 inhibitor to demonstrate improved OS, PFS benefit, and a tolerable safety profile in previously untreated patients with advanced GEA in conjunction with chemotherapy against chemotherapy alone ⁴³. 60% of dMMR/MSI-high CRC patients who received nivolumab + ipilimumab before surgery had a pathological CR ¹⁸⁹.

Lastly, in an important trial that employed PD-1 inhibitor Dostarlimab for locally advanced MSI-high rectal cancer, all 12 patients that finished therapy displayed full clinical responses¹⁹⁷. These PD-1 targets have shown promise in CRCs, but further clinical investigations need to be done in MSI-high GEAs to determine if similarly promising results in patients are possible.

1.4 Project Rationale, Objectives & Hypothesis

The current clinical standard of care for GEAs is a triplet-based chemotherapy regimen of docetaxel, 5-FU, and cisplatin/oxaliplatin. This regimen tends to be the best approach, but the strategy varies with GEA molecular subtype. MSI-high is characterized by MMR deficiency, leading to an increased mutation burden and an augmented chance of intrinsic chemoresistance. Due to the lack of clinical evidence, it is not possible to determine the epidemiology of patients within the MSI-high GEA group responding to chemotherapy, and which chemotherapies work best. We hypothesize that the poor response of MSI-high GEAs to chemotherapies is due to the increased mutational burden, which can be overcome by concurrently identifying and targeting multiple genetic alterations.

Aim 1) Identify a matched retrospective cohort using pathologist-indicated mismatch repair protein functionality (MLH1, MSH2, MSH6, PMS2) which reveals MSI status

- An ideally matched MSI-high and MSS patient cohort was selected from a >350 GEA patient biobank.

Aim 2) To develop PDOs/PDXOs

- Selected PDOs/PDXOs were developed, regularly thawed, maintained, and passaged in a Matrigel-based environment. Organoids are grown for ~3-14 days in an incubator at 37°C, 5% CO₂, and 3% O₂.

Aim 3) Analyze MMR protein function/loss in 3D PDO/PDXO models, confirming that the primary tumour microsatellite status is recapitulated

- Tumour content and MSI status of PDOs/PDXOs were confirmed with paraffin block embedding, subsequent slide sectioning, H&E staining, and MMR protein staining.
- To identify differentially and frequently altered genes per PDO line, >1 million cells were frozen for WES to compare with primary tumour WES.

Aim 4) Utilize PDX biobank to develop PDXOs in absence of appropriate PDOs

- Amplify tumour cells in mice for relatively rare MSI-high cases.

Aim 5) Test standard of care chemotherapies with 3D PDO/PDXO models and explore alternative approaches to prevent chemoresistance by evaluating targeted agents based on WES data.

- Cells were treated with the same chemotherapy received by the patient.
- Briefly, cells were seeded in 96 well plates. After maturation, they were treated with 10 different drug concentrations using a drug dispenser. Organoid viability is determined 72 hours later with a plate reader.

CHAPTER 2: EXPERIMENTAL DESIGN & METHODOLOGY

2.1 Clinical data & cohort

A retrospective cohort was established using the electronic records OACIS Clinical Information System at the Montreal General Hospital (MGH) following the MUHC code of ethics. Firstly, MSI-high patients were identified, and corresponding PDO/PDXO culture growth success was determined from an internal biobank containing over 350 GEA patient samples. Using available clinicopathological information, MSS patients were then matched to MSI-high on a rolling basis for cohort inclusion in the priority order of MSI , PDO/PDXO availability (refer to **Supplementary Table 1**), tumour location, tumour grade, neoadjuvant chemotherapy, sex, and age.

2.2 Patient sample collection

GEA tissues and blood samples were collected at endoscopic biopsy or surgical resection from consenting patients at the MGH under MUHC Research Ethics Board guidelines; Institutional Review Board projects 2007-856 and 2014-1119 respectively. Prior to samples being used for research purposes, written informed consent was received from participants.

2.3 Tumour volume change

Through comparing surgeon-evaluated computerized tomography (CT) scans around the time of biopsy before neoadjuvant treatment to after treatment around the time of surgical resection, % tumour volume reduction was classified according to the RECIST ²⁵ criteria for solid tumours. Relative gastric/esophageal wall inflammation thickening distance or cross-

sectional area of a lymph node when present were used to best evaluate pre-post % treatment effectiveness. Percentage increases and decreases were classified into RECIST categories depending on % value.

$$\text{Percentage Increase} = \frac{\text{Final Value} - \text{Starting Value}}{|\text{Starting Value}|} \times 100$$

$$\text{Percentage Decrease} = \frac{\text{Starting Value} - \text{Final Value}}{|\text{Starting Value}|} \times 100$$

Complete response (CR) is the disappearance of all target lesions, partial response (PR) is at least a 30% decrease from baseline, stable disease (SD) is between a 30% decrease to 20% increase, and progressive disease (PD) is at least 20% increase in target lesion size.

2.4 Patient-derived organoid culture

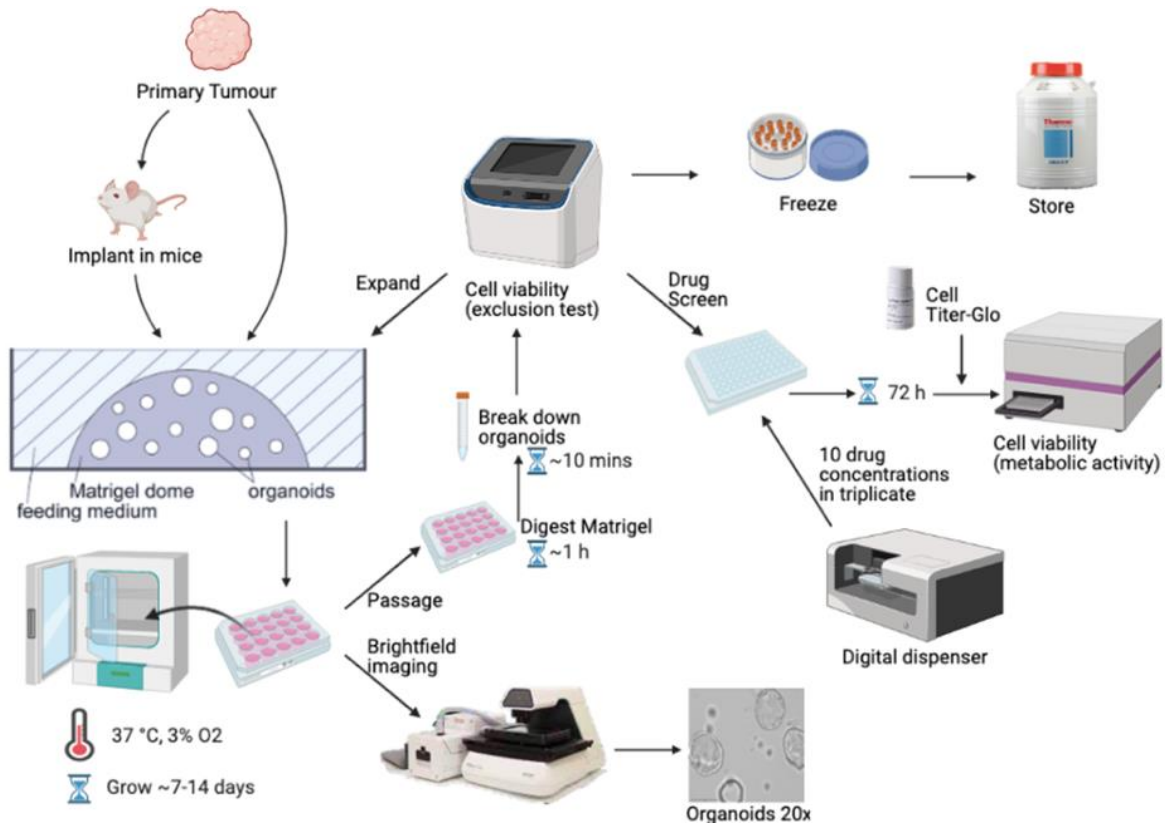


Figure 1. Organoids prepared from primary tumour samples are processes for storage, drug screening, and imaging

Selected primary tumour samples are chemically and mechanically digested to be processed as PDOs directly from primary tumours or implanted in mice as PDXs to amplify cells for PDXOs. Single cells are cultured in Matrigel domes plated in the center of 24-well plates forming 3-dimensional spheroids with cell culture medium on top. Organoids grow in an incubator at 37°C, 5% CO₂, and 3% O₂ for 3 to 14 days. Once mature, they can be imaged, passaged, frozen for later use in liquid nitrogen storage, or plated for high-throughput drug screens as described below. This figure was created with BioRender.com.

Organoids were passaged in a sterile biosafety cabinet with a digestion buffer 1:100 dilution of 100mg/ml stock Collagenase/Dispase (Sigma 10269638001) with AD-DF+++ [Advanced DMEM/F12 (Invitrogen 12634-010), supplemented with Glutamax-1(Invitrogen 35050-061), HEPES (Invitrogen 15630-080) and Pen/Strep (Sigma P4333)] medium to digest the Matrigel (Corning, 356231). The medium is then removed with a p1000 pipette tip. A 500ul digestion buffer is added in each well, pipetting up and down to break the Matrigel domes. After digesting for ~1 hour, the media is collected in a 15mL tube and spun at 500xg for 5 mins at 4°C. The supernatant is carefully removed without disturbing the pellet. 1mL of 0.25% Trypsin (Gibco, 15050-065) is mixed with a p1000 tip and left to incubate at 37°C in a water bath for 5 min. Pulse vortex for ~5 seconds, looking for single organoids under a microscope. 5mL of 5% FBS-PBS is then added to inactivate the trypsin. This is followed by a vortex step to generate a smooth suspension of cells. The tube is then Spun at 500xg for 5 mins at 4°C. Supernatant is removed and 1ml AD-DF+++ medium is added to wash. Cells are counted by taking 10uL of cell suspension + 10uL of Trypan Blue (Gibco, 15250-061), with cell counting slides (Invitrogen, C10283) then recording the viability of live cells. At this point, cells are plated for expansion or experiments, and frozen for storage or DNA extractions.

The next steps are planned according to 30 000 cells per well for PDO, 100 000 cells per well for PDX-derived PDOs. To freeze cells for storage, 750µl CryoStor media (Sigma) is used with CryoPure (Sarstedt, 9081911) 1.8mL freezing tubes. The tube(s) are placed in a CoolCell (Corning, 432002) freezing container and put in -80° Freezer. To freeze cells for DNA extraction, the supernatant is removed and the cell pellet is flash-frozen in a 1.5ml tube with liquid nitrogen, then placed in a -80° Freezer.

To plate PDO cells in Matrigel: a dome of 80uL Matrigel and cells is dispensed onto a 24-well plate using a p200 pipette per well. The plate is left to incubate for 1 min at room temperature, before transferring it to a HERAcell V10S 160i incubator (Thermo scientific) at 37°C, 3% O₂, and 5% CO₂ for ~30 mins to allow the Matrigel to become a solid dome. 600uL of complete organoid growth medium is then added to each well.

To plate PDXOs in Matrigel: 24 well plates are put on ice, and 80µl of 100% Matrigel per well is added in a zigzag pattern, covering the entire bottom of the well. Plates are left to sit at 37°C in a 3% O₂ incubator for ~30 mins, allowing the Matrigel to solidify. Cells are resuspended in 5% Matrigel complete gastric media solution that is prepared on ice in a 15mL/50mL tube and 500µl is added per well.

Notably, cell culture media is refreshed every 3-4 days: For PDOs, 600uL of media is removed and 600uL of complete gastric organoid growth media is added using a p1000 pipette. For PDXOs, ~500uL of cell culture media per well is removed using a p1000 pipette, but should leave some to not disrupt the Matrigel coat on the bottom. ~500uL of 5% Matrigel complete gastric organoid growth media solution is added. Passaging occurs every 10-14 days depending on organoid growth. Complete gastric cell culture media is prepared by adding human IntestiCult (components A (Stemcell, 06011) and B (Stemcell, 06012)), Pen/Strep (Sigma P4333), and

ROCK inhibitor to gastric organoid media (Fujii, Clevers, and Sato 2019). Additionally, *mycoplasma* testing was performed with the TransDetect Luciferase Mycoplasma Detection Kit (FM301) according to their standardized protocol when new lines were added to cell culture, and at regular 1-month intervals.

2.5 Mice surgery & patient-derived xenograft organoids

2.5.1 Mouse Surgery for PDX:

On the day of implantation, fresh tumour samples were collected and stored in a 4°C cell culture medium. The right flanks of two mice are then subcutaneously implanted with a tiny part of the GEA primary tumour, about 3x3 mm in size and split into two pieces. The tumour is collected and the mouse is euthanized once it reaches about 1cmx1cm (0.52 cm³) in volume. Once removal occurs, the tumour is implanted into two recipient mice as passage 1, while the remainder of the tumour will be kept for future research. The passage of these mice in succession will continue until passage 3. At the 3rd passage, the tumour will be excised and stored for analysis or to develop PDXO cultures.

Mice from an in-house colony of immunocompromised NSG (Jackson Laboratory, 005557) between 7 and 12 weeks old, both males and females, are implanted. Six months after surgery, mice are euthanized if there is no tumour development. All mice experiments were conducted in strict conformity with the requirements of the Canadian Council on Animal Care's Guide to the Care and Use of Experimental Animals', and under the conditions and techniques authorized by the McGill University Animal Care Committee (Animal Use Protocol 8081).

2.5.2 Tumour xenograft subcutaneous implantation

Carprofen (20 mg/kg per day) is given subcutaneously, 30 minutes prior to the beginning of surgery. The animal is anesthetized and kept under isoflurane. Using a heating disc or warming pad, the body temperature is maintained. The use of ophthalmic ointment prevents corneal dryness and damage. Before putting a mouse in a surgical area, its right flank is shaved using an electric razor. The mouse is maintained with a nasal cone, and the region for surgical implantation is swabbed with 0.5% chlorhexidine solution followed by 70% ethanol, three times. A 3-5 mm incision is performed right across the flank to establish a subcutaneous pocket. The tumour is chopped into 3x3mm pieces and implanted subcutaneously on the mouse's right flank. After the tumour fragment has been implanted, a combination of lidocaine and bupivacaine is applied to the surgical site before closing the skin wound. The skin margins are held together with forceps while a mouse autoclip or Vicryl 5-0 suture is used to close the incision.

2.5.3 PDXO derivation

Using a MACS Miltenyi Biotech tumour dissociation kit (130-095-929), PDX tumour pieces were digested into single cells. In a sterile biosafety cabinet, sterilized forceps and a razor were used to chop the tumour into very fine pieces. Subsequently, the tumour is added to the Miltenyi gentleMACS tube (130-093-237) and chemically digested with enzymes (200 µl Enzyme H, 100µl enzyme R, and 25µl enzyme A) that are added to 4.7mL of AD-DF+++ medium in a Miltenyi gentleMACS tube. Tumour pieces were then mechanically digested with a gentleMACS Octo Dissociation machine for 1 hour. All tube contents were poured onto a 100-micron strainer that was placed on top of a 50mL tube, followed by a 40-micron strainer, filtering the larger crushed tumour pieces from the solution, and washing each strainer with

2.5mL PBS (Gibco, 14190-144). Contents were transferred to a 15mL tube, and centrifuged at 500xg for 5 min at 4°C. The supernatant is removed and 1mL PBS is added and mixed using a P1000 pipette. Before depletion cell count is conducted, 10uL of cell suspension mixed with 10uL of Trypan Blue is taken to count and record the viability of live cells. The tubes are then centrifuged at 500xg for 5 min at 4°C. The supernatant is removed with a p1000 pipette and 80uL AD-DF+++ medium with 20uL of mouse depletion antibody cocktail (Miltenyi Biotech 130-104-694) (20uL of mouse depletion cocktail is good for 2 million cells) is added and left to incubate on ice for 15min. A MACS multistand is set up using LS columns (Miltenyi Biotech 130-042-401) to remove mouse cells. 3mL AD-DF+++ is added to the column to prepare it for the wash. Then 500uL of AD-DF+++ is added to incubating tubes and the mixture is added to the column followed by an additional 5mL of AD-DF+++ to the column filter. Cells were centrifuged at 500xg for 5 min at 4°C. The supernatant is removed and 1mL PBS is added and mixed using a P1000 pipette. An after-depletion cell count is then performed as described above. The next steps are planned while considering: 100 000 cells per well for PDXOs using the cell plating methods above.

2.6 Histology & Antibodies

Tissue blocks of organoids were prepared so immunohistochemical analysis can be conducted. In 4-well-chambered cell culture slides (Corning, 354114) organoids were cultured until fully developed. Histogel tube (ThermoFisher HG-4000-012) was heated in a microwave oven for about 20 seconds or until it liquefies. The PDO/PDXO medium is removed and washed with PBS twice, 400ul each. The PDOs/PDXOs are fixed with 800ul of room temperature 4% Paraformaldehyde (PFA) for 2 hours. Cryomolds (Tissue-Trek, 4565) are placed on ice and

150uL of Histogel per cryomold is added and kept on ice for 10 minutes. The PFA solution is removed and 800ul diluted Harris Hematoxylin Solution (Sigma HHS32-1L), 1:1 with H₂O is added incubating for 10 mins. It is then washed 3x with ddH₂O, 400 ul each. The plastic chamber is removed and Kimwipes are used to remove excess water. The PDOs/PDXOs are removed and transferred onto the first Histogel layer. 150ul of Histogel is added on top of the Matrigel layer in the cryomold, and left to cool on ice for 10 min. The histogel is flipped into a tissue cassette and fixed with 10% Formalin (Sigma Aldrich, HT501128) for 16-24 hours. Cassettes were stored in 70% ethanol until histopathology core processing for paraffin embedding.

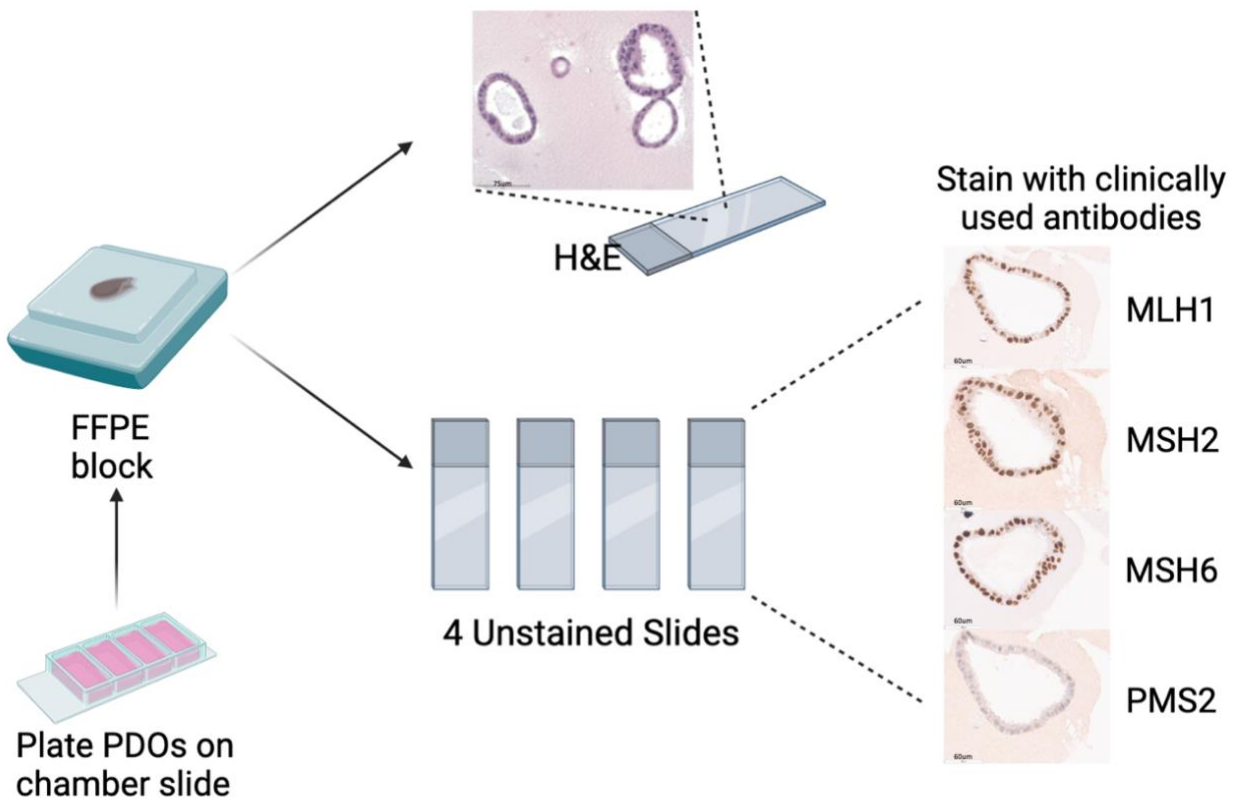


Figure 2. MMR protein staining process for PDO/PDXO slides

Organoids are plated on chamber slides and processed to establish FFPE blocks as described above. Blocks are sectioned to create unstained organoid slides that can be stained with

Hematoxylin and eosin (H&E), and/or 4 MMR antibodies. This figure was created with BioRender.com.

MMR status to determine MSI-high classification was assessed using the same clinically used IHC antibodies for MLH1 (mutL homologue 1; G168-15, Roche Diagnostics), MSH2 (mutS homolog 2; G219-1129, Roche Diagnostics), MSH6 (mutS homolog 6; SP93, Roche Diagnostics), PMS2 (postmeiotic segregation increased 1 homolog 2; A16-4, Roche Diagnostics). Formalin-fixed, paraffin-embedded (FFPE) blocks per cell line (as described above) are established to create unstained organoid slide sections that are stained with antibodies of interest through the standard protocols for the Ventana (Roche Diagnostics) automated immunostainer. IHC will be coupled with TMB results from WES analysis (described below) to confirm MMR status.

PDO/PDXO tumour content was analyzed by a pathologist by looking at corresponding H&E stained slides, typically based on the identification of malignant cells due to the presence of marked loss of polarity and macronuclei abnormalities compared to normal tissue. Nonetheless, organoid tumour content decisions were taken as rough estimates with the consideration that the exact clonal heterogeneity is not possible to be replicated due to the slide sectioning representing a sample of the larger tumour.

2.7 Brightfield imaging

An EVOS M7000 microscope was used for brightfield and live 3D cell imaging. Corresponding image sizes are 4x = 650 μ m, 10x = 275 μ m, 20x = 150 μ m, and 40x = 75 μ m.

2.8 *In vitro* drug screening

Medium throughput 300 000 organoid cells total/3000 cells per well are plated in 30 wells of a 96-well plate. After 3-5 days, depending on organoid maturation, pre-aliquoted drugs from -80°C are digitally dispensed with Tecan D300e. Cell media is replaced 24 hours before drug addition, and EVOS M7000 brightfield images are taken right before drug dispensing. In a sterile tissue culture hood, a T8+ Dispensehead Cassette (Tecan, 30097370) is loaded into the drug dispenser, as 10 different program-delegated drug compounds and normalization fluid (DMSO/DMSO +Tween20) concentrations are added in triplicate. After 72 hours in an incubator, wells are brightfield imaged, cell media is removed, and CellTiter-Glo 3D Cell Viability Assay (Promega) is added. A Varioskan Lux plate reader (Thermo Scientific) conducts a 5-minute shaking followed by a 30-minute incubation in darkness. The luminescence protocol measured metabolic ATP activity, determining relative cell viability. Dose-response curves and IC50 concentrations were calculated with Excel and GraphPad PRISM.

High throughput 16-drug compound screening was conducted at the Institute for Research in Immunology and Cancer. A Multidrop Combi Reagent Dispenser (Thermo Scientific) was used to seed Matrigel-encapsulated cells onto white 384-well plates. Organoid cells were allowed to mature for 4 days, then treated with 10 different concentrations in quadruplicate using an Echo 555 acoustic dispenser (Labcyte). After 1 week, a 405 Touch Microplate Washer (BioTek) was used to aspirate media and replenish with Cell Titer Glo 3D using the Multidrop Combi Reagent Dispenser. The plates were shaken for 5 minutes and then incubated at room temperature in darkness for 30 minutes. A Synergy Neo HTS plate reader (BioTek) was used to determine luminescence cell viability measurements. XLfit (IDBS)

integrated with Excel was used to create IC50 concentrations and dose-response curves, which were then reformatted in GraphPad PRISM.

2.9 Drug Stocks

All drugs were diluted in DMSO (Sigma, SHBL2891) except for cisplatin which was diluted in 0.9% saline. Drug compounds used include Docetaxel (Cayman, 11637), Cisplatin (Cayman, 13119), 5-fluorouracil (5-FU)(Cayman, 14416), Irinotecan (Cayman, 22566), Oxaliplatin (Cayman, 13106), VEGFR inhibitor Sorafenib (Cayman, 10009644), EGFR inhibitor Gefitinib (Cayman, 13166), ERK1/2 inhibitor Ulixertinib (Cayman, 18298), PIK3CA/mTOR inhibitor Gedatolosib (Cayman, 14567), MEK inhibitor Trametinib (Cayman, 16292), HSP90 inhibitor Luminespib/NVP-AUY922 (Cayman, 10012698), EZH2 inhibitor UNC 1999 (Cayman, 14621), WRN helicase inhibitor NSC 19630 (Cayman 14858). Ratios used are: DOF (1:1.7:10 for Docetaxel, Oxaliplatin, 5-FU), DCF (1:1:10 for Docetaxel, Cisplatin, 5-FU), FOLFIRI (1:2 for 5-FU, Irinotecan), and Luminespib + UNC 1999 (1:1). Drug selection for high-throughput screening including alternative targets was based on preliminary PDX genomic sequencing grant data.

2.10 DNA collection, extraction & sequencing

To identify differentially and frequently altered genes per PDO line, >1 million cells were frozen for WES to compare with primary tumour WES. Additionally, patient-specific buffy coat samples were available for all patients, acting as germline controls. AllPrep DNA/RNA Protein Mini Kit #80004. Buffer RLT with b-Mercaptoethanol was prepared in a fume hood. 350ul Buffer RLT was then added and vortexed to disrupt frozen tissue. Samples are placed on ice and

then vortexed for 1 minute. The lysate is pipetted directly into the QIA shredder spin column placed in a 2ml collection tube and centrifuged for 2 min at full speed. The QIA shredder column is discarded and the tube is capped. The lysate is centrifuged for 3 min at full speed. The supernatant is transferred to an AllPrep DNA spin column placed in a 2ml collection tube and centrifuged for 30s at 8000xg. The AllPrep DNA spin column was placed in a new 2ml collection tube and stored at room temp or 4°C for DNA purification. The flow-through for RNA purification was not required. 500ul Buffer AW1 is added to the AllPrep DNA spin column and centrifuged for 15s, 8000xg, discarding the flow-through. While reusing the collection tube, 500ul Buffer AW2 is added to the AllPrep DNA spin column and centrifuged for 2 mins, 8000xg to wash the spin column membrane. The collection tube is emptied and the spin column is centrifuged for 1 min at full speed. The AllPrep DNA spin column is placed in a new 1.5ml collection tube. 50ul of preheated to 70°C Buffer EB is added directly to the spin column. For 2 mins it is incubated at room temp (15-25°C), then centrifuged for 1 min, 8000xg to elute the DNA. The collection tube is reused, to further elute the DNA through centrifuging for 1.5 min, 8000xg, 1 min vortex. The measurements are done using a Nanodrop (Thermo Fischer ND-2000).

Firstly, to process whole exome sequencing (WES) data the quality was determined with FastQC (v0.11.9). Pre-processing of sequencing data to yield analysis-ready reads was conducted as per the Genome Analysis ToolKit 4 (GATK4 v4.2.2.0). GATK4 runs on Java (runtime: OpenJDK 64-Bit Server VM v1.8.0_302-b08), using the Java libraries HTSJDK (v2.24.1) and Picard (v2.25.4). During the pre-processing, mapping the reads to the human reference genome GRCh38 and alignment is performed by bwa-mem (v0.7.17). Somatic Single Nucleotide Variant (SNV) and Insertion/Deletion (Indel) calling were performed using GATK Mutect2. Variants

were annotated using annovar, which is Perl (v5.30.2) script. Copy Number Variant (CNV) calling was performed with the R (v4.1.0) package sequenza (v3.0.0), which uses external tools such as samtools (v1.15.1) and tabix. Lastly, oncoplots of the annotated variants were generated with the R package maftools (v2.14.0). Given inferred background mutation processes, MutSig2CV identifies genes altered more often than anticipated by chance (caveats: not enough samples to extract significant information).

2.11 Statistical analysis

All statistical and graph analyses were performed using Excel or GraphPad prism (v9.2.0). Fisher's exact test was used to test the independence of two categorical variables. The unpaired student's t-test was used to analyze the mean differences between experimental groups. The chi-square test was used to identify how much of a difference exists between the observed count vs. the expected counts. The stratified cox proportional hazard and log-rank test were applied for survival analysis. Of note, some percentages might not add up to 100 due to rounding. The statistical details are explained further in each figure legend, *P* values of < 0.05 were considered statistically significant in all experiments, while ns = not significant.

CHAPTER 3: RESULTS

3.1 MSI-high patients are clinicopathologically well-matched to MSS

3.1.1 Characteristics of patient cohort display effective matching

Due to the rarity of MSI-high patients, all applicable (n=23) were selected while referring to the OACIS clinical database in conjunction with a 350-patient biobank (**Table 1**). To control for this group, MSS patients were selected based on the priority of PDO/PDXO samples available, tumour location, tumour grade, neoadjuvant treatment, sex, and age. Characteristics include median age in years, sex, tumour location of distal esophageal/GEJ and gastric, T stage of 1-4, N stage of 1-4, histologic grade of well, moderately, and poorly differentiated and treatment arm of treatment naïve or neoadjuvant chemotherapy (n=28). The pathological response was recorded as good, moderate, and poor of the patients administered peri-operative chemotherapy. The MSI-high group has a nearly equal distribution between males and females. The distribution between distal esophageal/GEJ and gastric is close to even. Most patients are late-stage and grade. The pathological response for most patients is poor. Importantly, neoadjuvant chemotherapy was given to 14 MSI-high patients and their matched MSS pair. Out of these 24 patients given neoadjuvant chemotherapy, their clinical responses were PR or SD according to the clinical response RECIST criteria.

Patients are introduced at variable times so five-year clinical follow-up is not possible for all patients (**Figure 3**). Individual patient treatment trajectories are followed until endpoints of follow-up time end or death. Of note, each patient number in **Figure 3** corresponds with the same patient numbers in **Supplementary Table 1**.

The specific MSI-high to MSS matched pairing process is visually described with black text rows representing MSI-high in accordance with their pair one row below in red text (**Supplementary Table 1**). For all 46 patients (23 MSI-high, 23 MSS) their relevant clinical and laboratory information is recorded including biobank ID, MSI status, tumour site, histologic grade, neoadjuvant treatment, sex, age at collection, clinical stage, % tumour size reduction, RECIST clinical response, pathological staging, pathological response, PDO/PDXO used, organoid from biopsy/resection, organoid derived from the clinically treated patient, and medical record number (MRN).

Table 1. Clinicopathological overview comparing MSI-high with MSS

The 46-patient cohort was ideally matched between 23 MSI-high/dMMR and 23 MSS/pMMR.

The unpaired t-test, Fischer's exact test and chi-squared test were used to evaluate the statistical significance in GraphPad Prism.

Characteristic	Whole Series (N=46)	MSI High (n=23)	MSI Low/MSS (n=23)	P
Median (range) age, years	69 (18-88)	72 (18-88)	67 (28-85)	0.37
Sex				
Male	27 (59%)	11 (48%)	16 (70%)	0.24
Female	19 (41%)	12 (52%)	7 (30%)	
Tumour localization				
Esophageal, distal/GEJ	22 (48%)	11(48%)	11 (48%)	>0.999
Gastric	24 (52%)	12 (52%)	12 (52%)	
T stage				
1	6 (13%)	3 (13%)	3 (13%)	0.91
2	5 (11%)	2 (9%)	3 (13%)	
3	21 (46%)	10 (43%)	11 (48%)	
4	14 (30%)	8 (35%)	6 (26%)	
N stage				
0	20 (43%)	11 (48%)	9 (39%)	0.77
1	9 (20%)	5 (22%)	4 (17%)	
2	6 (13%)	3 (13%)	3 (13%)	
3	11 (24%)	4 (17%)	7 (31%)	
Histologic Grade				
Well differentiated	5 (11%)	4 (17%)	1 (4%)	0.2
Moderately differentiated	20 (43%)	11 (48%)	9 (39%)	
Poorly differentiated	21 (46%)	8 (35%)	13 (57%)	
Treatment Arm				
Treatment Naïve	18 (39%)	9 (39%)	9 (39%)	>0.999
Chemotherapy	28 (61%)	14 (61%)	14 (61%)	
Pathological response (n=28)				
Good	3 (11%)	3 (21%)	0	0.18
Moderate	5 (18%)	2 (14%)	3 (21%)	
Poor	20 (71%)	9 (65%)	11 (79%)	
Clinical Response (RECIST) (n=28)				
CR (complete response)	0 (0%)	0 (0%)	0	0.98
PR (partial response)	12 (43%)	5 (36%)	7 (50%)	
SD (stable disease)	11 (39%)	6 (43%)	5 (36%)	
PD (progressive disease)	0	0	0	
NE (inevaluable)	5 (18%)	3 (21%)	2 (14%)	

Figure 3. Clinical treatment timeline overview comparing MSI-high to MSS

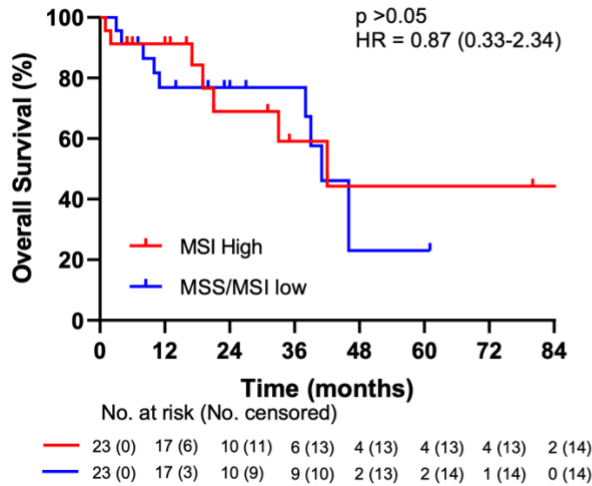
The clinical timeline for each of the 46 patients in the cohort is noted, and separated into MSI high (red) and MSS (blue) sections. All 46 patients on the Y-axis are followed in accordance with a timeline bar graph that follows each respective patient's treatment timeline in time (months) on the X-axis. Each bar follows patients for as long as they are included in the study or until death. The green diamond shows neoadjuvant start time, the yellow circle shows the time of surgical resection, the purple triangle shows tumour recurrence if present, well the black x corresponds to patient death.

3.1.2 No significant differences in survival were observed between MSI-high & MSS patients given neoadjuvant chemotherapy

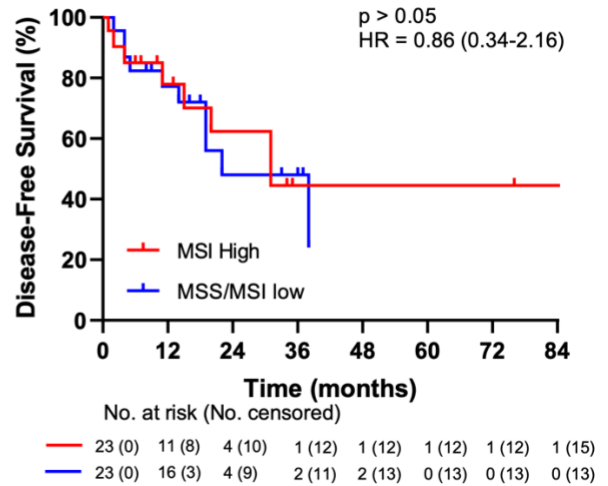
Figure 4A OS with HR= 0.87 (0.33-2.34), and **Figure 4B** DFS with HR = 0.86 (0.34-2.16), show a nonsignificant difference between 23 MSI-high and 23 MSS/MSI-low patients without differentiating between chemotherapy given. **(Figure 4C)** MSI High Pre-Op Chemo vs. MSS/MSI low Pre-Op Chemo: HR = 1.19 (95% CI, 0.31-4.50) with p = 0.79, a non-significant difference between 14 MSI-high given neoadjuvant chemotherapy and surgical resection (red) vs. 14 MSS/MSI-low given neoadjuvant chemotherapy and surgical resection (blue). MSI High Pre-Op Chemo vs. MSI High Treatment Naïve: HR = 0.74 (95% CI, 0.16-3.48) with p = 0.69, a non-significant difference between 14 MSI-high given neoadjuvant chemotherapy and surgical resection (red) vs. 9 MSI-high treatment naïve (green) with surgical resection only. MSS/MSI low Pre-Op Chemo vs. MSS Treatment Naïve: HR = 0.28 (95% CI, 0.051-1.52) p = 0.024*, a statistically significant difference between 14 MSS/MSI-low given neoadjuvant chemotherapy and surgical resection (blue) vs. 9 MSS/MSI-low treatment naïve (purple) with surgical resection only. MSI High Treatment Naïve vs. MSS Treatment Naïve: HR = 0.62 (95% CI, 0.14-2.75) p = 0.50, a non-significant difference between 9 MSI-high treatment naïve (green) with surgical resection only vs. MSS/MSI-low treatment naïve (purple) with surgical resection only. **(Figure 4D)** MSI High Pre-Op Chemo vs. MSS/MSI low Pre-Op Chemo: HR = 1.1 (95% CI, 0.33-3.63) with p = 0.87, a non-significant difference between 14 MSI-high given neoadjuvant chemotherapy and surgical resection (red) vs. 14 MSS/MSI-low given neoadjuvant chemotherapy and surgical resection (blue). MSI High Pre-Op Chemo vs. MSI High Treatment Naïve: HR = 1.03 (95% CI, 0.25-4.05) with p = 0.97, a non-significant difference between 14 MSI-high given neoadjuvant chemotherapy and surgical resection (red) vs. 9 MSI-high treatment

naïve (green) with surgical resection only. MSS/MSI low Pre-Op Chemo vs. MSS Treatment Naïve: HR = 0.47 (95% CI, 0.11-2.01) with $p = 0.2$, a non-significant difference between 14 MSS/MSI-low given neoadjuvant chemotherapy and surgical resection (blue) vs. 9 MSS/MSI-low treatment naïve (purple) with surgical resection only. MSI High Treatment Naïve vs. MSS Treatment Naïve: HR = 0.74 (95% CI, 0.17-3.25) with $p = 0.66$, a non-significant difference between 9 MSI-high treatment naïve (green) with surgical resection only vs. MSS/MSI-low treatment naïve (purple) with surgical resection only. **Figure 4E** OS with HR = 0.40 (0.13-1.26) and **Figure 4F** DFS with HR = 0.62 (0.24-1.82), both compare the survival of 28 neoadjuvant treated patients + surgical resection groups (14 MSI-high, 14 MSS/MSI-low) vs. the 18 patients in the treatment naïve with surgical resection only group (9 MSI-high, 9 MSS/MSI-low). **Figure 4E** shows a statistically significant difference with a $p < 0.05$, while **Figure 4F** is not statistically significant with $p > 0.05$.

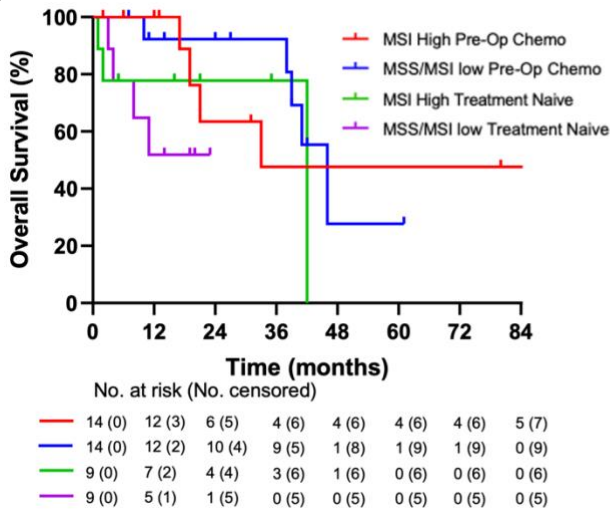
A



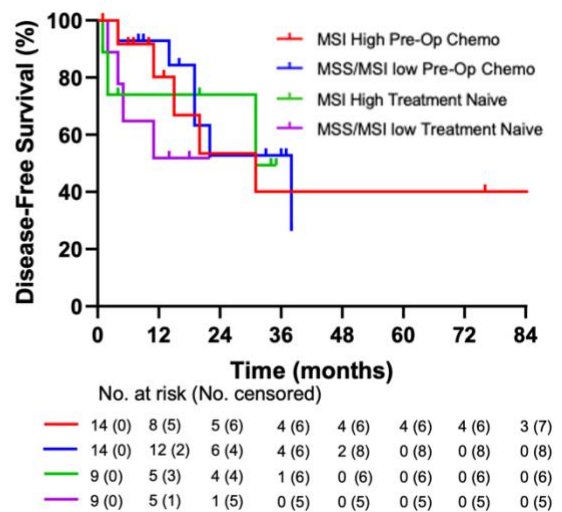
B



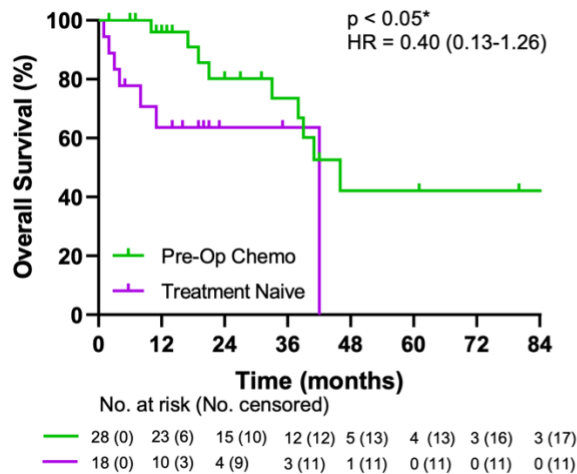
C



D



E



F

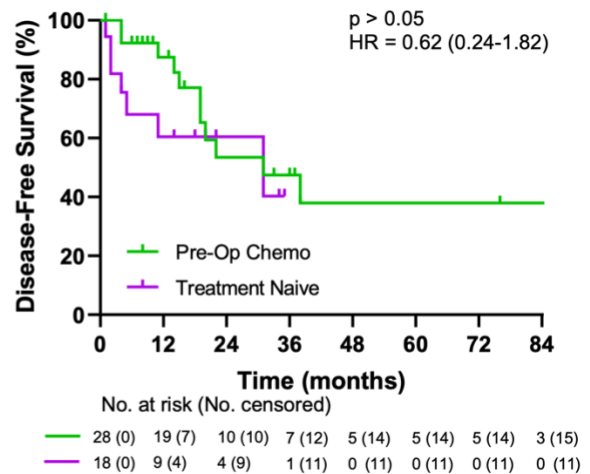


Figure 4. Kaplan-Meier curves of overall survival & disease-free survival according to MSI status (MSI-high vs. MSS) &/or treatment (surgery only vs. surgery & neoadjuvant chemotherapy)

(A)(B) Kaplan-Meier curves of overall survival & disease-free survival according to MSI status (MSI-high vs. MSS) MSI-high is in red with MSS/MSI low in blue. (C)(D) Kaplan-Meier curves of overall survival & disease-free survival according to MSI status (MSI-high vs. MSS) & treatment (surgery only vs. surgery & neoadjuvant chemotherapy). MSI-high Pre-Op Chemo is red, MSS/MSI-low Pre-Op Chemo is blue, MSI-high treatment naïve is green, and MSS/MSI-low treatment naïve is purple. (E)(F) Kaplan-Meier curves of overall survival & disease-free survival according to treatment (surgery only vs. surgery & neoadjuvant chemotherapy). Using GraphPad Prism software, the stratified cox proportional hazard regression model was used to estimate hazard ratios and corresponding confidence intervals. The log-rank test was used to determine the p-value significance. Time in months on the X-axis is compared to OS/DFS on the Y-axis. The number at risk is noted below the survival graph with censored patients mentioned at every 12-month timepoint.

3.2 Tumour histology & MSI status is recapitulated between primary tumour & PDOs/PDXOs

To confirm that PDOs/PDXOs recapitulate the tumour histology from the primary tumour to organoids, H&E structural images corresponding to 2 MSI-high patients (201435 & 0628) were taken (**Figure 5A**). Pathologist identified cancerous morphology was observed in the primary tumour and conferred to derived organoids. Of note, the tumour content of PDOs/PDXOs is estimated by a pathologist to their best ability in comparison to normal organoids. Once approved to have a sufficient % tumour content of greater than 50%, the extracted DNA of the PDO/PDXO can be sent for WES analysis.

Clinically at biopsy, the patient's tumour is taken for slide sectioning. H&E staining can then identify cancerous tumour structure, while deficiency in any of the MMR proteins of interest (MLH1, MSH2, MSH6, and/or PMS2) using a Ventana (Roche Diagnostics) immunostainer would classify the patient as MSI-high. As shown in **Figure 5B**, the above stains mentioned reveal the MSI status of an MSI-high (201465) and MSS (2016130) patient primary tumour. The MSI-high patient is classified as dMMR through demonstrating a deficiency in MSH2 and MSH6 (lack of brown pigment), while proficient in MLH1 and PMS2. In contrast, the MSS patient is classified as pMMR by showing proficiency in all 4 MMR proteins examined.

To justify that the organoid models retain their MSI status from primary tumour to organoid, MSI-high (0645) and MSS (1020) PDOs were stained (**Figure 5C**) in the same manner as clinically conducted in **Figure 5B**. The MSI-high organoids displayed deficiency in PMS2, the same protein that was lacking in the primary tumour for this patient, showing conferred MSI-high status between primary tumour and PDO. The MSS patient had pMMR status in all 4 primary tumour protein images and clearly retains this proficiency in the PDO MLH1, MSH2

and MSH6 stains. However, a follow-up PMS2 stain may be necessary for this patient to confirm that the MSS classification is recapitulated in organoids.

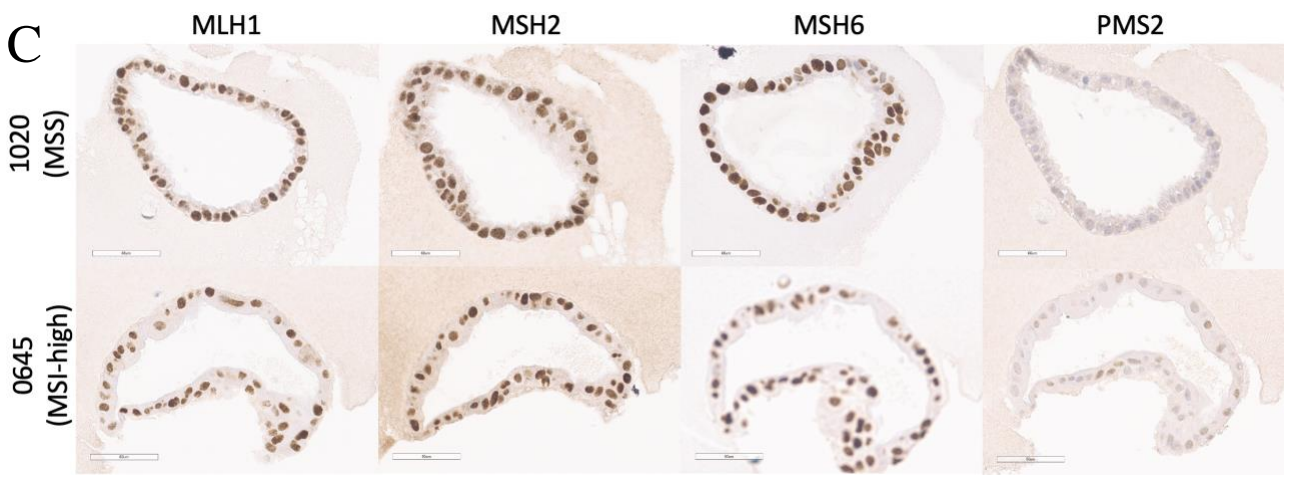
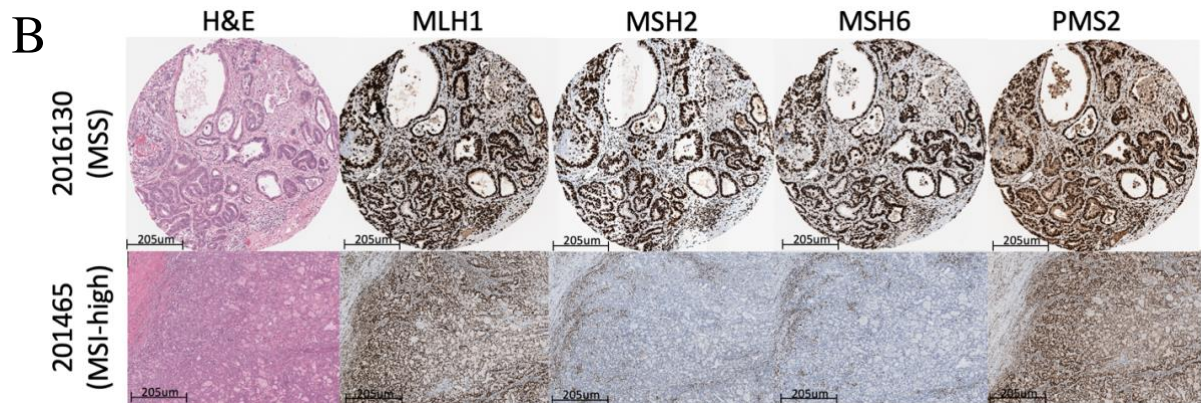
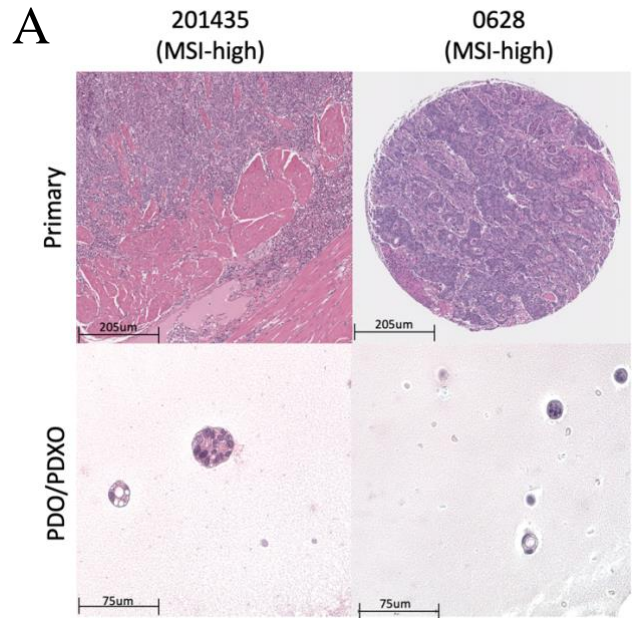


Figure 5. Primary tumour & PDO/PDXO H&E & mismatch repair protein staining images of MSI-high & MSS

H&E images of primary tumour (205µm) are compared to derived organoids (75µm) for 2 MSI-high cell lines 201435 (PDXO) and 0628 (PDO) (**A**). H&E and 4 MMR protein (MLH1, MSH2, MSH6, PMS2) primary tumour images (205µm) are compared between a MSI-high (201465) and MSS (2016130) patient (**B**). 4 MMR protein PDO images (60µm) are compared between a MSI-high (0645-PMS2 deficient) and MSS (1020) patient (**C**).

3.3 Clinical chemosensitivity correlates with patient-derived organoid/xenograft organoid chemosensitivity

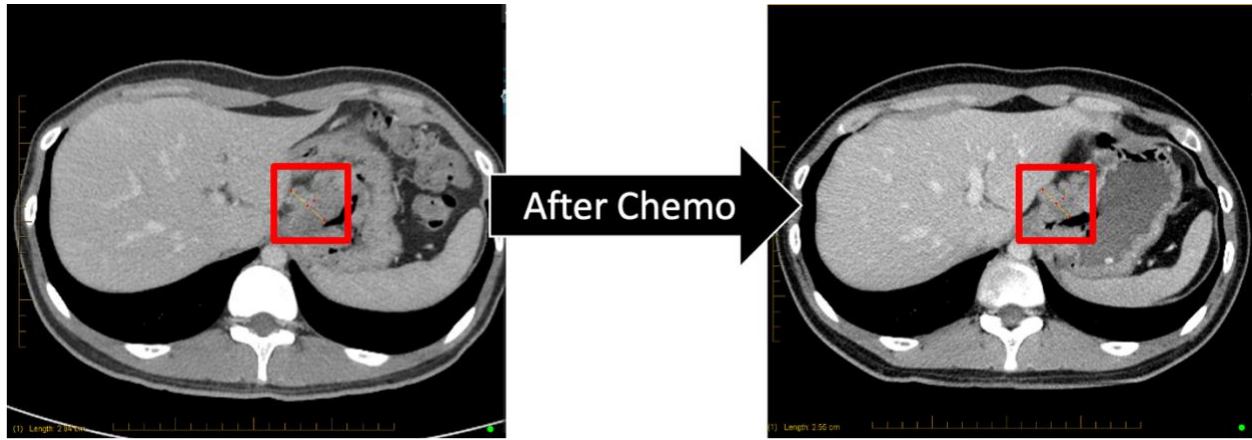
3.3.1 Most PDOs/PDXOs recapitulated the clinical response of respective patients'

To justify that PDO/PDXO models are a good representation of the primary tumours' response to chemotherapy clinically, PDO/PDXO models are treated with the same chemotherapy received by the patient while the responses *in vivo* vs. *in vitro* are compared. MSI-high patient ESO-21-1190 displayed a late clinical-stage T4N2 tumour (**Figure 6B**). The organoids were derived from the biopsy taken before the patient was clinically treated with DCF + PD-L1 target avelumab. CT scans revealed a 10.21% tumour change decrease from 2.84cm to 2.55cm was observed from pre-treatment to post-treatment, indicating SD (**Figure 6A**). This same patient's corresponding chemosensitivity curves (**Figure 6C**) at 10 different concentrations in triplicate from 3 biological replicates with R^2 of 0.97, displays a moderate AUC value of 0.25 that matches the clinical SD RECIST status observed in **Figure 6A**. After 72 hours of DCF treatment in organoids that are sensitive to chemotherapy, they will lose luminal structure, shrink and explode, as demonstrated in ESO-21-1190 brightfield 75um scale images (**Figure 6D**). Next, MSI-high patient GP 201435 showed a clinical stage of T3N1. The PDXO was attained from the surgical resection after the patient was clinically treated with DCF (**Figure 6F**). As a result, this patient may exhibit some acquired resistance since the organoids were already exposed to clinical chemotherapy. CT scans demonstrated a GEJ wall length decrease of 3.55cm to 1.98cm, indicative of a 43.43% tumour change and PR according to RECIST status (**Figure 6E**). This patient's chemosensitivity curves (**Figure 6G**) at 10 different concentrations in triplicate from 4

biological replicates with R^2 of 0.96, show a low AUC value of 0.11 that matches the PR observed clinically in **Figure 6E**.

The correlations between clinical RECIST response and PDO/PDXO chemosensitivity response for 9 patients are summarized in **Table 2**. Data is available for 7 MSI-high and 2 MSS patients, all falling into either SD or PR classifications. Accordingly, 7/9 (78%) of PDOs/PDXOs recapitulated the clinical response of patients. Since most organoids were derived from surgical resections, patients were clinically treated with chemotherapy before organoid derivation in 7/9 (78%) of these patients, thus an acquired resistance could be present.

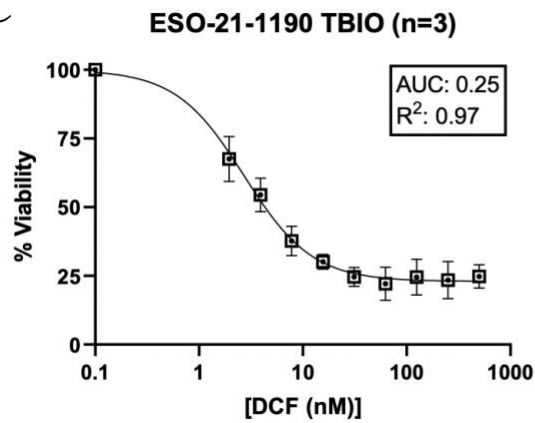
A



B

MMR Status	Age	Sex	Grade	Path Stage	Clinical Stage	Location	Treatment	% Tumour Change	RECIST Status
MSI-high	18	M	II	T4bN1	T4N2	GEJ	DCF + Avelumab	10.21% decrease	Stable disease

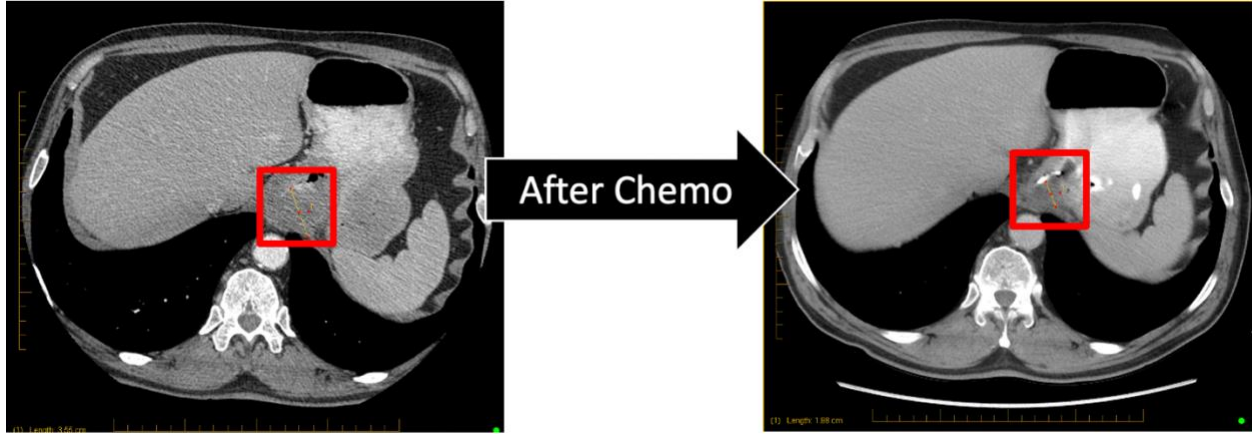
C



D



E



F

MMR Status	Age	Sex	Grade	Path Stage	Clinical Stage	Location	Treatment	% Tumour Change	RECIST Status
MSI-high	71	M	III	T4aN2	T3N1	GEJ	DCF	43.43% decrease	Partial response

G

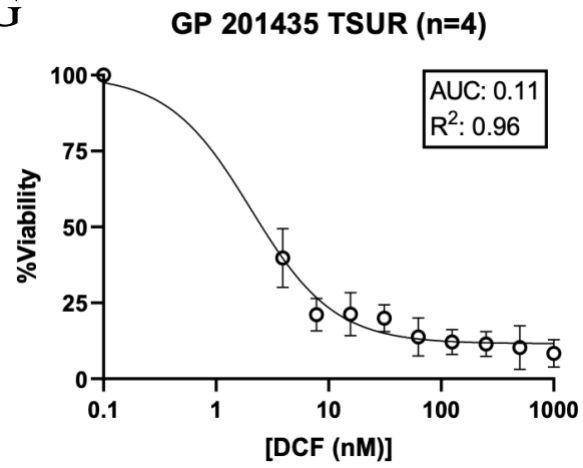


Figure 6. RECIST % tumour change CT images & corresponding PDO/PDXO chemosensitivity curves

Cross-sectional CT images of pre-treatment around biopsy and post-treatment around surgical resection are taken of patients' GEJs **(A)(E)**. Red boxes indicate the relevant area, while the yellow line with red dots shows the length of GEJ wall thickening. Images were accessed using OACIS software. In accordance with CT images, patients' clinicopathologic characteristics are described, including RECIST status **(B)(F)**. Chemosensitivity curves *in vitro* to the same treatment given clinically **(C)(G)**. % Viability is on the Y-axis with DCF concentration on the X-axis was created with GraphPad Prism. PDO brightfield images at *in vitro* pre-treatment to post-treatment after 72 hours using an EVOS microscope **(D)**.

Table 2. PDOs/PDXOs recapitulate the clinical response of patients

Patient-specific clinical RECIST response is compared to their derived *in vitro* organoid chemotherapy responses. Potential acquired resistance is also recorded depending on if the patients' organoids were established before/after the patient was clinically treated.

ID	PDO/PDXO AUC	MSI Status	RECIST	Organoids match clinical chemosensitivity	Potential acquired resistance
1190	0.25	MSI-high	Stable disease	Yes	No
201435	0.11	MSI-high	Partial response	Yes	Yes
0645	0.4	MSI-high	Partial response	No	Yes
0751	0.31	MSI-high	Stable disease	Yes	Yes
201452	0.34	MSI-high	Partial response	No	Yes
201465	0.43	MSI-high	Stable disease	Yes	Yes
1199	0.37	MSI-high	Stable disease	Yes	No
1000	0.56	MSS	Stable disease	Yes	Yes
1075	0.44	MSS	Stable disease	Yes	Yes

3.3.2 No significant neoadjuvant chemotherapy response difference between MSI-high & MSS patients clinically, & MSI-high & MSS PDOs/PDXOs *in vitro*.

As observed in **Table 1** and **Figure 7A**, all patients examined fell into the RECIST categories of either SD, between a 20% increase to a 30% decrease, or PR of more than a 30% decrease. No patients fell into the classifications of DP of an over 20% increase, or CR of entire tumour disappearance. The stratification between MSI-high and MSS groups appears to not correlate with RECIST status. This is confirmed in **Figure 7B**, as no significant chemotherapy response difference was observed through unpaired t-test analysis between MSI-high and MSS groups when comparing % tumour size changes to clinically administered neoadjuvant chemotherapy (DCF/DOF).

To determine if differences in chemosensitivity existed among MSI-high and MSS organoids, PDOs/PDXOs were treated with the same chemotherapy received by their respective patient and had their responses grouped by MSI status to compare. Through relatively comparing the two organoid groups in (**Figure 8A**), MSI-high (red) has a slightly lower AUC value of 0.36 and IC50 value of 2.40 compared to MSS (blue) with a slightly higher AUC of 0.46 and IC50 of 3.00. The AUC value best approximates the IC50 value coupled with where the percent viability starts to plateau, giving the best estimate of response. There appears to be a small visual separation between MSI-high and MSS responses, indicating from the graph that MSI-high might respond a bit better to chemotherapy in organoids than MSS. When the AUC values are compared between the two MSI status groups in (**Figure 8B**), MSS organoids (AUC=0.46) seemed more resistant to chemotherapy and dispersed than MSI-high organoids (AUC=0.36) which appeared more clustered and sensitive. However, after unpaired t-test analysis, no

significant chemosensitivity difference was observed between MSI-high and MSS PDOs/PDXOs.

Potentially, acquired resistance could be a factor in altering PDO/PDXO chemotherapy response if the primary tumour that the organoid is derived from was already exposed to chemotherapy clinically before *in vitro* organoid development. To investigate if this played a significant role, the data from **Table 2** is expanded upon with different patients in **Figure 8C**. MSI-high and MSS patients were subdivided into if they were treated with chemotherapy clinically or not. Using an unpaired t-test, **Figure 8D** analysis displayed no significant differences in AUC chemosensitivity between MSI-high organoids developed from clinically treated vs. clinically untreated, and MSS organoids derived from clinically treated vs. clinically untreated patients.

The 3D organoid cell death *in vitro* for MSI-high and MSS samples is shown with brightfield images at 650um and 150um (**Figure 8E**). MSI-high patient GAS-19-0645 and MSS patient ESO-20-1075 are both demonstrated to visually respond to chemotherapy DCF similarly. Control DMSO organoids have large spherical domes with an intact lumen, compared to after 72 hours of DCF treatment in which the organoids shrivel in size, lose spherical shape, and cells from the lumen explode outwards.

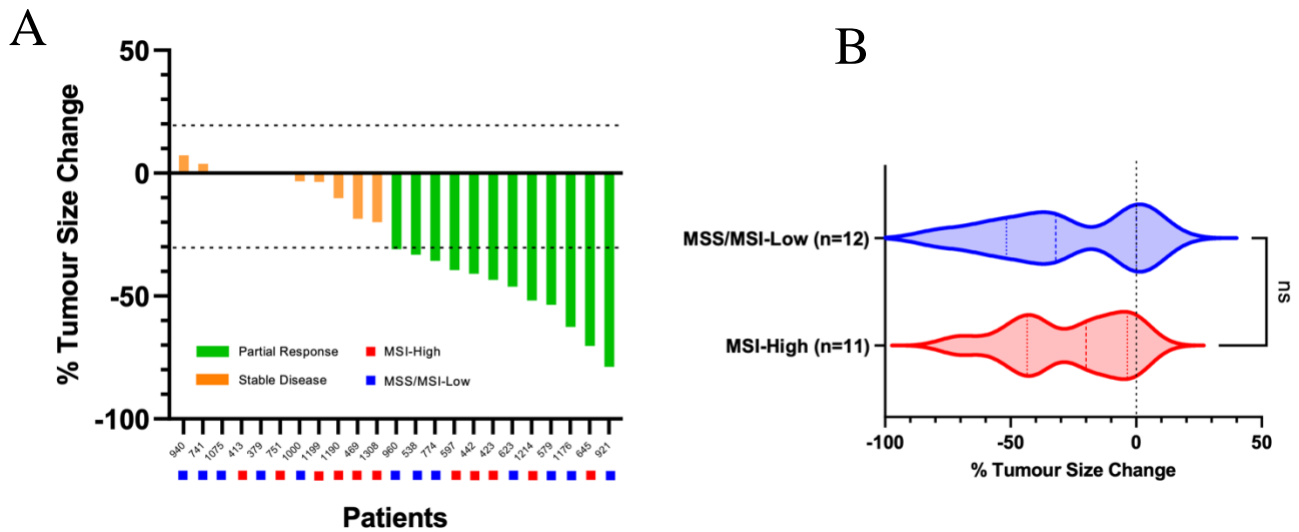


Figure 7. Clinical neoadjuvant chemosensitivity waterfall plot of RECIST % tumour change according to MSI status (MSI-high vs. MSS)

% tumour size change is on the Y-axis with the patients' biobank number on the X-axis. All patients fall into either PR (green) and SD (orange) RECIST classifications (A). MSI-high (red) and MSS (blue) as boxes indicated for 11 MSI-high and 12 MSS patients. (B) Box and violin plot of the % tumour change data from (A) describes the % tumour change on the X-axis for MSI-high (red) vs. MSS (blue) groups on the Y-axis. Graphs are created using GraphPad Prism.

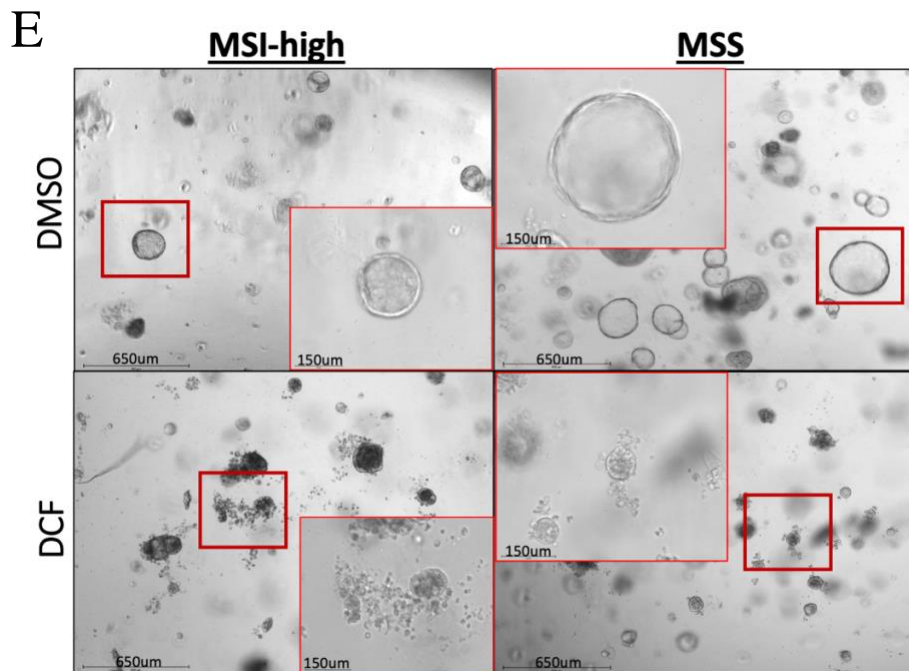
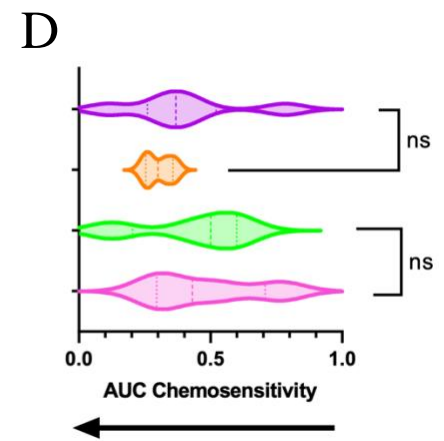
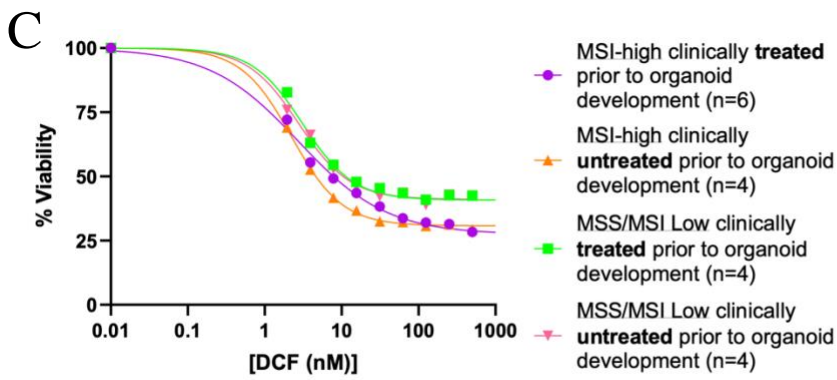
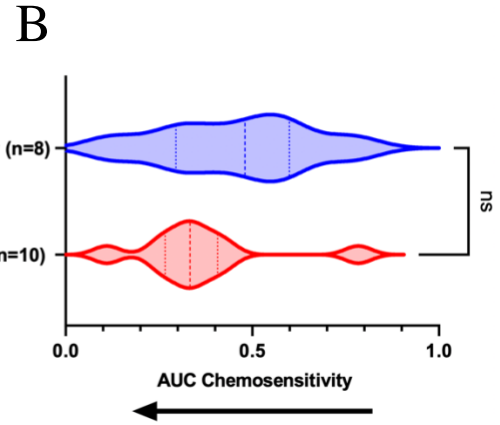
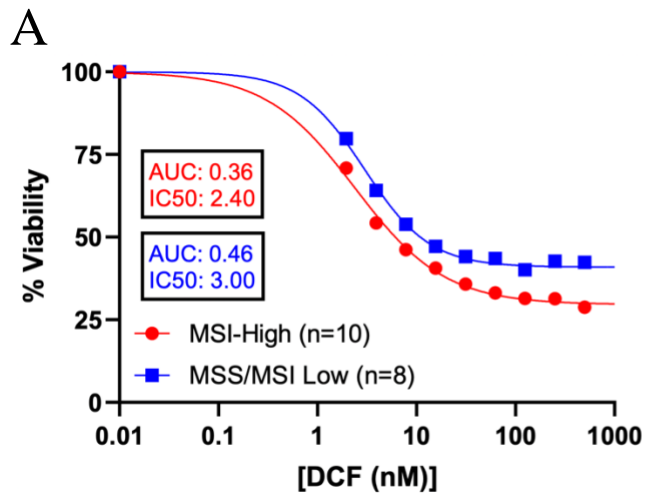


Figure 8. DCF-treated PDO/PDXO response curves according to MSI status (MSI-high vs. MSS)

10 MSI-high (red) and 8 MSS (blue) PDOs/PDXOs chemosensitivity curves are merged together to show relative DCF treatment response **(A)**. The average of 10 different concentrations in triplicate with 3 biological replicates per cell line is shown for the 18 lines, separated by MSI status. % viability is on the Y-axis with DCF concentration on the X-axis. **(B)** shows the corresponding box and violin plot using the AUC data of the 18 different organoid cell lines from **(A)**. MSI-high is separated from MSS on the Y-axis, with AUC-indicated chemosensitivity increasing from right to left on the X-axis. In **(C)** and **(D)**, organoid lines from **(A)** were separated further into 6 MSI-high clinically treated prior to organoid development (purple), 4 MSI-high clinically untreated prior to organoid development (orange), 4 MSS clinically treated prior to organoid development (green), and 4 MSS clinically untreated prior to organoid development (pink). % viability is on the Y-axis and DCF concentration is on the X-axis for **(C)**. Using the same colour legend as **(C)** for the Y-axis of **(D)**, AUC chemosensitivity increases from right to left. Graphs were created with GraphPad Prism. Brightfield images of MSI-high and MSS PDOs are shown in cytotoxic DCF and control DMSO conditions **(E)**.

3.4 Genomic sequencing & alternative targeted therapies exhibit promising outcomes

MSI-high sequencing can be used to confirm their MSI status through an elevated TMB. As observed in **Figure 9**, the MSI-high samples all show a greatly increased TMB score that differentiates them from MSS. Statistically speaking, since the most mutated genes in at least 3 of 8 samples are shown and MSI-high display much more mutations, there is a greater chance that the genes selected in this way are mutated in MSI-high. Actually, most genes selected in this manner are mutated in 3 of the MSI-high and 0 MSS or 2:1, and sometimes 1:2. This ratio is never 0:3 though, so no gene is mutated in at least 3 MSS and not mutated in any MSI-high. The specific mutations observed are mostly missense, frameshift and nonsense. Through examining the 4 MSI-high patients' mutations, *ARID1A* is mutated in $\frac{3}{4}$ primary tumours along with many other potential targets.

In an attempt to compare standard of care chemotherapy treatments to alternative targets, high throughput drug screening was conducted on 4 different organoid lines, 2 MSI-high and 2 MSS (**Table 3**). The chemotherapies were selected based on the combinations used worldwide for GEAs, while the alternative targets were selected based on internal lab data from PDX WES in combination with promising therapies demonstrated in the literature. 2/3 of the standard of care regimens DCF/DOF have docetaxel with notably low IC50s, while FOLFIRI only has fluorouracil and irinotecan. Notably, docetaxel itself has a particularly low IC50 value, indicating increased potency in comparison to the other standard of care singly of cisplatin, fluorouracil, oxaliplatin, and irinotecan. The alternative targets of luminespib (HSP90 inhibitor), trametinib (MEK inhibitor), and gefitinib (EGFR inhibitor) have comparably low IC50s indicating greater response to treatment and cancer cell death. In contrast ulixertinib (ERK1/2 inhibitor), sorafenib (VEGFR), gedatolisib (PIK3CA/mTOR), and UNC 1999 (EZH2 inhibitor)

displayed relatively higher IC50s indicating reduced treatment response and less cancer cell death. Of interest, the combination of luminespib and UNC 1999 had an effectively low IC50, however, this is the same value as luminespib alone, indicating that UNC 1999 had no effect in this 1:1 ratio drug combination.

The drug compounds with low IC50 scores from **Table 3** were selected and examined in further detail in **Figure 10 A-F** (R^2 good with over 0.830 in all). The chemotherapy regimen treatments of DCF (**Figure 10A**) and DOF/FLOT (**Figure 10B**) display MSI-high (AUC=0.26 and 0.27 respectively) to be slightly more resistant to chemotherapy than MSS (AUC=0.15 in both). Meanwhile, chemotherapy FOLFIRI, without docetaxel, shows less sensitivity and separation between MSI-high (AUC=0.38) and MSS (AUC=0.35) when compared to DCF and DOF/FLOT. HSP90 inhibitor luminespib showed a very sensitive response in MSI-high (AUC=0.029) and MSS (AUC=0.0085). MEK inhibitor trametinib revealed a slightly better response in MSI-high (AUC=0.06) than MSS (AUC=0.16). EGFR inhibitor gefitinib demonstrated a comparably moderate response between MSI-high (AUC=0.18) and MSS (AUC=0.15).

Next, the SL relationship was tested in MSI-high and control MSS PDOs (**Figure 10 G-H**). Drug NSC 19630 controls the *WRN* helicase biological activity and is primarily used for cell signaling applications. It selectively inhibits *WRN* helicase activity over its ATPase and exonuclease activities without affecting the other RecQ human helicases. The MSI-high PDOs from 1190-TBIO are developed from a clinically untreated patient with no concern of acquired chemoresistance. DCF AUC is 0.66, *WRN* inhibitor AUC is 0.46 and the combined synergistic AUC of DCF + *WRN* inhibitor is considerably more sensitive to treatment at 0.01. The MSS PDOs from 1000-TSUR are developed from a clinically treated FLOT patient with the

possibility of acquired chemoresistance. The AUC of DCF and *WRN* inhibitor alone are comparable at 0.30 and 0.32 respectively, however, their synergistic AUC is much more effective at 0.01. These patients cannot be compared with each other because they are not matched and have different survival outcomes. Nevertheless, there appears to be a synergistic effect of DCF + NSC 19630 in both MSI-high and MSS PDOs.

Figure 9. TMB & genomic alterations of MSI-high & MSS primary tumour oncoplot

A preliminary whole exome sequencing oncoplot of 4 MSI-high (red) and 4 MSS (blue) primary tumours are described, showing the most mutated genes in at least 3 of the 8 samples. The type of mutation is indicated on the Y-axis with the sample number on the X-axis. Specific mutations are separated into frame-shift deletion (blue), missense (green), frame-shift insertion (purple), nonsense (red), in-frame deletion (yellow), translation start site (orange), and multi-hit (black). TMB is indicated on the top. The software used to generate the plot is described in the methods section.

Table 3. IC50 organoid responses for 16 drug compounds

An IC50 [μM] table of four different organoid lines, 2 MSI-high and 2 MSS. 10 different concentrations are tested in quadruplicate using a high throughput robotic liquid handler. Drug compounds are grouped into standard of care regimen, standard of care singly, and alternative treatments.

	Drug Name	IC50 all 4 [μM]	Target
Standard of care <u>regimen</u>	DCF	0.00974	Chemo
	DOF	0.0119	Chemo
	FOLFIRI	0.619	Chemo
Standard of care <u>singly</u>	Docetaxel	0.000507	Chemo
	Cisplatin	13.057	Chemo
	5-FU	3.815	Chemo
	Oxaliplatin	7.792	Chemo
	Irinotecan	1.311	Chemo
<u>Alternative treatments</u>	Luminespib	0.0129	HSP90
	Luminespib + UNC 1999	0.0128	HSP90 + EZH2
	Trametinib	0.00394	MEK
	Gefitinib	0.174	EGFR
	Ulixertinib	0.776	ERK1/2
	Sorafenib	12.3	VEGFR
	Gedatolosib	5.547	PIK3CA/mTOR
UNC 1999	19.375	EZH2	

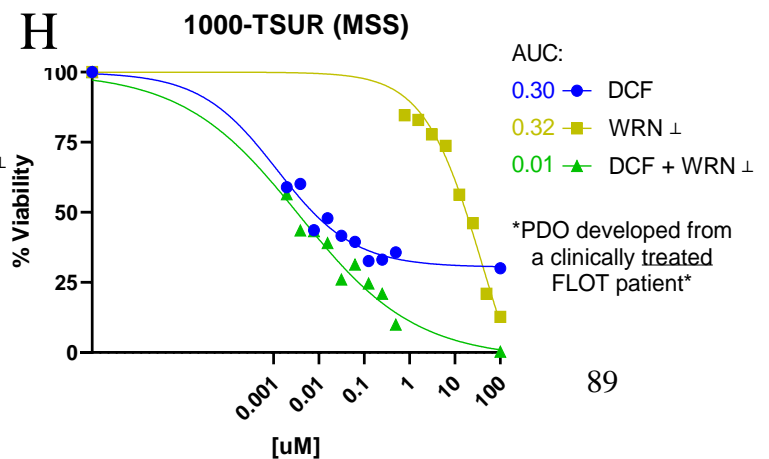
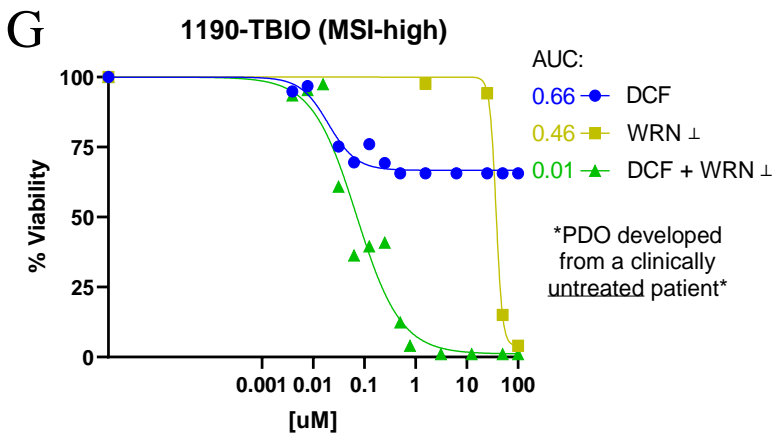
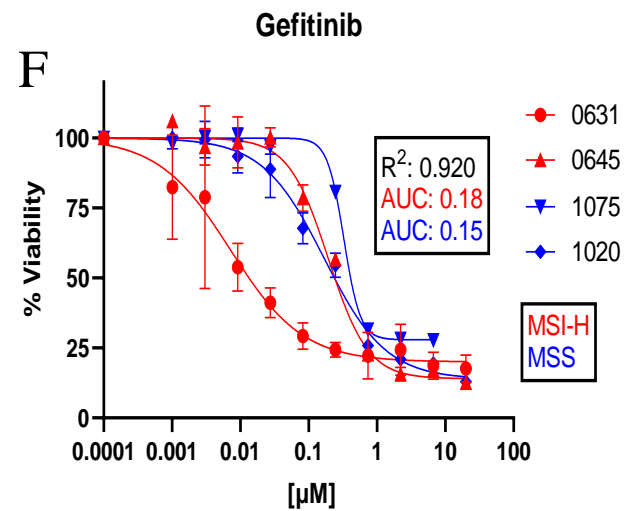
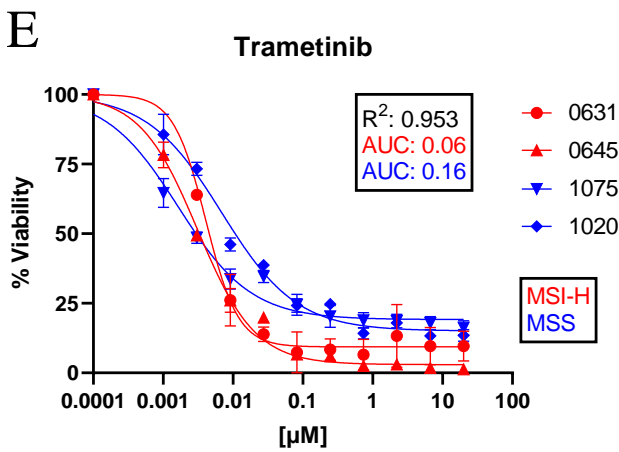
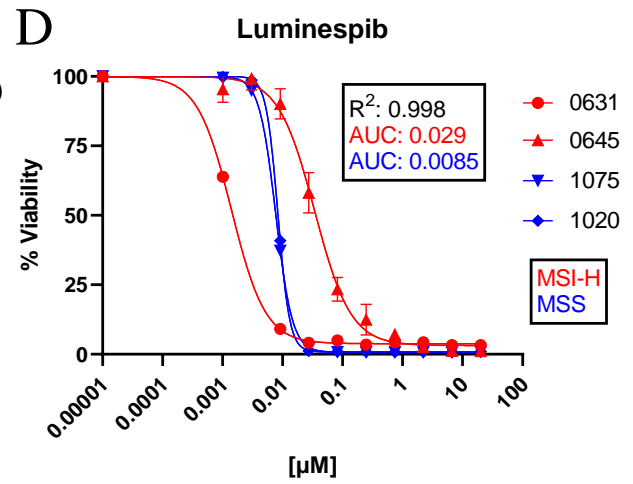
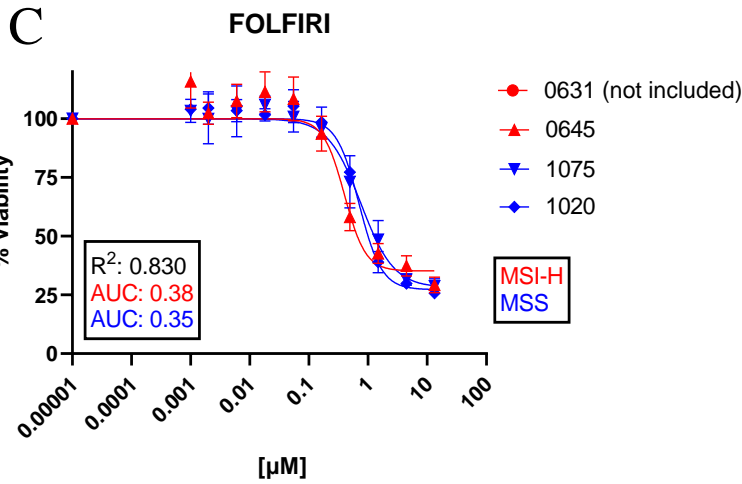
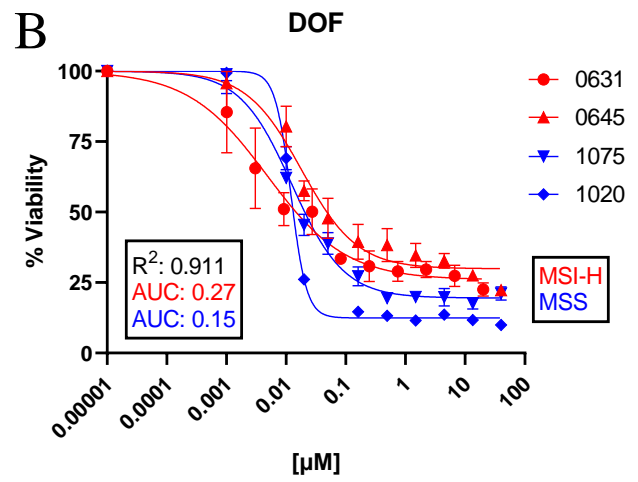
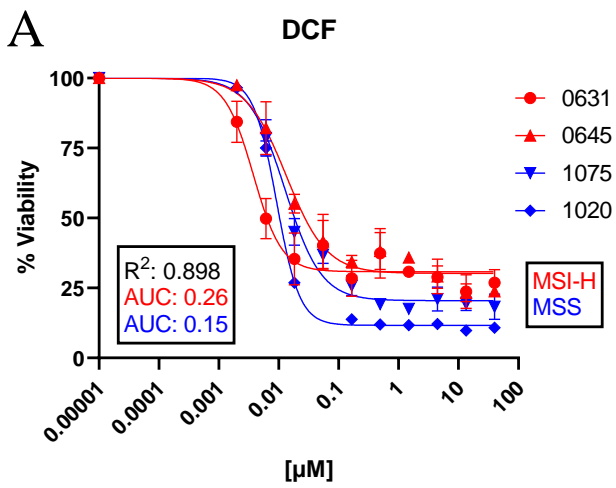


Figure 10. PDO drug compound response curves to chemotherapy regimens & alternative targets

Therapy sensitivity curves are generated for drug compounds tested at 10 different concentrations in 3-dimensional PDO cultures. % viability is on the Y-axis with drug concentration [μM] on the X-axis. **A-F** is data from 4 PDOs with each line on the curve representing a patient, 2 MSI-high (red) and 2 MSS (blue). **A-C** are standard of care chemotherapy regimens, while **D-F** are promising alternative targets. Data from **G** and **H** are from 1 MSI-high and 1 MSS cell line respectively. DCF (blue), *WRN* inhibitor (yellow) and synergistic conditions of DCF + *WRN* inhibitor (green) are tested.

CHAPTER 4: DISCUSSION

GEAs have limited biomarkers that can clinically guide treatment besides HER2, PD-L1, and MSI-high status in 6-30%, 16% and 12% of patients respectively ^{37,84,199,200}. Viable targeted therapies include trastuzumab for HER2 ³⁷ and immunotherapy PD-1 targets for MSI-high such as pembrolizumab ¹⁹⁴, nivolumab ¹⁸⁹, and dostarlimab ¹⁹⁷. Neoadjuvant chemotherapy FLOT is now often given to MSS GEA patients that are HER2 negative ^{26,27}, however, while the increase in median OS time is significant ²⁶, there is still much room for improvement as 40% of patients are innately resistant, with recurrence displayed in 50% of initial responders ³⁵. In an effort to improve OS for GEA patients, it is critical to focus on targeted therapies, maximizing the value of the available clinical biomarkers of HER2 and MSI-high.

This study importantly examines MSI-high GEA patients that are thought to be chemoresistant ¹²⁶, and attempts to first determine the degree that standard chemotherapy FLOT/DCF works as a viable treatment option in comparison to omitting it and recommending surgical resection only. Nevertheless, neoadjuvant FLOT/DCF in GEA MSI-high patients displayed comparable OS and DFS outcomes to MSS, according to RECIST criteria analyzed CT images clinically (**Figure 6A, 6E**) and in PDO/PDXOs chemosensitivity curves (**Figure 6C, 6G**). The MSI-high group compared to MSS/MSI-low showed non-significant differences in neoadjuvant chemotherapy-induced % tumour size change and DCF PDO/PDXO AUC chemosensitivity. These findings would allude to the recommendation of clinically treating MSI-high patients in the same manner as MSS with FLOT, in lack of better alternatives, since their responses are approximately the same. While it still requires further investigation, the thought of omitting neoadjuvant FLOT for MSI-high patients for surgical resection only would not be beneficial, as treating GEAs in general with neoadjuvant chemotherapy demonstrates expected

statistically significant OS benefits. This is demonstrated in Kaplan Meier curves (**Figure 4C, 4E**) in which MSS/MSI low Pre-Op Chemo vs. MSS Treatment Naïve and Pre-op chemo vs. Treatment Naïve groups showed statistical significance as chemotherapy plus surgery overall showed a benefit to survival as opposed to surgery alone.

The next stage of improving MSI-high outcomes is to identify treatment plans that establish survival benefits which overcast FLOT followed by surgical resection. Fortunately, there are multiple promising directions of future investigation for MSI-high GEAs such as PD-1 inhibitors, the discovery of novel genomically guided targets, and *WRN* helicase inhibitors. Immunotherapy PD-1 inhibitors are FDA approved for use in GEAs⁴³, and largescale clinical studies are required to determine their effectiveness. The recent emergence of immunotherapy translating to positive survival outcomes for MSI-high patients can be observed with cancer located in other anatomical locations. In particular, all 12 rectal cancer MSI-high patients in a study by Cercek *et al.* (2022) displayed complete responses with PD-1 inhibitor dostarlimab. The degree to which this rectal cancer treatment success applies to GEAs is unknown, but novel clinical analysis holds great potential. Through WES, one particular gene of interest is *ARIDIA*, which was mutated in 75% of MSI-high (**Figure 9**). This correlated with a study that looked at 14 MSI-high patients, showing *ARIDIA* was mutated in 71% of tumours¹³³. A potential therapy route for MSI-high GEAs with *ARIDIA* mutations is kinase inhibitor dasatinib, which demonstrated *ARIDIA*-related increased treatment sensitivity in pancreatic and ovarian cancer⁶⁵. Interestingly, the best treatment plan could end up being a combination of different options. Coupling chemotherapy FLOT with targeted inhibitors such as SL *WRN* helicase NSC 19630 or PD-1 dostarlimab followed by surgical resection could establish a beneficial synergistic relationship^{136,184,185}. Moreover, this synergistic effect of *WRN* helicase inhibition was observed

in both MSI-high and MSS patients (**Figure 10E-H**), in which NSC 19630 alone and DCF singly had minimal effect, but the combined effect was very compelling. MSI-high AUC improved from 0.66 in DCF singly to 0.01 in DCF + NSC 19630 while MSS AUC changed from 0.3 in DCF singly to 0.01 in DCF + NSC 19630. Inhibiting *WRN* helicase may also enhance the immunotherapy effect due to an elevated TMB and modified neoantigen landscape, resulting in a viable co-acting treatment concept that requires further study.

This project benefits from a well-matched cohort that increases the validity of the clinical and laboratory analysis, since studying MSI-high is often restricted by its rare occurrence and small sample size relative to MSS, with the strength of conclusions correlated to MSI-high group sample size¹³⁴. This project is fortunate to reap the benefits of having a large PDO/PDXO biobank already established. MSI-high patients were selected from a large >350-patient biobank in addition to being recruited on a rolling basis. GEA MSI-high/dMMR is a rare subtype with rates observed to be 12% internally and by Corso *et al.* (2019). The ability to have 23 MSI-high patients in the cohort with 10 MSI-high as viable PDOs/PDXOs for sequencing and chemosensitivity curves is uniquely valuable. Even though this is a relatively small sample size compared to survival studies that merge trials to get about 100 MSI-high patients, many were given non-FLOT/DCF chemotherapies and have not yet tested immunotherapy at a large scale in GEAs^{84,116,126,167}. A big advantage of having 10 MSI-high samples as PDO/PDXOs is that these samples can be prospectively analyzed in a high-throughput setting to apply genomically guided targets, and perhaps later in a low-throughput, high-fidelity on-a-chip setting that incorporates TME and fluid flow components to test successes from high throughput testing.

Furthermore, the WES from 4 primary tumour MSI-high compared to 4 MSS (**Figure 9**) successfully showed MSI-high have an increased TMB that can identify them. These genomic

findings are currently limited by a small sample size, however, WES for all 46 patients of the cohort shown in **Table 1** is in process. In addition, DNA extracted from 22 PDOs/PDXOs (10 MSI-high, 12 MSS) (identified in **Supplementary Table 1**) is completed and awaiting sequencing, which would help justify that MSI status is recapitulated between primary tumour to derived organoids, and give a much larger sample size to help identify alternative genomically guided targets to apply in subsequent high-throughput drug screens. After analyzing this data it could help explain the mechanism at play for intrinsic MSI-high chemoresistance and the explained potential sensitivity for immunotherapies and synthetic lethal *WRN* helicase interaction.

The MSI-high status has been proven to be conferred from the primary tumour to PDOs/PDXOs, from looking at the four clinically used mismatch repair proteins of interest in organoid slide staining samples (**Figure 5C**). 24 FFPE blocks (11 MSI-high, 13 MSS) are available for sectioning of unstained PDO/PDXO slides, and are in the process of being stained for MMR protein images. Resultantly, this would give a larger sample size to justify organoid MMR status recapitulation. These clinically used MMR stainings can be coupled with genomic data comparing the same patient's primary tumour and derived organoid TMBs for MSI status classifications.

Moreover, the primary tumours and PDOs/PDXOs have also been shown to be morphologically similar by analyzing corresponding H&E stains that are available for the 24 patients with FFPE blocks. Organoid tumour content was a recurring issue with no clear solution since the tumour organoid clusters themselves are heterogeneous populations within the same tumour. Sometimes getting multiple sections of the same block at different depths is required to get a higher % tumour content. The best possible evaluation was to have a trained pathologist

look at the PDO/PDXO H&E organoid slides and evaluate tumour content as an estimate. This can potentially be overcome by first staining slides for common tumour markers before pathologist approval to help tumour classification. Irregular nuclei and abnormal morphology of embedded organoids can be amplified with DAPI staining for the nucleus ²⁰¹. Furthermore, CK7, CK20, and CDX-2 staining in PDO/PDXO GEAs could be used as tumour markers, but there tends to be variability in their expression for GEAs, which would not typically give a distinct answer to the tumour being present for a given sample. However combining, H&E, DAPI, CK7, CK20, and CDX-2 staining for the same PDO/PDXO GEA sample could give the pathologist a better idea when indicating the % tumour content in comparison to H&E alone.

The success of PD-1 targeted immunotherapy in MSI-high cancer ¹⁹⁷ sparks the urgency to establish on-a-chip models that can co-culture tumour cells with TME components and fluid flow. Moreover, there is an urgency to apply this within a short clinical window time frame that is personalized to suit individual patient needs. Accordingly, an example clinical treatment plan may appear as the tumour being detected through endoscopic biopsy, with dMMR status determined using the four MMR proteins of interest to indicate MSI-high status. Afterwards, FLOT chemotherapy cycles can begin, and GEA PDOs can be co-cultured on-a-chip along with immune cells. Once cells are mature they can be treated with a PD-1 inhibitor such as dostarlimab in combination with FLOT, then corresponding drug sensitivity curves can reveal predicted treatment successes within a clinically relevant timeframe. To feasibly recommend neoadjuvant treatment in clinical practice, this process would require shortening to less than a month, however, at the very least it could guide adjuvant therapy, especially in cases that display neoadjuvant chemoresistance. Instead of giving the same neoadjuvant therapy that did not work

as an adjuvant, care can be guided better. For example, at a physician's discretion, the PD-1 inhibitor could be given in addition to chemotherapy based on patient-tailored *in vitro* results.

Some limitations to consider are the ethnicity of patients was not included in clinical data records, so it was not an aspect that matching was based on. MSI-high patients were added to the cohort on a rolling basis, as a result, the OS and DFS data did not follow all patients and their matched cohort pairs for equal amounts of time. It would require a follow-up analysis five years from now to evaluate all currently enrolled patient samples from a standardized time point. By matching the MSI-high patients, which mostly displayed moderate-poor tumour grade, matched MSS were accordingly selected to have moderate-poor tumour grade. Of note, randomly selected MSS patients would not necessarily have comparably progressed cancer as observed in the matched patient group selected. Consequently, the lack of statistically significant separation between MSI-high vs. MSS/MSI-low survival curves (**Figure 4A-B**) is expected and helps justify that the cohort is well-matched.

For chemosensitivity curves displayed in **Figures 6C, 6G, 8A-D, and 10A-H**, it is worth considering that AUC is a relative value which approximates IC₅₀ and % viability plateau. AUC is similarly used to analyze GC and interpret PDO responses in relevant papers^{56,202}.

As mentioned in **Table 2**, there is a potential acquired resistance that could influence the strength of the chemosensitivity curve comparisons as the time point that the primary tumour was collected and resulting organoids derived from could have been before the neoadjuvant was given to the patient clinically or after. For example, if chemotherapy was given before the primary tumour was collected for corresponding PDO, the potential required resistance is noted as yes (as shown in 7/9 patients examined).

Furthermore, there are differences in the manner that FLOT is administered clinically compared to organoid models. In the clinic, patients are given FLOT in 2-week cycles of 50 mg/m² docetaxel, 85 mg/m² oxaliplatin, leucovorin 200 mg/m², and 2600 mg/m² 5-FU as a 24-hour infusion ²⁶. This infusion step for 5-FU was not replicated in organoids, in which oxaliplatin was swapped for cisplatin and given at a DCF ratio of 1:1:10. Drugs were dispensed at time 0 in appropriate ratios and followed up for viability analysis 72 hours later. The drug screening and viability tests conducted could have been limited by human error at times, and future experiments might benefit from higher throughput robotic liquid handling that is now available in the lab for precision liquid dispensing.

Another aspect to consider is that the PMS2 staining for MSS samples (**Figure 5C**), seems to require further optimization. It is not visually obvious, typically indicated by the presence of brown pigment, that the PMS2 function is retained and proficient in MSS PDOs. It is possible that PMS2 expression is reduced in organoid culture, which can be explored further with RNA in situ hybridization to demonstrate loss/low levels of PMS2.

As future steps to improve this study, applying proteomic data to a wide range of cancer types and molecular backgrounds would have the utility to enhance the prediction ability to identify exploitable tumour weaknesses and understand the therapeutic resistance mechanism ^{203,204}. Moreover, by applying the upcoming primary tumour WES results on all 46 patients previously mentioned, shown so far in **Figure 9**, the throughput can be increased beyond the 16 drug compounds (**Table 3**) to be applied with MSI-high PDO drug screens *in vitro*. Lastly, to determine clinical therapy effectiveness, the RECIST criteria for tumour volume reduction could be coupled with observing a change in tumour markers such as CEA, CA 123 and CA 72.4 to get a bigger picture (Yin *et al.* 2020). Overall, much of the trial-and-error aspects of treating novel

therapies can be determined within PDO cultures, so personalized treatments for patients with MSI-high GEAs can be translated from bench to bedside in a clinically relevant manner that best improves patient survival outcomes.

REFERENCES

1. Sung, H. *et al.* Global Cancer Statistics 2020: GLOBOCAN Estimates of Incidence and Mortality Worldwide for 36 Cancers in 185 Countries. *CA Cancer J Clin* **71**, 209–249 (2021).
2. Brenner, D. R. *et al.* Projected estimates of cancer in Canada in 2022. *CMAJ* **194**, E601–E607 (2022).
3. Domper Arnal, M. J., Ferrández Arenas, Á. & Lanás Arbeloa, Á. Esophageal cancer: Risk factors, screening and endoscopic treatment in Western and Eastern countries. *World J Gastroenterol* **21**, 7933–7943 (2015).
4. Wong, H. H. & Chu, P. Immunohistochemical features of the gastrointestinal tract tumors. *J Gastrointest Oncol* **3**, 262–284 (2012).
5. Lauren, P. THE TWO HISTOLOGICAL MAIN TYPES OF GASTRIC CARCINOMA: DIFFUSE AND SO-CALLED INTESTINAL-TYPE CARCINOMA. AN ATTEMPT AT A HISTO-CLINICAL CLASSIFICATION. *Acta Pathol Microbiol Scand* **64**, 31–49 (1965).
6. Correa, P., Haenszel, W., Cuello, C., Tannenbaum, S. & Archer, M. A model for gastric cancer epidemiology. *Lancet (London, England)* **2**, 58–60 (1975).
7. Hayakawa, Y., Sethi, N., Sepulveda, A. R., Bass, A. J. & Wang, T. C. Oesophageal adenocarcinoma and gastric cancer: Should we mind the gap? *Nature Reviews Cancer* **16**, 305–318 (2016).
8. Uemura, N. *et al.* Helicobacter pylori infection and the development of gastric cancer. *N Engl J Med* **345**, 784–789 (2001).
9. Parsonnet, J. *et al.* Helicobacter pylori infection and the risk of gastric carcinoma. *N Engl J Med* **325**, 1127–1131 (1991).
10. Carneiro, F. *et al.* Model of the early development of diffuse gastric cancer in E-cadherin mutation carriers and its implications for patient screening. *J Pathol* **203**, 681–687 (2004).
11. Huang, J. Q., Zheng, G. F., Sumanac, K., Irvine, E. J. & Hunt, R. H. Meta-analysis of the relationship between cagA seropositivity and gastric cancer. *Gastroenterology* **125**, 1636–1644 (2003).
12. Goldblum, J. R. *et al.* Inflammation and intestinal metaplasia of the gastric cardia: the role of gastroesophageal reflux and H. pylori infection. *Gastroenterology* **114**, 633–639 (1998).
13. Wu, I.-C. *et al.* Association between Helicobacter pylori seropositivity and digestive tract cancers. *World J Gastroenterol* **15**, 5465–5471 (2009).
14. Quante, M. *et al.* Bile acid and inflammation activate gastric cardia stem cells in a mouse model of Barrett’s-like metaplasia. *Cancer Cell* **21**, 36–51 (2012).
15. Nowicki-Osuch, K. *et al.* Molecular phenotyping reveals the identity of Barrett’s esophagus and its malignant transition. *Science (New York, N.Y.)* **373**, 760–767 (2021).
16. Kim, R. *et al.* Early Tumor-Immune Microenvironmental Remodeling and Response to First-Line Fluoropyrimidine and Platinum Chemotherapy in Advanced Gastric Cancer. *Cancer discovery* **12**, 984–1001 (2022).
17. Bass, A. J. *et al.* Comprehensive molecular characterization of gastric adenocarcinoma. *Nature* **513**, 202–209 (2014).
18. Wang, K. *et al.* Whole-genome sequencing and comprehensive molecular profiling identify new driver mutations in gastric cancer. *Nat Genet* **46**, 573–582 (2014).
19. Kim, J. *et al.* Integrated genomic characterization of oesophageal carcinoma. *Nature* **541**, 169–174 (2017).

20. Wang, X. *et al.* Residual embryonic cells as precursors of a Barrett's-like metaplasia. *Cell* **145**, 1023–1035 (2011).
21. Muzny, D. M. *et al.* Comprehensive molecular characterization of human colon and rectal cancer. *Nature* **487**, 330–337 (2012).
22. Marshall, B. J. & Warren, J. R. Unidentified curved bacilli in the stomach of patients with gastritis and peptic ulceration. *Lancet* **1**, 1311–1315 (1984).
23. Bertuccio, P. *et al.* Recent patterns in gastric cancer: A global overview. *International Journal of Cancer* **125**, 666–673 (2009).
24. Wadhwa, R. *et al.* Gastric cancer-molecular and clinical dimensions. *Nat Rev Clin Oncol* **10**, 643–655 (2013).
25. Eisenhauer, E. A. *et al.* New response evaluation criteria in solid tumours: revised RECIST guideline (version 1.1). *Eur J Cancer* **45**, 228–247 (2009).
26. Al-Batran, S. E. *et al.* Perioperative chemotherapy with fluorouracil plus leucovorin, oxaliplatin, and docetaxel versus fluorouracil or capecitabine plus cisplatin and epirubicin for locally advanced, resectable gastric or gastro-oesophageal junction adenocarcinoma (FLOT4): a randomised, phase 2/3 trial. *The Lancet* **393**, 1948–1957 (2019).
27. Cunningham, D. *et al.* Perioperative Chemotherapy versus Surgery Alone for Resectable Gastroesophageal Cancer. *New England Journal of Medicine* **355**, 11–20 (2006).
28. Ychou, M. *et al.* Perioperative chemotherapy compared with surgery alone for resectable gastroesophageal adenocarcinoma: an FNCLCC and FFCD multicenter phase III trial. *J Clin Oncol* **29**, 1715–1721 (2011).
29. Noh, S. H. *et al.* Adjuvant capecitabine plus oxaliplatin for gastric cancer after D2 gastrectomy (CLASSIC): 5-year follow-up of an open-label, randomised phase 3 trial. *Lancet Oncol* **15**, 1389–1396 (2014).
30. Ferri, L. E. *et al.* Perioperative docetaxel, cisplatin, and 5-fluorouracil (DCF) for locally advanced esophageal and gastric adenocarcinoma: a multicenter phase II trial. *Ann Oncol* **23**, 1512–1517 (2012).
31. Farrokhi, P. *et al.* Efficacy and Safety of FLOT regimen vs. DCF, FOLFOX, and ECF regimens as Perioperative Chemotherapy Treatments for Resectable Gastric Cancer Patients. 2021.01.26.21250550 Preprint at <https://doi.org/10.1101/2021.01.26.21250550> (2021).
32. Montagnani, F., Turrisi, G., Marinozzi, C., Aliberti, C. & Fiorentini, G. Effectiveness and safety of oxaliplatin compared to cisplatin for advanced, unresectable gastric cancer: a systematic review and meta-analysis. *Gastric Cancer* **14**, 50–55 (2011).
33. Gürler, F. *et al.* Retrospective comparison of flot and modified dcf as first-line chemotherapy in metastatic gastric adenocarcinoma. *Turkish Journal of Medical Sciences* **52**, 1559–1568 (2022).
34. Bruno, P. M. *et al.* A subset of platinum-containing chemotherapeutic agents kill cells by inducing ribosome biogenesis stress rather than by engaging a DNA damage response. *Nat Med* **23**, 461–471 (2017).
35. Yoon, H. H. *et al.* Adverse Prognostic Impact of Intratumor Heterogeneous HER2 Gene Amplification in Patients With Esophageal Adenocarcinoma. *J Clin Oncol* **30**, 3932–3938 (2012).
36. Ott, P. A. *et al.* T-Cell-Inflamed Gene-Expression Profile, Programmed Death Ligand 1 Expression, and Tumor Mutational Burden Predict Efficacy in Patients Treated With Pembrolizumab Across 20 Cancers: KEYNOTE-028. *J Clin Oncol* **37**, 318–327 (2019).

37. Bang, Y.-J. *et al.* Trastuzumab in combination with chemotherapy versus chemotherapy alone for treatment of HER2-positive advanced gastric or gastro-oesophageal junction cancer (ToGA): a phase 3, open-label, randomised controlled trial. *Lancet* **376**, 687–697 (2010).
38. Nguyen, M. *et al.* Dissecting Effects of Anti-cancer Drugs and Cancer-Associated Fibroblasts by On-Chip Reconstitution of Immunocompetent Tumor Microenvironments. *Cell Reports* **25**, 3884–3893.e3 (2018).
39. Boku, N. *et al.* Safety and efficacy of nivolumab in combination with S-1/capecitabine plus oxaliplatin in patients with previously untreated, unresectable, advanced, or recurrent gastric/gastroesophageal junction cancer: interim results of a randomized, phase II trial (ATTRACTION-4). *Ann Oncol* **30**, 250–258 (2019).
40. Fuchs, C. S. *et al.* Safety and Efficacy of Pembrolizumab Monotherapy in Patients With Previously Treated Advanced Gastric and Gastroesophageal Junction Cancer: Phase 2 Clinical KEYNOTE-059 Trial. *JAMA Oncol* **4**, e180013 (2018).
41. Janjigian, Y. Y. *et al.* Pembrolizumab plus trastuzumab and chemotherapy for HER2+ metastatic gastric or gastroesophageal junction (G/GEJ) cancer: Initial findings of the global phase 3 KEYNOTE-811 study. *JCO* **39**, 4013–4013 (2021).
42. Kang, Y.-K. *et al.* Nivolumab in patients with advanced gastric or gastro-oesophageal junction cancer refractory to, or intolerant of, at least two previous chemotherapy regimens (ONO-4538-12, ATTRACTION-2): a randomised, double-blind, placebo-controlled, phase 3 trial. *Lancet* **390**, 2461–2471 (2017).
43. Janjigian, Y. Y. *et al.* First-line nivolumab plus chemotherapy versus chemotherapy alone for advanced gastric, gastro-oesophageal junction, and oesophageal adenocarcinoma (CheckMate 649): a randomised, open-label, phase 3 trial. *Lancet* **398**, 27–40 (2021).
44. Heinhuis, K. M. *et al.* Enhancing antitumor response by combining immune checkpoint inhibitors with chemotherapy in solid tumors. *Ann Oncol* **30**, 219–235 (2019).
45. Park, D. S. *et al.* The Goldilocks Window of Personalized Chemotherapy: Getting the Immune Response Just Right. *Cancer Res* **79**, 5302–5315 (2019).
46. Tel, J. *et al.* The chemotherapeutic drug oxaliplatin differentially affects blood DC function dependent on environmental cues. *Cancer Immunol Immunother* **61**, 1101–1111 (2012).
47. Wang, W. *et al.* Chemoimmunotherapy by combining oxaliplatin with immune checkpoint blockades reduced tumor burden in colorectal cancer animal model. *Biochem Biophys Res Commun* **487**, 1–7 (2017).
48. Galetto, A. *et al.* Drug- and cell-mediated antitumor cytotoxicities modulate cross-presentation of tumor antigens by myeloid dendritic cells. *Anticancer Drugs* **14**, 833–843 (2003).
49. Vincent, J. *et al.* 5-Fluorouracil selectively kills tumor-associated myeloid-derived suppressor cells resulting in enhanced T cell-dependent antitumor immunity. *Cancer Res* **70**, 3052–3061 (2010).
50. Li, J. *et al.* Randomized, Double-Blind, Placebo-Controlled Phase III Trial of Apatinib in Patients With Chemotherapy-Refractory Advanced or Metastatic Adenocarcinoma of the Stomach or Gastroesophageal Junction. *Journal of clinical oncology : official journal of the American Society of Clinical Oncology* **34**, (2016).
51. Shitara, K. *et al.* Trifluridine/tipiracil versus placebo in patients with heavily pretreated metastatic gastric cancer (TAGS): a randomised, double-blind, placebo-controlled, phase 3 trial. *Lancet Oncol* **19**, 1437–1448 (2018).

52. Qi, C. *et al.* Claudin18.2-specific CAR T cells in gastrointestinal cancers: phase 1 trial interim results. *Nature Medicine* **28**, 1189–1198 (2022).
53. Tuveson, D. & Clevers, H. *Cancer modeling meets human organoid technology*. <http://science.sciencemag.org/> (2019).
54. Weeber, F. *et al.* Preserved genetic diversity in organoids cultured from biopsies of human colorectal cancer metastases. *Proceedings of the National Academy of Sciences* **112**, 13308–13311 (2015).
55. Yin, S. *et al.* Patient-derived tumor-like cell clusters for drug testing in cancer therapy. vol. 12 1723–1723 <http://stm.sciencemag.org/> (2020).
56. Larsen, B. M. *et al.* A pan-cancer organoid platform for precision medicine. *Cell Reports* **36**, (2021).
57. Fujii, M. *et al.* A Colorectal Tumor Organoid Library Demonstrates Progressive Loss of Niche Factor Requirements during Tumorigenesis. *Cell Stem Cell* **18**, 827–838 (2016).
58. Sato, T. *et al.* Long-term Expansion of Epithelial Organoids From Human Colon, Adenoma, Adenocarcinoma, and Barrett’s Epithelium. *Gastroenterology* **141**, 1762–1772 (2011).
59. van de Wetering, M. *et al.* Prospective Derivation of a Living Organoid Biobank of Colorectal Cancer Patients. *Cell* **161**, 933–945 (2015).
60. Guillen, K. P. *et al.* A human breast cancer-derived xenograft and organoid platform for drug discovery and precision oncology. *Nature Cancer* **3**, 232–250 (2022).
61. Sachs, N. *et al.* A Living Biobank of Breast Cancer Organoids Captures Disease Heterogeneity. *Cell* **172**, 373–386.e10 (2018).
62. Broutier, L. *et al.* Human primary liver cancer-derived organoid cultures for disease modeling and drug screening. *Nat Med* **23**, 1424–1435 (2017).
63. Dijkstra, K. K. *et al.* Challenges in Establishing Pure Lung Cancer Organoids Limit Their Utility for Personalized Medicine. *Cell Rep* **31**, 107588 (2020).
64. Hu, Y. *et al.* Lung cancer organoids analyzed on microwell arrays predict drug responses of patients within a week. *Nature Communications* **12**, (2021).
65. Hirt, C. K. *et al.* Drug screening and genome editing in human pancreatic cancer organoids identifies drug-gene interactions and candidates for off-label treatment. *Cell genomics* **2**, 100095–100095 (2022).
66. Osuna de la Peña, D. *et al.* Bioengineered 3D models of human pancreatic cancer recapitulate in vivo tumour biology. *Nature Communications* **12**, (2021).
67. Tiriac, H. *et al.* Organoid Profiling Identifies Common Responders to Chemotherapy in Pancreatic Cancer. *Cancer discovery* **8**, 1112–1129 (2018).
68. Boj, S. F. *et al.* Organoid models of human and mouse ductal pancreatic cancer. *Cell* **160**, 324–338 (2015).
69. Gao, D. *et al.* Organoid cultures derived from patients with advanced prostate cancer. *Cell* **159**, 176–187 (2014).
70. Karthaus, W. R. *et al.* Identification of multipotent luminal progenitor cells in human prostate organoid cultures. *Cell* **159**, 163–175 (2014).
71. Paczkowski, M. *et al.* Reciprocal interactions between tumour cell populations enhance growth and reduce radiation sensitivity in prostate cancer. *Commun Biol* **4**, 6 (2021).
72. Boretto, M. *et al.* Patient-derived organoids from endometrial disease capture clinical heterogeneity and are amenable to drug screening. *Nat Cell Biol* **21**, 1041–1051 (2019).

73. Turco, M. Y. *et al.* Long-term, hormone-responsive organoid cultures of human endometrium in a chemically defined medium. *Nat Cell Biol* **19**, 568–577 (2017).
74. Karakasheva, T. A. *et al.* Generation and Characterization of Patient-Derived Head and Neck, Oral, and Esophageal Cancer Organoids. *Curr Protoc Stem Cell Biol* **53**, e109 (2020).
75. Kijima, T. *et al.* Three-Dimensional Organoids Reveal Therapy Resistance of Esophageal and Oropharyngeal Squamous Cell Carcinoma Cells. *Cell Mol Gastroenterol Hepatol* **7**, 73–91 (2019).
76. Li, X. *et al.* Oncogenic transformation of diverse gastrointestinal tissues in primary organoid culture. *Nature Medicine* **20**, 769–777 (2014).
77. Yan, H. H. N. *et al.* A Comprehensive Human Gastric Cancer Organoid Biobank Captures Tumor Subtype Heterogeneity and Enables Therapeutic Screening. *Cell Stem Cell* **23**, 882–897.e11 (2018).
78. Costa, E. C. *et al.* 3D tumor spheroids: an overview on the tools and techniques used for their analysis. *Biotechnol Adv* **34**, 1427–1441 (2016).
79. Drost, J. & Clevers, H. Organoids in cancer research. *Nat Rev Cancer* **18**, 407–418 (2018).
80. Hogenson, T. L. *et al.* Culture media composition influences patient-derived organoids ability to predict therapeutic response in gastrointestinal cancers. *JCI Insight* e158060 (2022) doi:10.1172/jci.insight.158060.
81. Pauli, C. *et al.* Personalized In Vitro and In Vivo Cancer Models to Guide Precision Medicine. *Cancer Discov* **7**, 462–477 (2017).
82. Vlachogiannis, G. *et al.* Patient-derived organoids model treatment response of metastatic gastrointestinal cancers. *Science* **359**, 920–926 (2018).
83. Hidalgo, M. *et al.* Patient-derived xenograft models: an emerging platform for translational cancer research. *Cancer Discov* **4**, 998–1013 (2014).
84. Corso, S. *et al.* A comprehensive PDX gastric cancer collection captures cancer cell–intrinsic transcriptional MSI traits. *Cancer Research* **79**, 5884–5896 (2019).
85. Dang, H. X. *et al.* *The clonal evolution of metastatic colorectal cancer*. vol. 6 9691–9701 <https://pdmr.cancer.gov/> (2020).
86. Byrne, A. T. *et al.* Interrogating open issues in cancer precision medicine with patient-derived xenografts. *Nat Rev Cancer* **17**, 254–268 (2017).
87. Pham, N.-A. *et al.* Patient-derived tumor xenograft and organoid models established from resected pancreatic, duodenal and biliary cancers. *Sci Rep* **11**, 10619 (2021).
88. Veninga, V. & Voest, E. E. Tumor organoids: Opportunities and challenges to guide precision medicine. *Cancer Cell* **39**, 1190–1201 (2021).
89. Rosenbluth, J. *et al.* Organoid cultures from normal and cancer-prone human breast tissues preserve complex epithelial lineages. *Nature Communications* **11**, (2020).
90. Verduin, M., Hoeben, A., De Ruyscher, D. & Vooijs, M. Patient-Derived Cancer Organoids as Predictors of Treatment Response. *Frontiers in Oncology* **11**, (2021).
91. Wang, H. *et al.* 3D cell culture models: Drug pharmacokinetics, safety assessment, and regulatory consideration. *Clinical and Translational Science* **14**, 1659–1680 (2021).
92. Kao, J. *et al.* Molecular profiling of breast cancer cell lines defines relevant tumor models and provides a resource for cancer gene discovery. *PLoS One* **4**, e6146 (2009).
93. Sachs, N. & Clevers, H. Organoid cultures for the analysis of cancer phenotypes. *Current Opinion in Genetics & Development* **24**, 68–73 (2014).

94. Kopper, O. *et al.* An organoid platform for ovarian cancer captures intra- and interpatient heterogeneity. *Nat Med* **25**, 838–849 (2019).
95. Shen, X. *et al.* KLF5 inhibition overcomes oxaliplatin resistance in patient-derived colorectal cancer organoids by restoring apoptotic response. *Cell Death and Disease* **13**, (2022).
96. Hill, S. J. *et al.* Prediction of DNA Repair Inhibitor Response in Short-Term Patient-Derived Ovarian Cancer Organoids. *Cancer Discov* **8**, 1404–1421 (2018).
97. Ooft, S. N. *et al.* Patient-derived organoids can predict response to chemotherapy in metastatic colorectal cancer patients. *Science Translational Medicine* **11**, (2019).
98. de Witte, C. J. *et al.* Patient-Derived Ovarian Cancer Organoids Mimic Clinical Response and Exhibit Heterogeneous Inter- and Inpatient Drug Responses. *Cell Reports* **31**, 107762 (2020).
99. Kondo, J. & Inoue, M. Application of Cancer Organoid Model for Drug Screening and Personalized Therapy. *Cells* **8**, 470 (2019).
100. Driehuis, E. *et al.* Oral Mucosal Organoids as a Potential Platform for Personalized Cancer Therapy. *Cancer Discov* **9**, 852–871 (2019).
101. Ferguson, F. M. *et al.* Discovery of a selective inhibitor of doublecortin like kinase 1. *Nat Chem Biol* **16**, 635–643 (2020).
102. Mo, S. *et al.* Patient-Derived Organoids from Colorectal Cancer with Paired Liver Metastasis Reveal Tumor Heterogeneity and Predict Response to Chemotherapy. *Adv Sci (Weinh)* e2204097 (2022) doi:10.1002/advs.202204097.
103. Settleman, R. L. C. and J. From Cancer Genomics to Precision Oncology—Tissue’s Still an Issue | EndNote Click.
<https://click.endnote.com/viewer?doi=10.1016%2Fj.cell.2014.05.027&token=WzI5MDk1MDYsIjEwLjEwMTYvai5jZWxsLjIwMTQuMDUuMDI3Ii0.J71XguIJ1XGdD7-ECpxoeleqt-M> (2014).
104. Woolston, A. *et al.* Genomic and Transcriptomic Determinants of Therapy Resistance and Immune Landscape Evolution during Anti-EGFR Treatment in Colorectal Cancer. *Cancer Cell* **36**, 35-50.e9 (2019).
105. Biffi, G. *et al.* IL1-Induced JAK/STAT Signaling Is Antagonized by TGF β to Shape CAF Heterogeneity in Pancreatic Ductal Adenocarcinoma. *Cancer Discovery* **9**, 282–301 (2019).
106. Neal, J. T. *et al.* Organoid Modeling of the Tumor Immune Microenvironment. *Cell* **175**, 1972-1988.e16 (2018).
107. Zhang, W., Li, J., Zhou, J., Rastogi, A. & Ma, S. Translational organoid technology – the convergence of chemical, mechanical, and computational biology. *Trends in Biotechnology* **40**, 1121–1135 (2022).
108. Bhatia, S. N. & Ingber, D. E. Microfluidic organs-on-chips. *Nat Biotechnol* **32**, 760–772 (2014).
109. Ingber, D. E. Reverse Engineering Human Pathophysiology with Organs-on-Chips. *Cell* **164**, 1105–1109 (2016).
110. Chen, D. S. & Mellman, I. Elements of cancer immunity and the cancer-immune set point. *Nature* **541**, 321–330 (2017).
111. Huh, D. *et al.* Microfabrication of human organs-on-chips. *Nat Protoc* **8**, 2135–2157 (2013).
112. Kasendra, M. *et al.* Development of a primary human Small Intestine-on-a-Chip using biopsy-derived organoids. *Scientific Reports* **8**, (2018).

113. Boland, C. R., Koi, M., Chang, D. K. & Carethers, J. M. The biochemical basis of microsatellite instability and abnormal immunohistochemistry and clinical behavior in Lynch syndrome: from bench to bedside. *Fam Cancer* **7**, 41–52 (2008).
114. Lopez, G., Venetis, K., Sajjadi, E. & Fusco, N. Mismatch Repair System Genomic Scars in Gastroesophageal Cancers: Biology and Clinical Testing. *Gastrointestinal Disorders* **2**, 341–352 (2020).
115. Kim, T.-M., Laird, P. W. & Park, P. J. The landscape of microsatellite instability in colorectal and endometrial cancer genomes. *Cell* **155**, 858–868 (2013).
116. Smyth, E. C. *et al.* Mismatch Repair Deficiency, Microsatellite Instability, and Survival: An Exploratory Analysis of the Medical Research Council Adjuvant Gastric Infusional Chemotherapy (MAGIC) Trial. *JAMA Oncol* **3**, 1197–1203 (2017).
117. Bahsi, S. *et al.* Clinicopathological and Prognostic Significance of MSI Status and PD-L1 Expression in Turkish Patients with Gastric Cancer. *International Journal of Hematology and Oncology* **31**, 9 (2021).
118. Kwon, M. *et al.* Determinants of response and intrinsic resistance to pd-1 blockade in microsatellite instability–high gastric cancer. *Cancer Discovery* **11**, 2168–2185 (2021).
119. Kim, K.-J. *et al.* Differential clinicopathologic features in microsatellite-unstable gastric cancers with and without MLH1 methylation. *Hum Pathol* **44**, 1055–1064 (2013).
120. Toyota, M. *et al.* Aberrant methylation in gastric cancer associated with the CpG island methylator phenotype. *Cancer Res* **59**, 5438–5442 (1999).
121. Mi, T.-M. *et al.* Prevalence and prognosis of microsatellite instability in oesogastric adenocarcinoma, NORDICAP 16-01. *Clinics and research in hepatology and gastroenterology* **45**, (2021).
122. Polom, K. *et al.* Meta-analysis of microsatellite instability in relation to clinicopathological characteristics and overall survival in gastric cancer. *Br J Surg* **105**, 159–167 (2018).
123. Imamura, Y. *et al.* Recent Incidence Trend of Surgically Resected Esophagogastric Junction Adenocarcinoma and Microsatellite Instability Status in Japanese Patients. *DIG* **99**, 6–13 (2019).
124. Salem, M. E. *et al.* Comparative Molecular Analyses of Esophageal Squamous Cell Carcinoma, Esophageal Adenocarcinoma, and Gastric Adenocarcinoma. *Oncologist* **23**, 1319–1327 (2018).
125. Polom, K. *et al.* Molecular key to understand the gastric cancer biology in elderly patients- The role of microsatellite instability. *J Surg Oncol* **115**, 344–350 (2017).
126. Pietrantonio, F. *et al.* *Individual Patient Data Meta-Analysis of the Value of Microsatellite Instability As a Biomarker in Gastric Cancer*. vol. 37 3392–3400 <http://ascopubs.org/> (2019).
127. Lin, S. J. *et al.* Signatures of tumour immunity distinguish Asian and non-Asian gastric adenocarcinomas. *Gut* **64**, 1721–1731 (2015).
128. Fang, W.-L. *et al.* The Clinicopathological Features and Genetic Mutations in Gastric Cancer Patients According to EMAS and MSI Status. *Cancers (Basel)* **12**, 551 (2020).
129. Zang, Y.-S. *et al.* Comprehensive analysis of potential immunotherapy genomic biomarkers in 1000 Chinese patients with cancer. *Cancer Med* **8**, 4699–4708 (2019).
130. An, J. Y. *et al.* Microsatellite instability in sporadic gastric cancer: its prognostic role and guidance for 5-FU based chemotherapy after R0 resection. *International Journal of Cancer* **131**, 505–511 (2012).

131. Kim, Y. *et al.* Profiling cancer-associated genetic alterations and molecular classification of cancer in Korean gastric cancer patients. *Oncotarget* **8**, 69888–69905 (2017).
132. Vos, E. L. *et al.* The interaction between microsatellite instability high (MSI-high) gastric cancer and chemotherapy on survival. *JCO* **39**, 244–244 (2021).
133. Zheng, K. *et al.* A novel NGS-based microsatellite instability (MSI) status classifier with 9 loci for colorectal cancer patients. *Journal of Translational Medicine* **18**, 1–9 (2020).
134. Janjigian, Y. Y. *et al.* Genetic predictors of response to systemic therapy in esophagogastric cancer. *Cancer Discovery* **8**, 49–58 (2018).
135. Lieb, S. *et al.* Werner syndrome helicase is a selective vulnerability of microsatellite instability-high tumor cells. *eLife* **8**, e43333 (2019).
136. Picco, G. *et al.* Werner Helicase Is a Synthetic-Lethal Vulnerability in Mismatch Repair–Deficient Colorectal Cancer Refractory to Targeted Therapies, Chemotherapy, and Immunotherapy. *Cancer Discovery* **11**, 1923–1937 (2021).
137. Marrelli, D. *et al.* Strong Prognostic Value of Microsatellite Instability in Intestinal Type Non-cardia Gastric Cancer. *Ann Surg Oncol* **23**, 943–950 (2016).
138. Garattini, S. K. *et al.* Molecular classifications of gastric cancers: Novel insights and possible future applications. *World J Gastrointest Oncol* **9**, 194–208 (2017).
139. Wang, K. *et al.* Exome sequencing identifies frequent mutation of ARID1A in molecular subtypes of gastric cancer. *Nat Genet* **43**, 1219–1223 (2011).
140. Dulak, A. M. *et al.* Exome and whole-genome sequencing of esophageal adenocarcinoma identifies recurrent driver events and mutational complexity. *Nat Genet* **45**, 478–486 (2013).
141. Schlauch, D. *et al.* Tumor-Specific and Tumor-Agnostic Molecular Signatures Associated With Response to Immune Checkpoint Inhibitors. *JCO Precision Oncology* 1625–1638 (2021) doi:10.1200/PO.21.00008.
142. Cocco, E. *et al.* Colorectal Carcinomas Containing Hypermethylated MLH1 Promoter and Wild-Type BRAF/KRAS Are Enriched for Targetable Kinase Fusions. *Cancer Res* **79**, 1047–1053 (2019).
143. Drilon, A. *et al.* Efficacy of Larotrectinib in TRK Fusion–Positive Cancers in Adults and Children. *New England Journal of Medicine* **378**, 731–739 (2018).
144. Pietrantonio, F. *et al.* ALK, ROS1, and NTRK Rearrangements in Metastatic Colorectal Cancer. *J Natl Cancer Inst* **109**, (2017).
145. Cocco, E. *et al.* Resistance to TRK inhibition mediated by convergent MAPK pathway activation. *Nat Med* **25**, 1422–1427 (2019).
146. Misale, S. *et al.* Blockade of EGFR and MEK intercepts heterogeneous mechanisms of acquired resistance to anti-EGFR therapies in colorectal cancer. *Sci Transl Med* **6**, 224ra26 (2014).
147. Russo, M. *et al.* Acquired Resistance to the TRK Inhibitor Entrectinib in Colorectal Cancer. *Cancer Discov* **6**, 36–44 (2016).
148. Hampel, H. *et al.* Screening for the Lynch syndrome (hereditary nonpolyposis colorectal cancer). *N Engl J Med* **352**, 1851–1860 (2005).
149. Mensenkamp, A. R. *et al.* Somatic mutations in MLH1 and MSH2 are a frequent cause of mismatch-repair deficiency in Lynch syndrome-like tumors. *Gastroenterology* **146**, 643–646.e8 (2014).
150. Rodríguez-Soler, M. *et al.* Risk of cancer in cases of suspected lynch syndrome without germline mutation. *Gastroenterology* **144**, 926–932.e1; quiz e13–14 (2013).

151. Haraldsdottir, S. *et al.* Colon and endometrial cancers with mismatch repair deficiency can arise from somatic, rather than germline, mutations. *Gastroenterology* **147**, 1308-1316.e1 (2014).
152. Vivanco, I. & Sawyers, C. L. The phosphatidylinositol 3-Kinase AKT pathway in human cancer. *Nat Rev Cancer* **2**, 489–501 (2002).
153. Samuels, Y. *et al.* High frequency of mutations of the PIK3CA gene in human cancers. *Science* **304**, 554 (2004).
154. Jung, B., Staudacher, J. J. & Beauchamp, D. Transforming Growth Factor β Superfamily Signaling in Development of Colorectal Cancer. *Gastroenterology* **152**, 36–52 (2017).
155. Zhang, Q. *et al.* Inhibition of ATM Increases Interferon Signaling and Sensitizes Pancreatic Cancer to Immune Checkpoint Blockade Therapy. *Cancer Res* **79**, 3940–3951 (2019).
156. Bilbao, C. *et al.* The relationship between microsatellite instability and PTEN gene mutations in endometrial cancer. *Int J Cancer* **119**, 563–570 (2006).
157. Catasús, L., Matias-Guiu, X., Machin, P., Muñoz, J. & Prat, J. BAX somatic frameshift mutations in endometrioid adenocarcinomas of the endometrium: evidence for a tumor progression role in endometrial carcinomas with microsatellite instability. *Lab Invest* **78**, 1439–1444 (1998).
158. Lee, J.-H. *et al.* Inverse Relationship between APC Gene Mutation in Gastric Adenomas and Development of Adenocarcinoma. *The American Journal of Pathology* **161**, 611–618 (2002).
159. Grasso, C. S. *et al.* Genetic Mechanisms of Immune Evasion in Colorectal Cancer. *Cancer Discov* **8**, 730–749 (2018).
160. Lin, E. I. *et al.* Mutational profiling of colorectal cancers with microsatellite instability. *Oncotarget* **6**, 42334–42344 (2015).
161. Kim, J. C. *et al.* Promoter methylation of specific genes is associated with the phenotype and progression of colorectal adenocarcinomas. *Ann Surg Oncol* **17**, 1767–1776 (2010).
162. Dulak, A. M. *et al.* Gastrointestinal adenocarcinomas of the esophagus, stomach, and colon exhibit distinct patterns of genome instability and oncogenesis. *Cancer Res* **72**, 4383–4393 (2012).
163. Kim, M. A. *et al.* EGFR in gastric carcinomas: prognostic significance of protein overexpression and high gene copy number. *Histopathology* **52**, 738–746 (2008).
164. Hong, L. *et al.* Prognostic value of epidermal growth factor receptor in patients with gastric cancer: a meta-analysis. *Gene* **529**, 69–72 (2013).
165. Richards, F. M. *et al.* Germline E-cadherin gene (CDH1) mutations predispose to familial gastric cancer and colorectal cancer. *Hum Mol Genet* **8**, 607–610 (1999).
166. Knijnenburg, T. A. *et al.* Genomic and Molecular Landscape of DNA Damage Repair Deficiency across The Cancer Genome Atlas. *Cell Rep* **23**, 239-254.e6 (2018).
167. Nie, R. C. *et al.* Adjuvant Chemotherapy for Gastric Cancer Patients with Mismatch Repair Deficiency or Microsatellite Instability: Systematic Review and Meta-Analysis. *Ann Surg Oncol* **29**, 2324–2331 (2022).
168. Amirouchene-Angelozzi, N., Swanton, C. & Bardelli, A. Tumor Evolution as a Therapeutic Target. *Cancer Discov* (2017) doi:10.1158/2159-8290.CD-17-0343.
169. Xie, Y.-H., Chen, Y.-X. & Fang, J.-Y. Comprehensive review of targeted therapy for colorectal cancer. *Signal Transduct Target Ther* **5**, 22 (2020).
170. Bernards, R. A missing link in genotype-directed cancer therapy. *Cell* **151**, 465–468 (2012).

171. Holohan, C., Van Schaeybroeck, S., Longley, D. B. & Johnston, P. G. Cancer drug resistance: an evolving paradigm. *Nat Rev Cancer* **13**, 714–726 (2013).
172. Brosh, R. M. DNA helicases involved in DNA repair and their roles in cancer. *Nat Rev Cancer* **13**, 542–558 (2013).
173. Chu, W. K. & Hickson, I. D. RecQ helicases: multifunctional genome caretakers. *Nat Rev Cancer* **9**, 644–654 (2009).
174. Chan, E. M. *et al.* WRN helicase is a synthetic lethal target in microsatellite unstable cancers. *Nature* **568**, 551–556 (2019).
175. Kategaya, L., Perumal, S. K., Hager, J. H. & Belmont, L. D. Werner Syndrome Helicase Is Required for the Survival of Cancer Cells with Microsatellite Instability. *iScience* **13**, 488–497 (2019).
176. Behan, F. M. *et al.* Prioritization of cancer therapeutic targets using CRISPR–Cas9 screens. *Nature* **568**, 511–516 (2019).
177. McDonald, E. R. *et al.* Project DRIVE: A Compendium of Cancer Dependencies and Synthetic Lethal Relationships Uncovered by Large-Scale, Deep RNAi Screening. *Cell* **170**, 577–592.e10 (2017).
178. Meyers, R. M. *et al.* Computational correction of copy number effect improves specificity of CRISPR–Cas9 essentiality screens in cancer cells. *Nat Genet* **49**, 1779–1784 (2017).
179. van Wietmarschen, N., Nathan, W. J. & Nussenzweig, A. The WRN helicase: resolving a new target in microsatellite unstable cancers. *Current Opinion in Genetics and Development* **71**, 34–38 (2021).
180. Nickoloff, J. A., Jones, D., Lee, S.-H., Williamson, E. A. & Hromas, R. Drugging the Cancers Addicted to DNA Repair. *J Natl Cancer Inst* **109**, djx059 (2017).
181. O'Brien, V. & Brown, R. Signalling cell cycle arrest and cell death through the MMR System. *Carcinogenesis* **27**, 682–692 (2006).
182. Prince, P. R., Emond, M. J. & Monnat, R. J. Loss of Werner syndrome protein function promotes aberrant mitotic recombination. *Genes Dev* **15**, 933–938 (2001).
183. Bou-Hanna, C. *et al.* Acute cytotoxicity of MIRA-1/NSC19630, a mutant p53-reactivating small molecule, against human normal and cancer cells via a caspase-9-dependent apoptosis. *Cancer Lett* **359**, 211–217 (2015).
184. Germano, G. *et al.* Inactivation of DNA repair triggers neoantigen generation and impairs tumour growth. *Nature* **552**, 116–120 (2017).
185. Mackenzie, K. J. *et al.* cGAS surveillance of micronuclei links genome instability to innate immunity. *Nature* **548**, 461–465 (2017).
186. Mandal, R. *et al.* Genetic diversity of tumors with mismatch repair deficiency influences anti-PD-1 immunotherapy response. *Science* **364**, 485–491 (2019).
187. Schrock, A. B. *et al.* Tumor mutational burden is predictive of response to immune checkpoint inhibitors in MSI-high metastatic colorectal cancer. *Ann Oncol* **30**, 1096–1103 (2019).
188. Le, D. T. *et al.* PD-1 Blockade in Tumors with Mismatch-Repair Deficiency. *New England Journal of Medicine* **372**, 2509–2520 (2015).
189. Chalabi, M. *et al.* Neoadjuvant immunotherapy leads to pathological responses in MMR-proficient and MMR-deficient early-stage colon cancers. *Nat Med* **26**, 566–576 (2020).
190. Le, D. T. *et al.* Mismatch repair deficiency predicts response of solid tumors to PD-1 blockade. *Science* **357**, 409–413 (2017).

191. Overman, M. J. *et al.* Durable Clinical Benefit With Nivolumab Plus Ipilimumab in DNA Mismatch Repair–Deficient/Microsatellite Instability–High Metastatic Colorectal Cancer. *JCO* **36**, 773–779 (2018).
192. Mlecnik, B. *et al.* Integrative Analyses of Colorectal Cancer Show Immunoscore Is a Stronger Predictor of Patient Survival Than Microsatellite Instability. *Immunity* **44**, 698–711 (2016).
193. Chao, J. *et al.* Assessment of Pembrolizumab Therapy for the Treatment of Microsatellite Instability–High Gastric or Gastroesophageal Junction Cancer Among Patients in the KEYNOTE-059, KEYNOTE-061, and KEYNOTE-062 Clinical Trials. *JAMA Oncology* **7**, 895–902 (2021).
194. Fuchs, C. S. *et al.* Pembrolizumab versus paclitaxel for previously treated PD-L1-positive advanced gastric or gastroesophageal junction cancer: 2-year update of the randomized phase 3 KEYNOTE-061 trial. *Gastric Cancer* **25**, 197–206 (2022).
195. Shitara, K. *et al.* Efficacy and Safety of Pembrolizumab or Pembrolizumab Plus Chemotherapy vs Chemotherapy Alone for Patients With First-line, Advanced Gastric Cancer: The KEYNOTE-062 Phase 3 Randomized Clinical Trial. *JAMA Oncol* **6**, 1571–1580 (2020).
196. André, T. *et al.* Neoadjuvant Nivolumab Plus Ipilimumab and Adjuvant Nivolumab in Localized Deficient Mismatch Repair/Microsatellite Instability-High Gastric or Esophagogastric Junction Adenocarcinoma: The GERCOR NEONIPIGA Phase II Study. *J Clin Oncol* 0–0 (2022) doi:10.1200/JCO.22.
197. Cercek, A. *et al.* PD-1 Blockade in Mismatch Repair–Deficient, Locally Advanced Rectal Cancer. *New England Journal of Medicine* **386**, 2363–2376 (2022).
198. Fujii, M., Clevers, H. & Sato, T. Modeling Human Digestive Diseases With CRISPR-Cas9-Modified Organoids. *Gastroenterology* **156**, 562–576 (2019).
199. Gravalos, C. & Jimeno, A. HER2 in gastric cancer: a new prognostic factor and a novel therapeutic target. *Ann Oncol* **19**, 1523–1529 (2008).
200. Morihiro, T. *et al.* PD-L1 expression combined with microsatellite instability/CD8+ tumor infiltrating lymphocytes as a useful prognostic biomarker in gastric cancer. *Sci Rep* **9**, 4633 (2019).
201. Tarnowski, B. I., Spinale, F. G. & Nicholson, J. H. DAPI as a useful stain for nuclear quantitation. *Biotech Histochem* **66**, 297–302 (1991).
202. Calandrini, C. & Drost, J. Normal and tumor-derived organoids as a drug screening platform for tumor-specific drug vulnerabilities. *STAR Protocols* **3**, (2022).
203. Coppé, J. P. *et al.* Mapping phospho-catalytic dependencies of therapy-resistant tumours reveals actionable vulnerabilities. *Nature Cell Biology* **21**, 778–790 (2019).
204. Gonçalves, E. *et al.* Pan-cancer proteomic map of 949 human cell lines. *Cancer cell* **40**, 835-849.e8 (2022).